EXPERIMENTAL INVESTIGATION ON THE SYNTHESIS OF CARBON NANOTUBES (CNTs) BY ARC-DISCHARGE METHOD USING A MIG WELDER

By

HARIPRASAD RAMAKRISHNAN VENKATANATH

Bachelor of Engineering

UNIVERSITY OF MADRAS

CHENNAI, India 2002

Submitted to the Faculty of the
Graduate College of the
Oklahoma State University
in partial fulfillment of
the requirements for
the Degree of
MASTER OF SCIENCE
December, 2005

EXPERIMENTAL INVESTIGATION ON THE SYNTHESIS OF CARBON NANOTUBES (CNTs) BY ARC-DISCHARGE METHOD USING A MIG WELDER

Thesis Approved:

Dr. Ranga Komanduri (Thesis Adviser)

Dr. Hongbing Lu

Dr. C.E. Price

A. Gordon Emslie (Dean of the Graduate College)

SUMMARY

The arc-discharge is a simple and inexpensive method for producing carbon nanotubes (CNTs) on a large scale. The arc-discharge apparatus in the vertical configuration in conjunction with an MIG welder was built for conducting this study. To synthesize multi-walled carbon nanotubes (MWNTs) a 0.25" diameter graphite anode was used. For the synthesis of single-walled carbon nanotubes (SWNTs), 4at% nickel, 1at% yttrium, 95at% carbon anode was used. The anodes were prepared by filling the graphite rod with metal catalyst. Critical process parameters such as process gas, and gas pressure have been varied to study its effect on MWNT yield. The desired pressure condition for the synthesis of MWNTs is found to be between 315 and 355 torr of helium. In this pressure range 137 mg of MWNT containing material was formed in 5 minutes. Since the multiwalled carbon nanotubes are formed along with amorphous carbon, the effect of time, temperature and air flow during purification has been studied. The optimum purification time is found to be 15 mins at 700 ^{0} C or 5 mins at 750 ^{0} C. In the study of SWNTs, the helium pressure and flow rate was varied to study its effect on yield. Maximum yield of SWNTs containing deposit is obtained at 506 torr of helium with a flow rate of 2l/min. The growth mechanism of single-walled carbon nanotubes is studied using the SEM and TEM and explained according to the vapor-liquid-solid model.

ACKNNOWLEDGEMENT

I would like to express my indebtedness to my advisor Dr. Ranga Komanduri, for his encouragement, support, facilities and guidance. I thank you for the opportunity to work in your labs. I would like thank my committee members Dr. Lu and Dr. Price for serving on my committee.

I would like to thank Mrs. Phoebe Doss and Mr. Terry Colberg of the electron microscopy lab for their help with the SEM and TEM work. I would like to thank Mrs. Sharon Green of Mechanical and Aerospace Engineering department for the TEM images. I would also like to thank Madhan, Raju, and Deva of the microwave CVD group for the useful discussions. I would like to thank Anand and Katie for their assistance with the experiments. I would like to thank the ATRC lab manager Mr. Jerry Dale for the help and useful suggestions.

I would like to thank my parents, brothers and sister-in-law for their constant support, encouragement, and motivation throughout my graduate program.

TABLE OF CONTENTS

Chapter **Page**

LIST OF TABLES

Table **Page**

LIST OF FIGURES

FIGURE **PAGE**

CHAPTER 1

INTRODUCTION TO CARBON NANOTUBES

1.1 Introduction

The discovery of the third allotrope of carbon, namely fullerene by Smalley in 1985 [1], spurred the interest in other allotropes of carbon. The forth allotrope of carbon, carbon nanotubes, was first observed by high resolution TEM Iijima in 1991 [2]. In 1993, Iijima and Ichihashi of NEC, Japan [3] and Bethune *et al.* [4] at IBM Almaden research center in California, independently reported the synthesis of single walled nanotubes. Today carbon nanotubes are considered as one of the most important molecules in nanotechnology.

1.2 Structure

A carbon nanotube is made of graphite sheets rolled into a hollow cylinder. A single-walled carbon nanotube (SWNT) is made by rolling one graphite sheet. When multiple graphite sheets are stacked upon each other and rolled into a cylinder with a common axis it is called multi-walled carbon nanotube (MWNT). MWNTs consist of two or more concentrically arranged single-walled nanotubes. In the graphene sheet, the carbon atoms are arranged in a hexagonal array such that each carbon atom is surrounded by three carbon atoms.

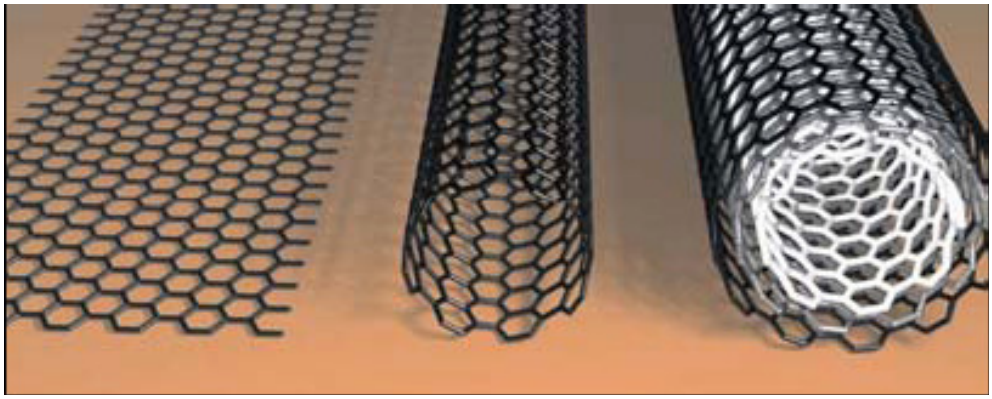

Figure 1.1 Structure of single graphite sheet where carbon atoms are arranged in a hexagonal array, a SWNT (middle) and, MWNT (right) [5]

There are infinitely many ways to roll a graphene sheet into a cylinder, resulting in different physical and electronic properties of the tubes [6]. The unit cell of the graphene lattice can be described by two vectors a_1, a_2 and contains two carbon atoms at the position 1/3 (a_1+a_2) and 2/3 (a_1+a_2) as shown in Figure 1.2. In the nanotube, the graphene sheet is rolled up in such a way that the graphene lattice vector $c = na_1 + ma_2$ becomes the circumference of the tube. It is also called chiral vector which uniquely defines the particular nanotube. The chiral vector is represented by a pair of integers (n, m). The chiral angle θ determines the amount twist in the tube. For each tube, θ is between 0^o and 30^o, the tubes with $\theta = 0^o$ are called zig-zag tubes because they exhibit a zig-zag pattern along the circumference. It is denoted by (n, 0) and the tubes where $\theta = 30^o$ are called armchair tubes and is denoted by (n, n) as shown in Fig 1.3 [6]. All the other nanotubes are called chiral or helical nanotube and have a longer unit cell along the axis.

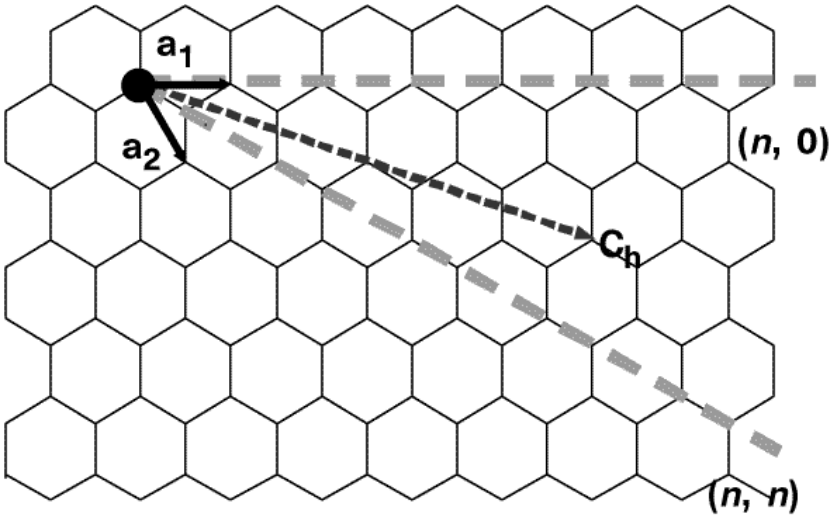

Figure 1.2 A two-dimensional graphene sheet with lattice vectors $\mathbf{a_1}$ and $\mathbf{a_2}$, and the roll-up vector. $\mathbf{c_h} = n\mathbf{a_1} + m\mathbf{a_2}$. The limiting cases of (n, 0) zigzag and (n, n) armchair tubes are indicated with dashed lines [6].

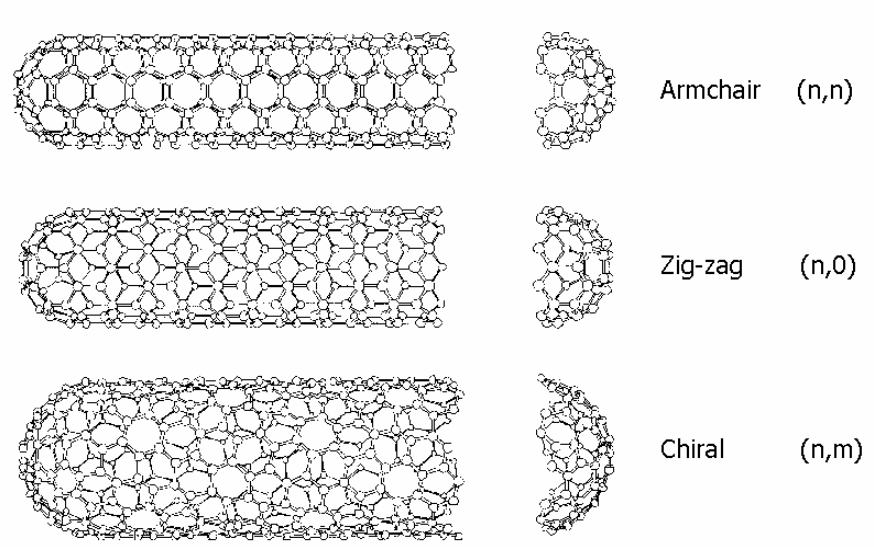

Figure 1.3 Schematic models of armchair, zig-zag and chiral single walled tubes [6].

1.3 Properties

Carbon nanotubes are of great interest due to their unique properties. Theoretical and experimental studies have shown that carbon nanotubes have outstanding mechanical properties, (e.g. Young's modulus 1-1.28 TPa [7, 8, 14] in their axial direction and yield

strength 120 GPa [9]). They perform better in compression than carbon fibers. It has also been observed that the nanotubes exhibit highly elastic behavior when loaded using an AFM probe [10]. Apart from the unique mechanical properties, they have very high thermal conductivity (~ 2000 W/mK [11, 12]), and minimum electrical resistance (10^{-4} Ω-cm [13]). Due to their one dimensional structure, sp2 and π bonding between the carbon atoms, they have very interesting electronic properties. The electronic properties of a SWNT completely depend on the chiral vector (n, m), and they can be semiconducting or metallic [6]. The nanotube is metallic when the difference n-m is a multiple of three, semiconducting when the difference is not three. The difference in electronic properties is caused by the different molecular structure leading to different band gap.

1.4 Applications

Carbon nanotubes can be used as reinforcing fiber in composites due to their unique mechanical, thermal properties and high aspect ratio. Nanotubes in composites can lead to extraordinary, strength to weight ratio in composites [15, 16]. The high aspect ratio and strength of carbon nanotubes allows them to be used as probes in AFM, the small diameter allows the CNTs to probe biomolecules and nanostructures [17, 18]. Carbon nanotubes are ideal candidates for next generation nano-electronic devises due to their unique electronic properties. Carbon nanotubes can be used in field emitting devices such as flat panel display [19], electron guns in cathode ray tubes [20]. The ability to fill carbon nanotubes with metals leads to the use of nanotubes as moulds to fabricate nanowires [21]. Due to their high surface area per unit weight, single walled nanotubes can be used to store large amounts of hydrogen atoms by adsorption [22]. Sheets of single

walled nanotube can be used as electro-mechanical actuators, substituting the actuator mechanism present in natural muscles [23]. Active research is in progress for finding new applications for the exceptional one dimensional structures of carbon.

1.5 Outline

Chapter 2 examines various methods by which carbon nanotubes are synthesized. Chapter 3 presents the literature review of the nanotubes produced by DC arc-discharge method. Chapter 4 provides the problem statement and the motivation behind the study. Chapter 5 deals with the experimental setup used in the synthesis of carbon nanotube. Chapter 6 presents the results, Chapter 7 discussion, and Chapter 8 contains the conclusions and suggested future work.

CHAPTER 2

SYNTHESIS OF CARBON NANOTUBES

2.1 Introduction

Since the discovery of nanotubes in the DC arc evaporation apparatus [2, 3, 4], extensive research has been conducted for synthesizing both multiwalled and singlewalled carbon nanotubes. There are four most promising methods for synthesizing nanotubes, namely, arc-discharge, laser ablation, chemical vapor deposition, and high pressure CO disproportionation (HiPco).

2.2 Arc-discharge

The DC arc-discharge method was the first method by which multi-walled and single-walled carbon nanotubes were produced and analyzed [2, 3 and 4]. In the DC arc-discharge method a graphite electrode is evaporated in an inert atmosphere as shown in Figure 2.1. When direct current of 50 to 100 A is applied between two graphite electrodes separated by a gap of ~ 1 mm at low pressure (below 650 torr), a deposit called cathode deposit is formed on the cathode. The deposit consists of a hard outer shell of graphite and a soft inner core consisting of bundles of MWNTs [24]. The average temperature in the inter electrode arc plasma region is on the order of 4000 K [25].

The same apparatus can be used for synthesis of SWNT using an anode which is doped with a transition metal catalyst, such as iron, nickel or cobalt. The SWNTs are found in the form of dark deposit, called, the soot formed around the cathode deposit. The soot consists of bundles of SWNTs entangled with carbon nanoparticles and amorphous carbon. Mass production of SWNTs was achieved by Journet *et al.* [26] using a bimetallic Ni-Y (4.2%:1%) catalyst in a He atmosphere. The temperature in the arc-discharge apparatus is higher that other methods. So the crystallinity and yield per unit time is higher than the other methods [26]. The primary parameters that control the process are inert gas, pressure of the inert gas, anode-cathode distance, current density and nature and ratio of metal catalyst.

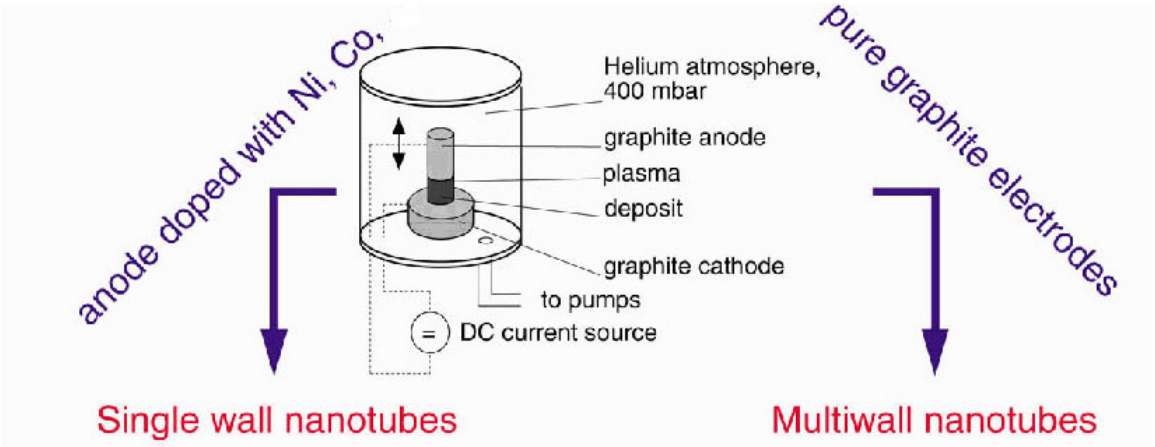

Figure 2.1 Apparatus used for synthesizing carbon nanotubes [27]

2.3 Laser ablation

The laser ablation process was developed in 1995 by Smalley's research group at Rice University [27]. A pulsed or continues laser is used to vaporize the graphite-metal target which is placed in a furnace at 1200^0 C as shown in Fig 2.2. The pressure in the chamber is typically 500 torr and argon flow is maintained to condense the carbon-catalyst vapor on the

collector. When the laser beam strikes the composite graphite target a very hot plume is formed which expands and cools rapidly thus forming SWNTs. The SWNTs are in the form of ropes bundled together by van der Waals forces. The diameter of the SWNTs ranges from 1-2 nm. MWNTs are produced when pure graphite target is used.

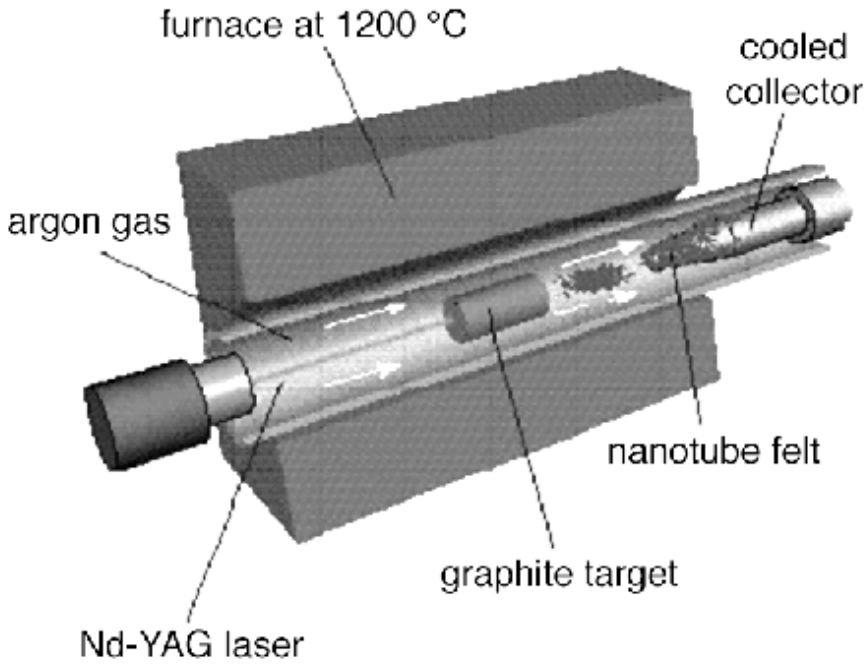

Figure 2.2 Laser ablation setup used for CNT synthesis [28]

The diameter of SWNTs can be controlled by controlling the furnace temperature, inert gas flow rates, and metal catalyst. Increasing the furnace temperature increases the diameter of the SWNTs, use of Ni-Y catalyst increases the diameter and use of Rh-Pd catalyst decreases the diameter of the SWNTs. The inert gas flow rate controls the diameter distribution. High quality SWNTs with minimal defects are produced using the laser ablation process. Highly crystalline SWNTs are produced in high power laser ablation due to homogenous annealing [27].

2.4 Chemical vapor deposition (CVD)

The first CVD method was developed by Endo *et al*. [29] at Shinshu University in Japan. In the CVD technique carbon source is in the gas phase (methane, acetylene, carbon monoxide). Thermal energy is used to ionize the carbon source to produce the reactive carbon ions. The carbon nanotubes are grown on the substrate (Si or SiO_2 or glass) which is coated with metal catalyst (iron, cobalt or nickel) particles. The temperature for the synthesis of CNTs is in the range of 650 to 1200^0 C and the pressure is below 30 torr. The use of hydrogen facilitates to reduce the amorphous carbon due to etching of by atomic hydrogen. The most commonly used CVD techniques are plasma enhanced CVD, thermal chemical CVD, alcohol catalytic CVD and laser assisted thermal CVD. The schematic of microwave plasma enhanced CVD apparatus is shown in Figure 2.3.

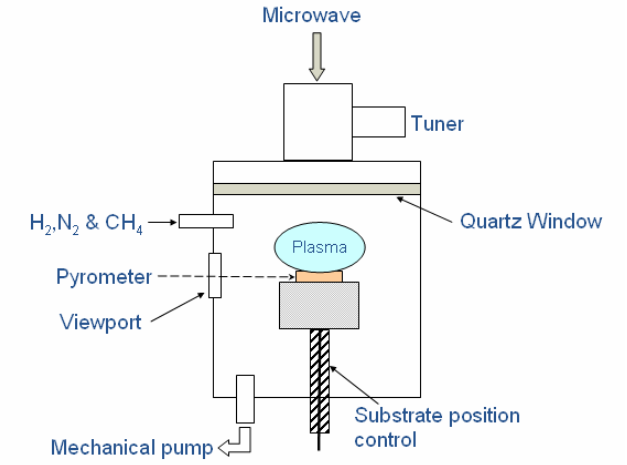

Figure 2.3 Microwave plasma enhanced CVD technique [30]

The CVD technique is ideal for growing aligned and patterned tubes. Due to the low temperature of synthesis, the CNTs are not defect free, diameter distribution is in the range of 50 nm. Aligned and patterned tubes synthesized by CVD technique can find extensive use in

nanoelectronics and microscopy. Recently aligned SWNTs up to 2.5 mm in height have been reported by adding about 100 ppm water during synthesis [31].

2.5 High pressure CO disproportionation (HiPCO) process

In 1999 Smalley and his team at Rice University reported the synthesis of SWNTs in a gas-phase catalytic process [32, 33]. The catalyst particles are formed *in situ* by the thermal decomposition of iron pentacarbonyl $Fe(CO)_5$. Continuous flow of carbon monoxide, at a pressure of 1-10 atm and temperature between 800 and 1200^0 C is used. The SWNT yield and diameter distribution is controlled by varying the pressure and temperature, SWNTs as small as 0.7 nm in diameter have been generated. The products of $Fe(CO)_5$ thermal decomposition reacts to form iron clusters in the gas phase. These clusters act as nucleation sites for the growth of SWNTs. Solid carbon is produced by the disproportionation of CO which occurs catalytically on the surface of the iron particles.

$$CO + CO \rightarrow C\ (s) + CO_2 \text{ (Boudouard reaction)}$$

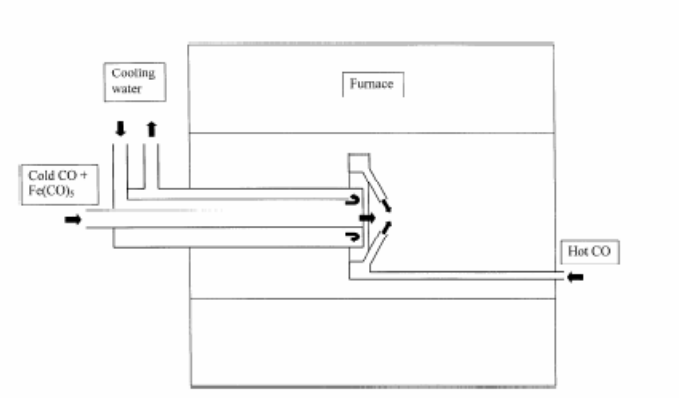

Figure 2.4 Schematic of high pressure carbon monoxide method (HiPco method) [33]

The apparatus used for the HiPco method is shown in Fig. 2.4. The temperature in the tube section inside the furnace is maintained between 800 and 1200^0 C, while the tube

entrance and exit was maintained at room temperature. Flow of CO/$Fe(CO)_5$ mixtures through the reactor results in the deposition of SWNTs on the walls of the quartz tube outside the furnace. Carbon nanotubes can also be grown by other methods such as CoMoCat process [34] and flame synthesis technique [35].

CHAPTER 3

LITERATURE REVIEW

3.1 Introduction

The history of carbon nanotube can be attributed to the discovery of carbon fibers, graphite whiskers, and fullerene. This chapter gives an introduction to the carbon fibers, carbon whiskers, fullerene and deals extensively with multi-walled and single-walled carbon nanotubes.

3.1.1 Carbon fibers

Carbon fibers are macroscopic structures that are analogous to carbon nanotubes [36]. Carbon fibers have high modulus of elasticity, low density, low thermal coefficient of expansion, chemical stability with strong acids and low electrical resistivity. All these properties make them ideal candidates for composite materials. Carbon fibers have been of interest from the second half of the 19^{th} century. In 1879, Edison discovered that a carbon filament in an oxygen-free atmosphere glows and did not burn up for 40 hours [37]. In 1889, Hughes and Chambers [38] patented a process for producing carbon fibers by pyrolyzing marsh gas in an iron crucible. The growth mechanism and the role played by the metal catalyst were not clearly understood till the development of electron microscopy in the 1950's [39]. Active research in the field of carbon fibers was conducted in the 1950's to develop light weight composite materials for the aircraft industry.

3.1.2 Carbon whiskers

Graphite whiskers were discovered by Roger Bacon in 1959 [40]. Graphite whisker is a graphitic material formed by rolling a graphene sheet into a scroll as shown in Fig. 3.1 b. Graphite whiskers are formed in D.C. arc-discharge between carbon electrodes by using current of 70-76 A and 75-80 volts. The discharge is carried out in an inert atmosphere of argon at a pressure of 92 atmospheres. The graphite whiskers are up to 3 cm long and 1-5μm in diameter [40]. The whiskers exhibit great crystalline perfection, and very high elastic modulus along the fiber axis. The growth of graphite whiskers is similar to the growth of MWNTs except that the whiskers are grown at high pressure.

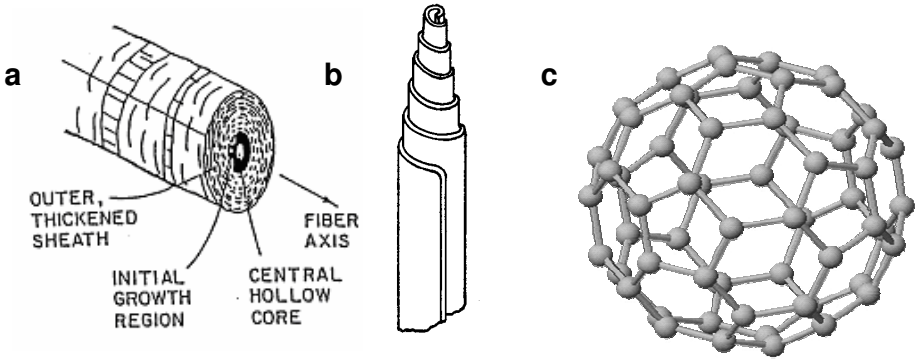

Figure 3.1 Sketch illustrating the morphology of a) carbon fiber b) Graphite whisker and c) C_{60} Buckminsterfullerene [38, 40, 41].

3.1.3 Fullerene

In 1985, R. E. Smalley, R. F. Curl, J. R. Heath, and S. O'Brien at Rice University, and H. W. Kroto of the University of Sussex in England discovered fullerenes [1]. They observed a hollow truncated icosahedron, similar in shape to a soccer ball consisting of 60 carbon atoms, C_{60} tends to form spontaneously when carbon vapor condenses. In 1990,

Wolfgang Kratscmer of Max Plank Institute at Heidelberg, Donald Huffman and co-workers of the University of Arizona used a carbon arc to vaporize graphite in a helium atmosphere. The soot collected on the walls of the chamber contained macroscopic amounts of solid C_{60}. This led to large scale production of fullerene and further stimulated interest in the allotropes of carbon [41].

Two groups of theoretical scientists one at the Naval Research Laboratory, in Washington, D.C [42] and the other at the Massachusetts Institute of Technology [43] submitted papers on the electronic properties of fullerene tubes just few weeks before Iijima's paper was published in Nature. Iijima [2] had reported on the existence of helical microtubules of graphitic carbon which was later called multi-walled carbon nanotubes. This led to the intense research in the field of carbon nanotubes.

3.2 Apparatus

The apparatus used for the synthesis of nanotubes can be classified based on the position of the anode and cathode, namely, horizontal and vertical. Nanotubes were first observed in the vertical arc-discharge used to generate fullerene (also called as Krätschmer-Huffman method [41]). The apparatus is connected to the gas supply lines for the synthesis of nanotubes; Helium, argon, hydrogen or nitrogen or its mixtures are used as the working gases. A vacuum pump is connected so that chamber can be evacuated completely to remove the oxygen present and to maintain the gas at a constant pressure during the arc-discharge.

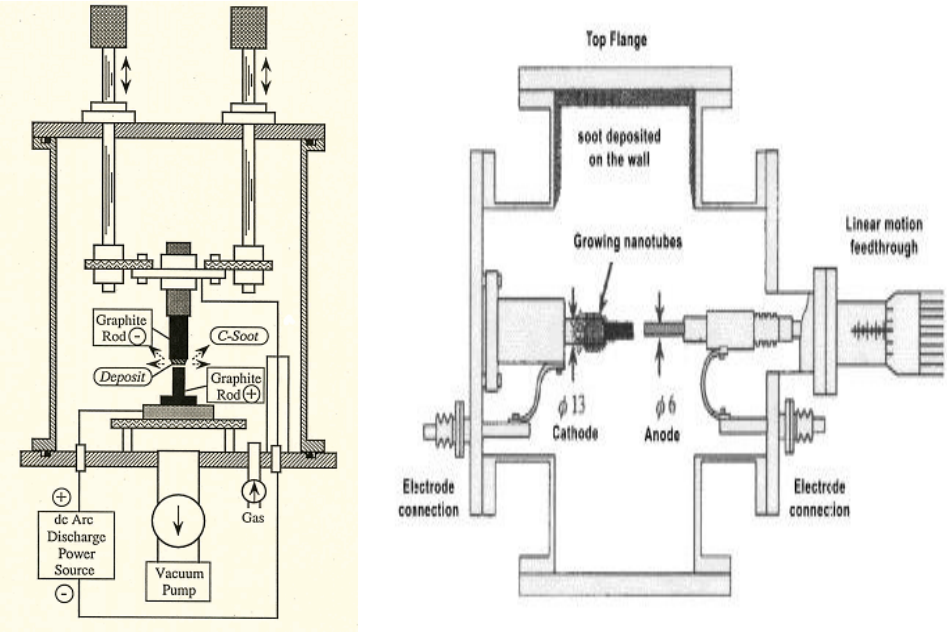

Figure 3.2 Schematic of arc-discharge setup in the vertical [2] and horizontal configurations [44].

The anode and cathode is made of pure graphite rods in generating MWNTs and a metal filled graphite rod is used as anode for SWNTs. The anode and cathode is connected to a welding machine to supply direct current at constant voltage. Direct current is used as the energy source to vaporize the anode and deposit it on the cathode. In both the vertical and horizontal arrangements, the anode is usually moved towards the cathode using a feed mechanism such that the distance between the anode and the cathode is held constant to maintain a stable arc [44]. Arc stability is essential to obtain good yield of nanotubes. A number of modifications have been made to the horizontal and vertical arrangements to increase yield and to optimize the process parameters for producing both MWNTs and SWNTs.

3.2.1 Automated system

Bera *et al.* [45] have developed an optoelectronically automated system for the synthesis of nanotubes in a liquid environment. The optoelectronic system maintains the anode-cathode distance constant allowing a continuous generation of nanotubes. The system works on a feed back loop, consisting of electrode gap detector and an analog electronic unit as a controller as shown in Figure 3.3

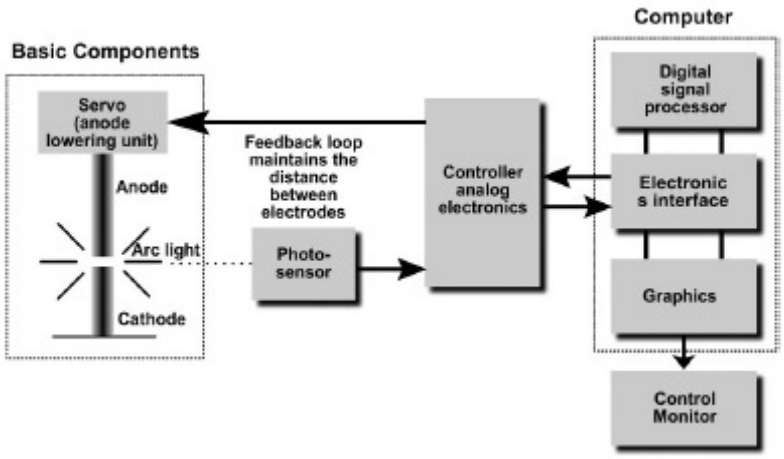

Figure 3.3 Block diagram of the optoelectronic feedback control system [45]

The system has two main advantages namely, (i) arc stability is maintained (since the anode-cathode distance is continuously monitored to adjust the position of the anode) thus increasing the yield, (ii) the system does not need human intervention thus the system can be operated even with gasses such as hydrogen safely.

3.2.2 Rotating cathode DC arc method

Yumura *et al.* [46] developed the rotating cathode DC arc method with the aim of decreasing the deposition time. The cathode deposit is removed from the cathode surface

within one turn of the cathode, as shown in Figure 3.4a. Thus the cathode surface is always clean before entering the discharge zone, thus maintaining a constant anode-cathode distance. The main advantage of this system is that it can be used for continuous production of the MWNTs.

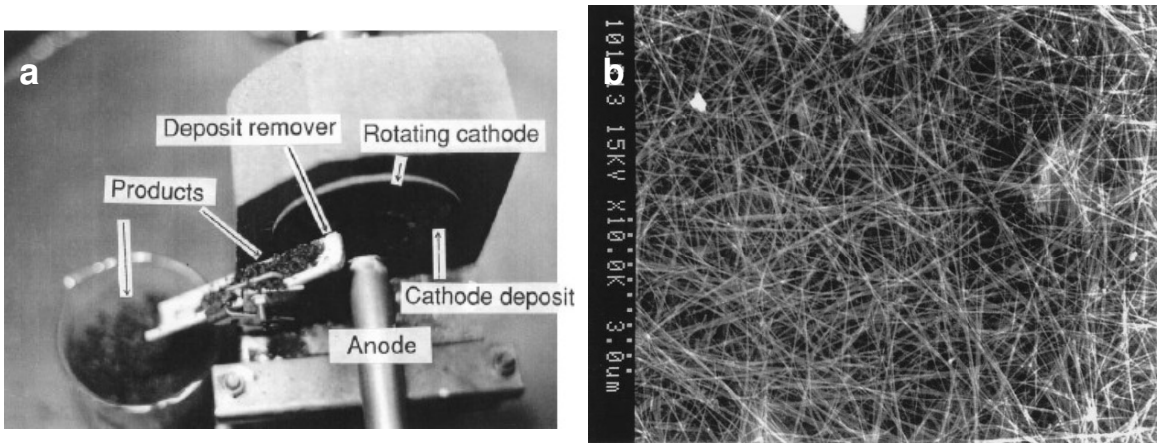

Figure 3.4 a) Rotating cathode, b) SEM image of purified MWNT using rotating cathode method [46].

3.2.3 Simplified arc-method

Ishigami *et al*. [47] developed a simplified arc-method that allows the continuous synthesis of MWNTs. A graphite anode is dipped into an open container of liquid nitrogen with a short graphitic cathode, as shown in Figure 3.5a. The electrodes are brought into contact to strike an arc, and the distance between anode and cathode is maintained constant. Nanotubes formed at the arc plasma region are collected in the bottom of the funnel shaped container which is opened periodically to flush the nanotubes. The level of liquid nitrogen is maintained constant using a sensor and a fill pipe. Nanotube rich material up to 44 mg per minute is synthesized using a 60 A stable arc current. The system eliminates components such as pumps, gas handling system, and seals. The liquid nitrogen maintains the necessary

oxygen free inert atmosphere and also provides the necessary thermal gradient. The surface of the nanotubes is pure without any trace of nitrogen.

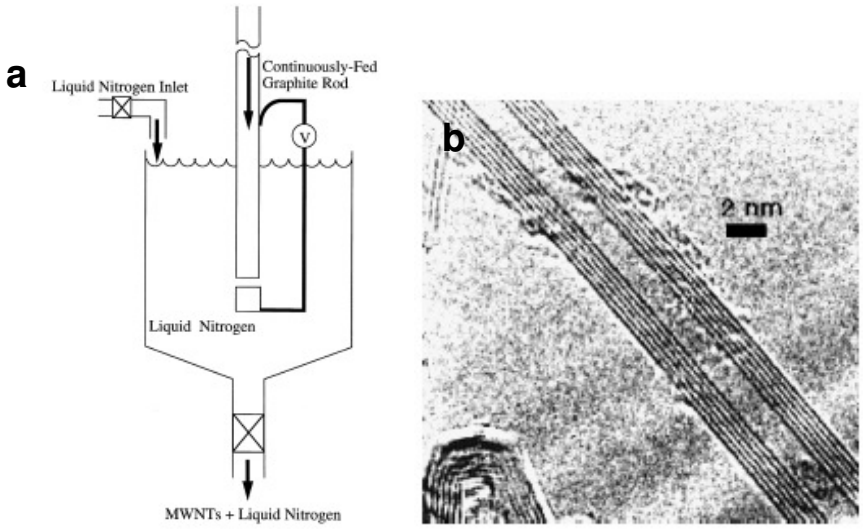

Figure 3.5 a) Schematic of continuous production chamber for MWNTs, b) HRTEM image of MWNTs [47].

3.2.4 Arc plasma jet method

Ando *et al.* [48] developed the arc plasma jet method for the mass production of SWNTs. The quantity of the nanotubes is increased by decreasing the cathode deposit. In a chamber of 300 mm in diameter and 400 mm height, 6 mm diameter doped graphite (Ni-4%, Y-1%, C- 95%) rod is used as anode and 6 mm pure graphite rod is used as cathode. The cathode is set at an angle of 30^0 to the anode to reduce the cathode deposit, as shown in Figure 3.6a.

When the anode is evaporated in a helium atmosphere by the DC current, carbon-arc plasma jet is formed in the direction of the cathode axis. When the DC current is 60 A and helium gas pressure is 500 torr, the length of arc plasma jet reaches 30 mm. In 3 mins three types of deposit are formed: 1) large quantity of cotton-like soot is formed on the chamber

walls; 2) small cathode deposit on the cathode; 3) small carbon aggregation-like the tail of a comet on the tip of the cathode. Most SWNTs are found in the cotton-like soot formed on the chamber walls.

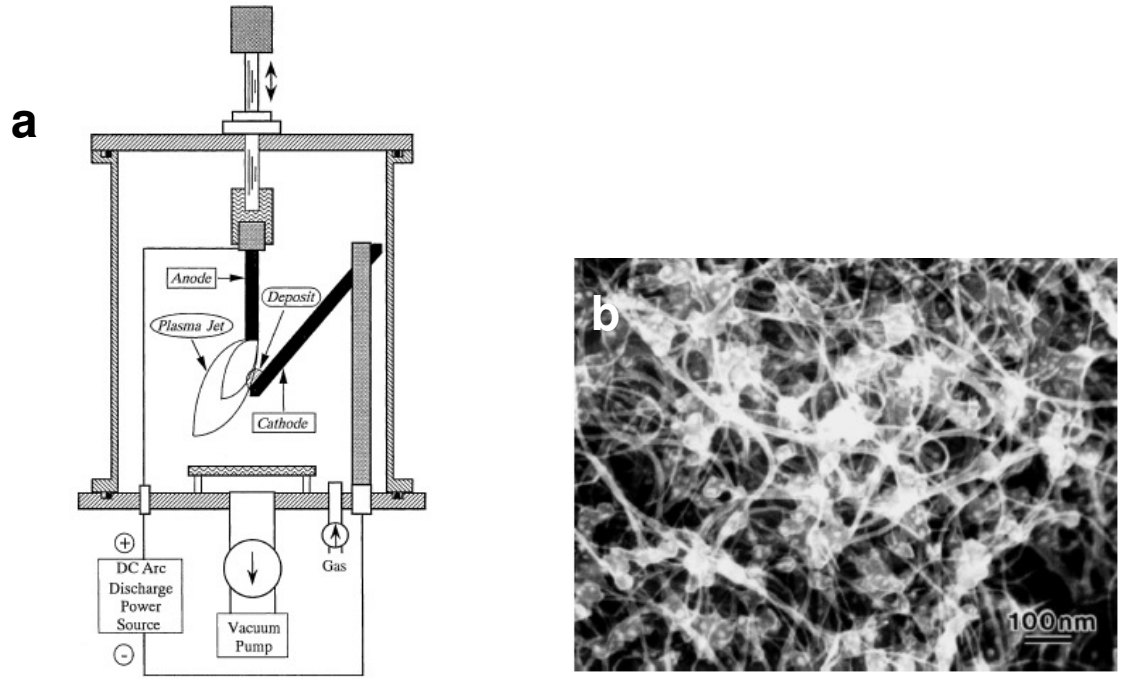

Figure 3.6 a) Schematic diagram of arc plasma jet apparatus, b) SEM micrograph of cotton-like soot [48].

The arc-plasma jet effectively reduces the formation of the cathode deposit and increases the yield of SWNTs. Cotton-like soot production is increased up to 1.24 g/min for 1.48 g/min of anode evaporated. The cotton-like soot contained up to 50% SWNTs with in the range diameter 1.34 to 1.53 nm.

3.2.5 Bowl shaped cathode

Huang *et al.* [49] modified the cathode design to increase the yield by using a bowl shaped graphite cathode as shown in Figure 3.7. The cathode is 20 cm diameter, 12 cm deep (side sloping at 60^0) with holes in the sides for the catalyst. The catalysts consist of Co 6%,

Ni 6%, Fe 3%, Ce 3%, mixed with 0.5% S as SWNT promoter and 0.5% Sn as nanowelding element. The presence of Sn helps in the formation of super bundles of SWNTs by welding together small bundles of SWNTs. This design of the cathode not only acts as a crucible but also provides substrate for growing SWNTs. The cathode directs the carbon species to be directed upwards and also allows the catalyst to be supplied at a more controlled rate. A mesh plate is placed on the top of the cathode to collect super bundles of SWNTs that grow. The anode is a square (15 X 15 mm^2) graphite rod doped evenly with 1.5% Ni and 1.5% Co. At a static helium pressure of 680 torr with operating current of 180 A, SWNTs bundles are produced.

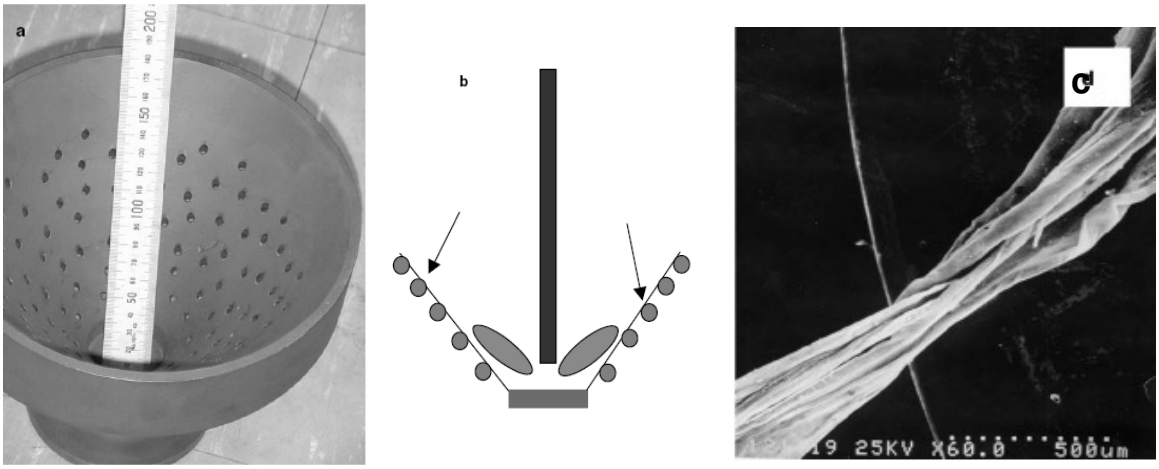

Figure 3.7 a) Bowl shaped cathode, b) Schematic of the electrodes with the distribution of catalyst marked by arrow, c) SWNT super bundle [49].

In 30 mins numerous very long and aligned carbon ropes are formed that fills the space between the surface of the cathode and mesh plate at the top. The ropes have a diameter of up to 100 μm with lengths up to 20 cm. The ropes consist of smaller bundles of nanotubes with diameter in the range 1.5 – 3.0 nm, as shown in Figure 3.7c. The main advantage of this design is that the metal catalyst in the carbon ropes is isolated from the

carbon species easily, with some of them sintered thus larger than the conventional arc-discharge. Thus, it is easy to remove the metal impurities and further purify the SWNTs without causing any damage to the nanotubes. The process is very sensitive to the process parameters like pressure, current and ambient gas. Maximum yield of 1.1 g/ h is achieved under optimal conditions.

3.3 Multi-walled carbon nanotube

The formation of MWNTs was first reported by Iijima at NEC, Japan in 1991 [2]. MWNTs with diameter ranging from 4 to 30 nm and up to 1µm long were observed on the negative end of the carbon electrode, the smallest tube was a double walled carbon nanotube. The D.C arc-discharge apparatus used here was similar to the apparatus used for mass production of C_{60} [41]. The D.C arc-discharge was carried out in an argon atmosphere at 100 torr.

3.3.1 Large scale synthesis of MWNTs

A major breakthrough came in 1992, when Ebbesen and Ajayan, of NEC, Japan reported large scale synthesis of nanotubes [24]. They studied the effects of pressure and buffer gas on the yield of nanotubes. They observed the yield of nanotubes to increase with increase in helium gas pressure. At 500 torr, the total yield of nanotubes as a proportion of the evaporated material was found to be optimal. The anode was 6 mm and, the cathode was 9 mm in diameter and a current of 100 A was used. They observed a cylindrical rod shaped deposit on the cathode as shown in Figure 3.8a. The deposit consist of a two distinct regions, an inner black core made of soft fibrous material surrounded by an outer grey metallic hard

shell as shown in Figure 3.8c. They reported that the black core material is made of only nanotubes and nanoparticles, as shown in Figure 3.8e. The outer grey shell does not contain nanotubes. The nanotubes in the core region were observed to be parallel to the direction of the current and the yield of fibrous core increased with plasma stability.

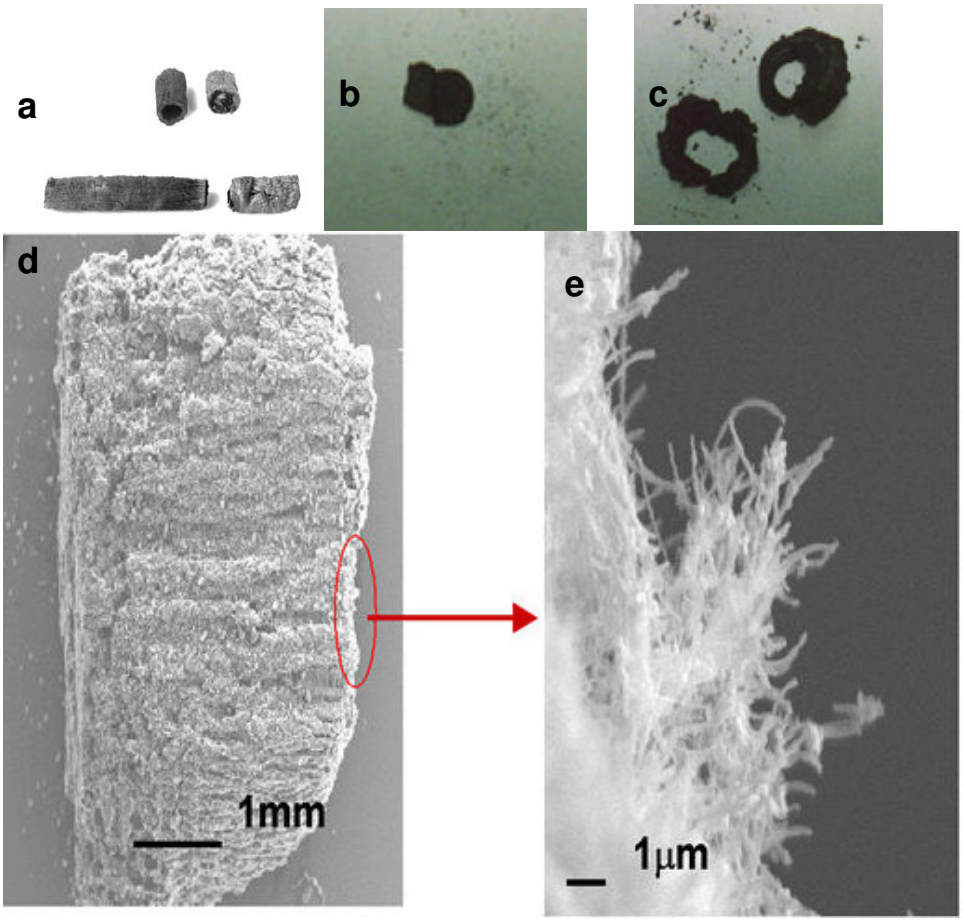

Figure 3.8 a) Cathode deposit, b) Core, c) Shell, d) and e) SEM image of the core material [111].

3.3.2 Effect of buffer gas

A) Helium

Seraphin *et al*. [50] studied the effect of process variables such as current density, voltage, current, and pressure on the yield of nanotubes. They observed that low pressure

(200 torr) and low current density produces only a few nanotubes along with graphitic particles. Any further increase in current density to 470 A/cm^2 decreases the nanotube formation and further increase in current density completely eliminates the formation of nanotubes and only carbon crumbs are produced.

Table 3.1, Effect of helium pressure on MWNTs yield [50].

Helium pressure (Torr)	Current density (A/cm2)	Voltage (Volts)	Current (A)	Tube length (μm)	Diameter (nm)	Comments
200	350	24	110	0.1-0.5	5 to 40	Few tubes
200	470	31	150	0.1-1.2	10 to 30	Very few tubes
200	690	24	220	No tubes	No Tubes	Only crump's
550	190	24	60	0.7- 6.0	15 to 60	Highest yield
550	220	27	70	0.4-3	10 to 30	most tubes > 1μm
550	240	34	75	0.2-1.1	10 to 30	most tubes 0.5μm
550	315	34	100	0.1-1.1	10 to 30	most tubes 0.5μm
550	380	33	30	0.1-1.5	5 to 20	Low yield
550	630	24	200	0.1-1.2	10 to 40	Low yield

Table3.1 shows effect of current density at a helium pressure of 550 torr. At a low current density of 190 A/cm^2, the yield is highest and the tubes are 2 to 6 μm long. By increasing the current density to 220 A/cm^2, the length of the tubes decreases to 1μm. Further increase in current density to 240 A/cm^2 leads to tubes of 0.5 μm. Any further increase in current density does not change the morphology of the nanotubes but decreases the yield of the nanotubes. Thus, the optimum conditions to produce long tubes were found to be at a helium pressure of 550 torr and a current density of 190 A/cm^2 at 24 Volts (as seen in Table 3.1 for details). Zhangyz *et al*. [51] also reported the increase in the formation of nanotubes with increase in helium pressure. At 80 torr the ratio between nanotubes to nanoparticles is

8%. The ratio of nanotubes to nanoparticles increases from 15% at 230 torr, to 20% at 400 torr and reaches 30% at 550 torr of helium as shown in Table 3.2.

Table 3.2, Effect of helium pressure on cathode deposit [51].

He pressure (torr)	80	150	230	300	450	600	700
mg/min	126	70	50	30	31	30	28

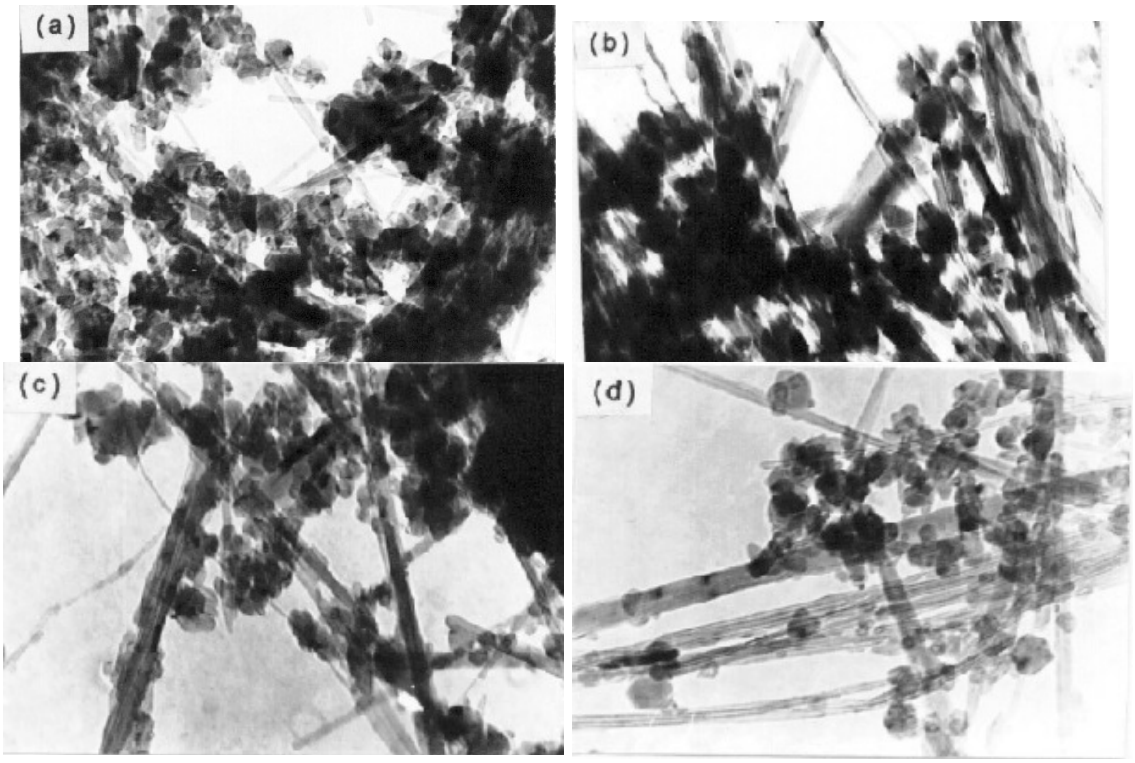

Figure 3.9 Effect of helium gas pressure a) 80 torr, b) 230 torr, c) 400 torr, d) 550 torr [51].

Synthesis of MWNT using helium as a buffer gas produces considerable amount of graphitic particles and carbon nanoparticles which are bonded to the tubes. So extensive purification procedure has to be followed to remove the nanoparticles. In order to improve purity arc-discharge has been carried out in hydrogen, nitrogen, argon or water to produce tubes with higher quality.

B) Hydrogen gas

In diamond coatings atomic hydrogen selectively etches graphite and stabilizes the sp^3 bonds thus facilitating the formation of diamond film. In the same way, atomic hydrogen in the hydrogen-arc can selectively etch amorphous carbon on the nanotubes by the formation of hydrocarbons. Atomic hydrogen also prevents the ends of the tubes from closing by forming dangling carbon bonds growing at the edge of the nanotube. The formation of open ended tubes makes them extremely useful for formation of metal filled nanotubes or nanowires. Hydrogen has very high thermal conductivity (1684 W/m K). Hence it is a more efficient quencher for carbon vapors which condense and form nanotubes. Since hydrogen is a reactive gas, it forms strong C-H covalent bonds which lowers the energy of the system and prevents the ends of the tubes from closing. The nanotube samples obtained with hydrogen is purer compared to the nanotubes obtained with helium [52].

Carbon nanotubes synthesized in a hydrogen-arc discharge has been studied extensively. For example Wang *et al.* [52] studied the effect of hydrogen pressure during arc-discharge. At a hydrogen pressure of 50 torr many clean and long tubes are produced where as no nanotubes are produced with helium at 50 torr. At 100 torr, the yield of nanotubes is comparable to that at 500 torr of helium gas. At 300 torr or higher, the number of open ended tubes increases. It has been reported that nanotubes produced using hydrogen are purer than that with helium gas, as shown in Fig 3.11.

Hahn *et al*. [53] used a 10 mm diameter cathode and a 6 mm diameter anode, at 60 A current with a constant flow of hydrogen. Maximum yield of 150 mg of black core material in 10 mins was obtained at 100 torr of hydrogen at a continuous flow rate of 200 sccm. A

cylindrical deposit as shown in Figure 3.10 is obtained. The deposit is made of hard shell of graphite sheets and a core material with nanotubes. The black core material consists of needle-like material which is ~50μm in diameter and a few mm in length. The needle-like material is hardly conglomerated by MWNTs and other impurities.

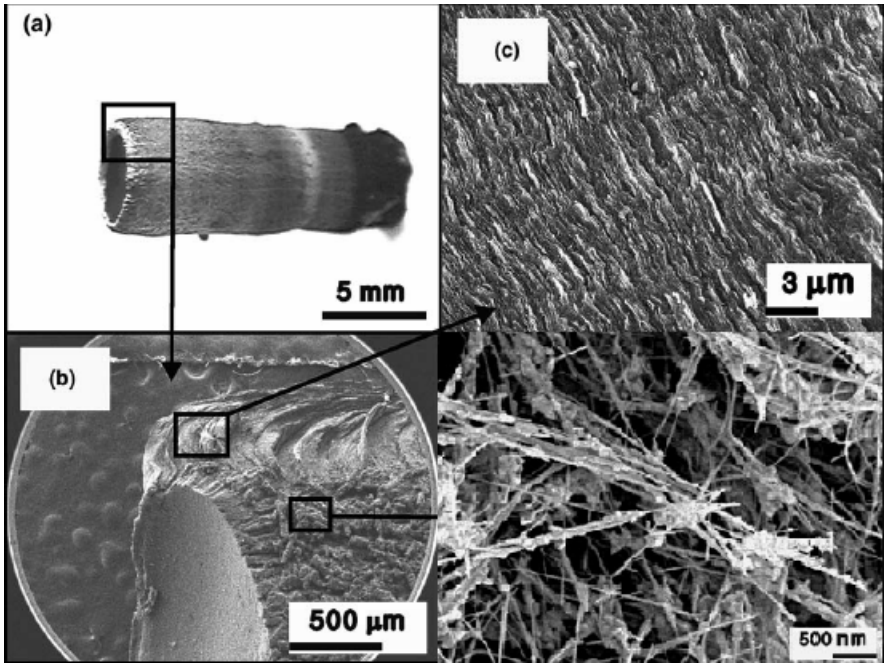

Figure 3.10 SEM images of (a) a cylindrical cathode deposit produced by hydrogen arc-discharge, (b) the cross section of cathode deposit, (c) graphene sheets of hard grey shell, and (d) MWNTs in the needle-like material from the black core material [53].

It is interesting to note that optimum pressure for nanotube formation is lower in the case of hydrogen than helium. This can be attributed to the fact that hydrogen has better quenching properties due to its high thermal conductivity. The surfaces of the nanotubes are very clean and covered with very little amorphous carbons or carbon nano particles. The nanotubes can be further purified by thermal oxidation in air. In order to purify the MWNTs, the sample is placed on a quartz specimen holder and heated using infrared radiation heating system as shown in Fig. 3.11a [54]. After 30 minute irradiation at 500^0C in air, extremely clean nanotubes are obtained as shown in Fig. 3.11c.

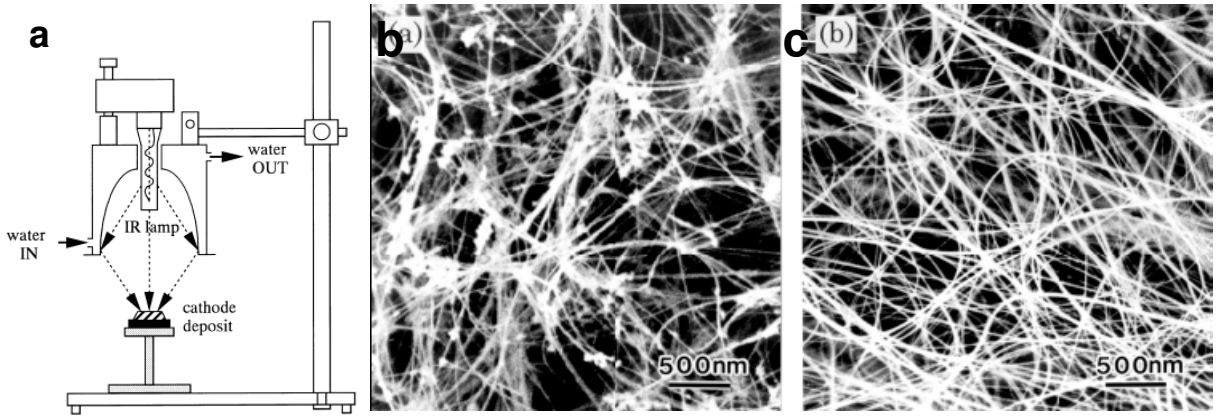

Figure 3.11 a) Purification of MWNTs [54], b) As-produced MWNTs, c) MWNTs after purification [109].

Even though the use of hydrogen in arc-discharge helps to synthesize MWNTs with higher purity, the use of hydrogen makes the system extremely dangerous. So, special safety precautions have to be taken to conduct the experiments.

3.3.3 Liquid environment

The role of buffer gas in arc-discharge is to provide an inert atmosphere for the reaction, stabilize the electric arc, and quench the sublimated carbon atoms so that they form nanotubes on the cathode. The effect of liquid environment has been studied using water, deionized water, polycyclic aromatic hydrocarbons, and liquid nitrogen. The role of liquid is to provide an oxygen free environment. Liquid environments also facilitates in cooling the cathode thus eliminating the need for a cooling circuit. Liquid environment helps to build extremely simple apparatus for the synthesis of nanotubes, thus eliminating the need of vacuum pump and other complex vacuum systems.

A) Liquid nitrogen

Jung *et al.* [55] synthesized MWNTs using a simple apparatus as shown in Figure 3.12. Use of liquid nitrogen to cool the surface of the cathode. The anode and cathode are made of graphite which are 8 and 10 mm in diameter, respectively. The electrodes are immersed in a Dewar flask filled with liquid nitrogen as shown. The gap between the anode and the cathode is adjusted using a control screw. Maximum yield of MWNTs deposit was obtained when the anode-cathode distance was less than 1 mm. The arc current was 80 A to vaporize the anode and deposit it on the cathode. The deposit consists of MWNTs along with round particles and amorphous carbon as shown in Fig. 3.12. The diameter of the tubes are in the range of 20-50 nm and length up to a few micrometers.

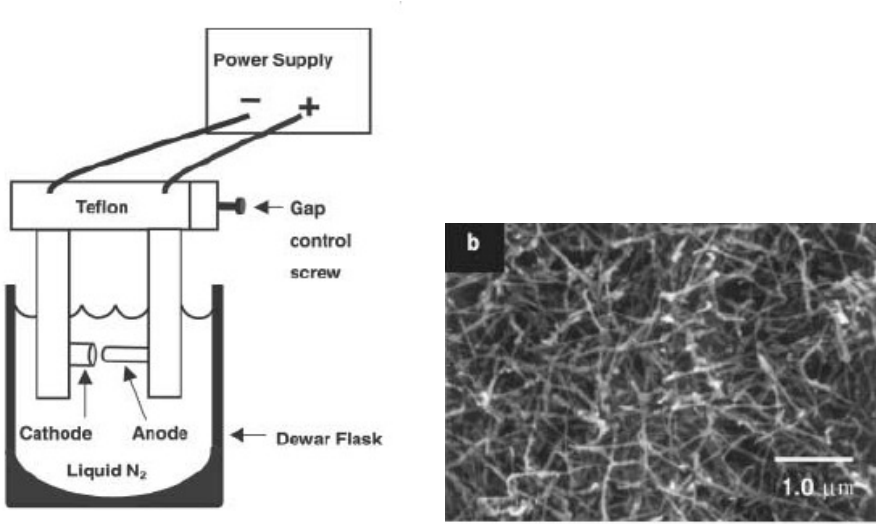

Figure 3.12 a) Apparatus for MWNTs synthesis b) MWNTs formed in liquid nitrogen [55]

Antisari *et al.* [56] synthesized nanotubes using a simple system in liquid nitrogen. A spectroscopically pure 6 mm diameter graphite rod was used as anode and the cathode was made of 15 mm diameter graphite block. A carbonaceous cylinder up to several mm long was

produced with 40-60 A current in a few mins. The deposit formed is reported to be extremely heterogeneous with nanotubes and nanoparticles.

The outer surface layer of the deposit consists of globular particles and no nanotubes. This is attributed to the fact that the temperature in the outer shell region is lower due to direct contact with liquid nitrogen and the temperature is too low for the formation of nanotubes. On the top surface of the cathode deposit is a less dense material with nanotubes nucleating at the underlying surface, as shown in Fig. 3.13.

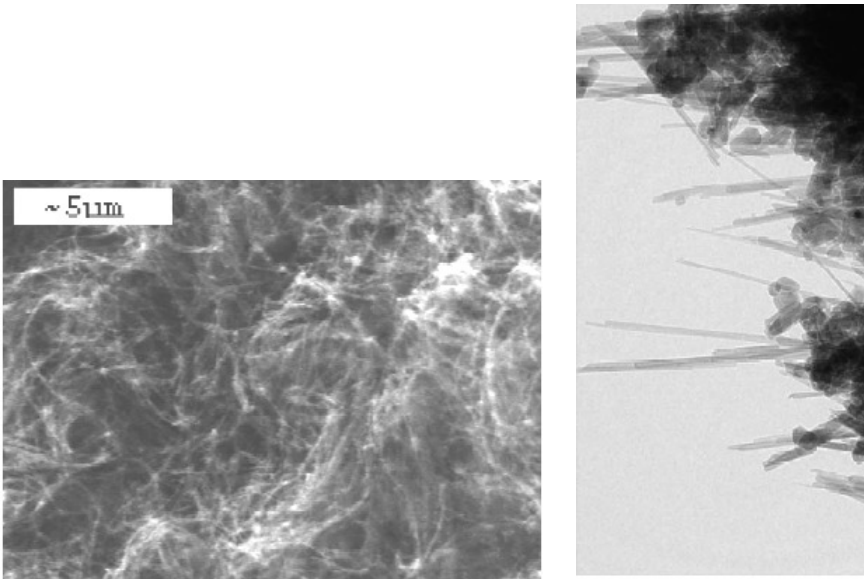

Figure 3.13 a) SEM image of MWNTs observed on the cathode surface b) TEM image of MWNTs [56].

Analysis of the inner core region of the deposit showed that nanotubes are highly degraded, (as shown in Fig. 3.13), suggesting that the tubes are destroyed during the arc-discharge process. This is attributed to the fact that very low liquid nitrogen temperatures leads to fast and violent evaporation. It does not allow direct heat exchange between the growing materials, leading to less efficient cooling. Although MWNTs can be synthesized in liquid nitrogen environment, the yield of nanotubes is very less due to degradation of the

nanotubes in the arc-discharge process. The efficiency can be increased by removing the nanotubes as soon as they are formed.

B) Deionized water

Sano *et al.* [57] studied the effect of arc-discharge in de-ionized water using a simple apparatus as shown in Figure 3.14. The arc-discharge was carried out in de-ionized water between two carbon electrodes submerged in 2.5 l of DI water in a Pyrex beaker. The arc was initiated between a 6 mm anode and a 12 mm cathode (both 99.9% pure graphite) submerged under 3 cm in DI water. A stable arc was generated with 30 A current when the anode-cathode distance was 1 mm. Anode was consumed at a rate of 117 mg/min during discharge.

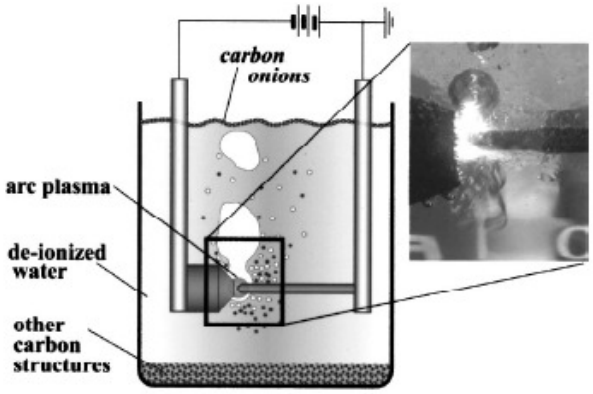

Figure 3.14 Schematic of the apparatus used for arc-discharge in water and a digital image of the discharge [57].

Floating particles were found on the surface consisting of many nested onion-like particles of 30-35 nm in diameter in agglomerated form along with nested particles, similar to MWNTs. The onion-like particles consist of well crystallized, well defined concentric shells, as shown in Fig. 3.15. They found that carbon onions have an extremely high surface area of 984.3 m^2/g, which is three times higher than the value of SWNTs.

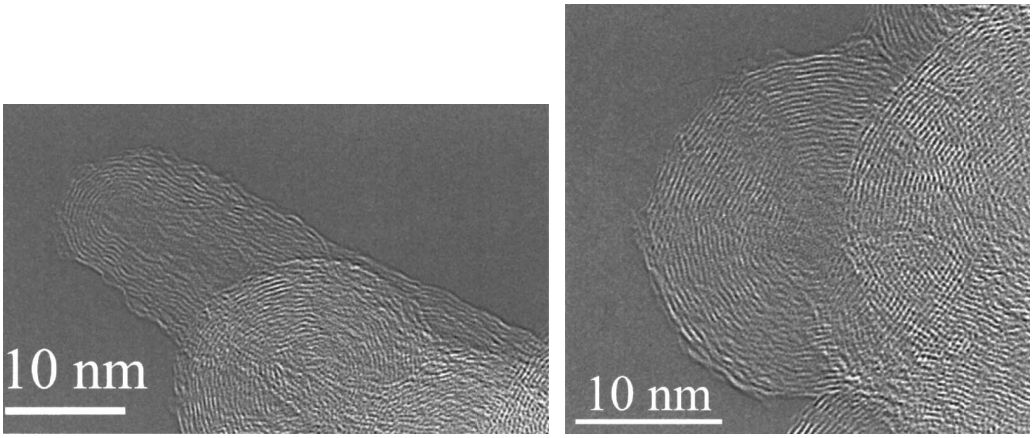

Figure 3.15 a) HRTEM image of elongated nano particles. b) Carbon nano onions [57].

Rosolen *et al*. [58] found that MWNTs are formed by arc-water method when deionized water is used. The particles deposited at the bottom of the reactor contained graphitic particles with diameter between 10 to 600 nm along with MWNTs with 20-30 nm in diameter and a few micrometer in length but the amount of nanotubes is very low, as shown in Fig 3.16.

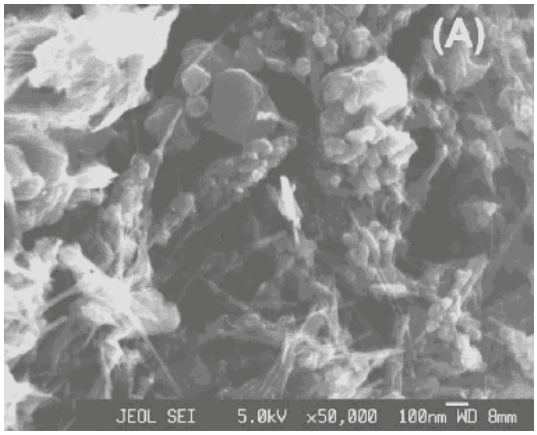

Fig. 3.16 SEM image of as-synthesized material by arc-water method in pure deionized water [58].

Rosolen *et al.* [58] also synthesized large amounts of MWNTs along with SWNTs by conducting the arc-discharge in H_3VO_4 aqueous solution from pure graphite rods (Fig. 3.17). The experiments were conducted at 60 A current by maintaining the distance between anode

and cathode of 1mm. Vanadium compound was chosen for the study based on their properties of promoting the formation of more ordered structure in the heat treatment of coke.

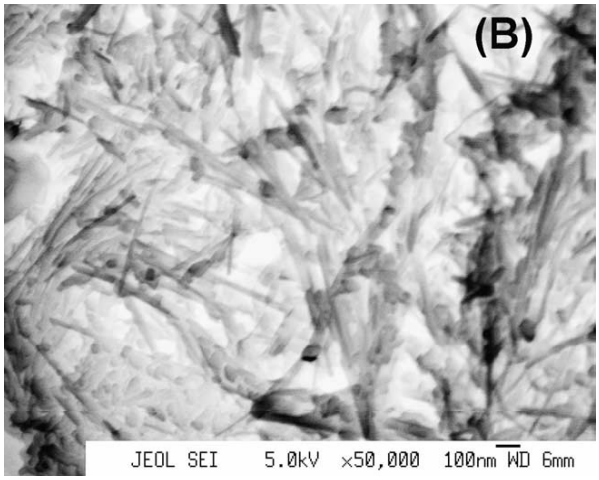

Figure 3.17 SEM image of MWNTs in H_3VO_4 aqueous solution [58].

C) Water

Antisari *et al*. [56] was successful in synthesizing large quantities of MWNTs in water submerged arc-method, as shown in Figure 3.18. MWNTs are formed on the cathode deposit by using deionized water. The cathode deposit consists of highly pure nanotubes. The purity of the nanotube is attributed to the effect of hydrogen resulting from the thermal decomposition of water into hydrogen and carbon monoxide gas. The formation of hydrogen during arc-discharge also leads to the formation of open ended tubes as explained in the previous section. Zhu *et al*. [59] have been successful in synthesizing MWNT containing material up to 7 mg/min by using aqueous solution of $NiSO_4$, $CoSO_4$ or $FeSO_4$ at 0.2 M concentration. The purity of the material produced is 20%.

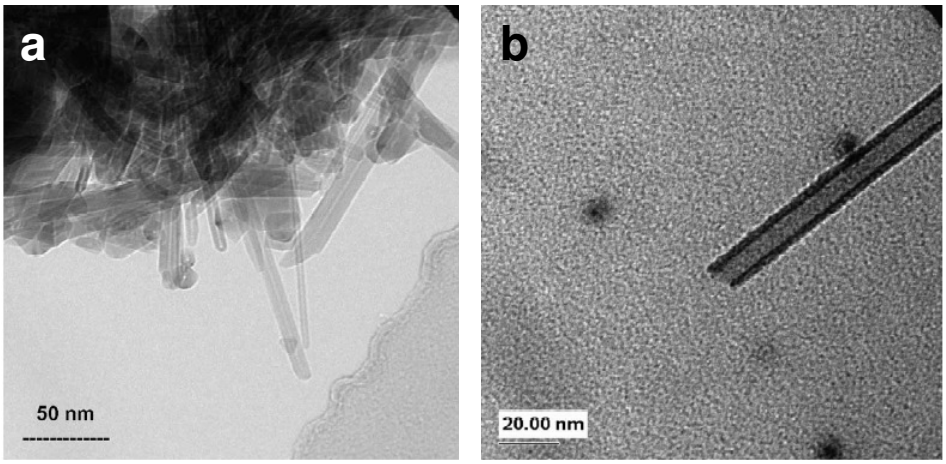

Figure 3.18 a) TEM image of as-grown MWNTs grown in water, b) HRTEM image of open ended tip [56].

Li *et al*. [60] have developed a water protected arc-discharge method which is capable of producing nanotube rich material up to 10 g/hr. Fig 3.19 is a schematic of the apparatus. Two vertical graphite electrodes are connected to 50 A, 30 V D.C power supply. The electrodes are immersed in cool de-ionized water. In the anode, a hole (3 mm diameter and 20 mm deep) is filled with nickel, yttrium (Ni:Y= 5:1), and graphite powder. Another hole (10 mm diameter, 10 mm deep) is drilled on the cathode to collect the product. A graphite cover (60 mm diameter and 100 mm long) is used to provide the chamber for the reaction. Before the reaction, the chamber is full of de-ionized water. Once the arc is struck between the electrodes, carbon monoxide and hydrogen gases are produced which create a gas atmosphere in the chamber during nucleation and tubular growth. TEM analysis shows that the as-prepared samples contain more than 50% MWNTs. The nanotubes are typically 10-20 nm in diameter and 0.5 to 1μm in length.

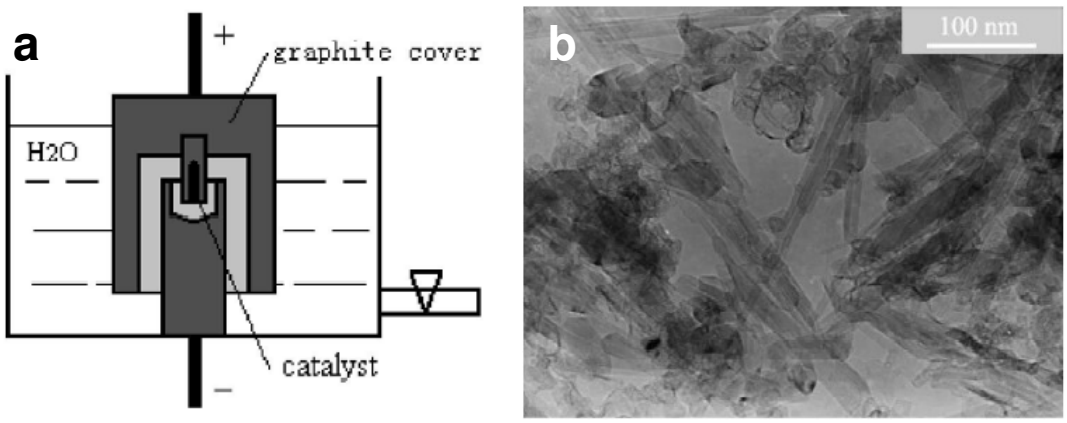

Figure 3.19 a) Schematic of water-protected arc-discharge apparatus, b) TEM image of the as-produced product [60].

The use of water over hydrogen has many advantages. Water has good electrical insulation properties, excellent cooling properties and vaporizes at higher temperatures compared to liquid nitrogen. During the discharge process in water, gases (CO and H_2) are formed from the reaction of carbon with water. The gas mixture further forms a quasi-inert gas chamber for the formation of MWNTs. The tubes grown using arc-water method have cleaner surfaces and higher degree of crystalline structure. Above all, the apparatus for arc-water discharge is very simple and does not require any vacuum chamber or other complex systems.

D) CF_4 gas

Yokomichi *et al.* [61] studied the effect of arc current in 99.999% CF_4 gas using 5 mm diameter carbon rods. SEM images of the cathode deposit showed that the nanotubes grew despite the presence of fluorine atoms which terminate the carbon bonding. TEM analysis showed that the nanotubes have an outer diameter of 20 nm and inner diameter of 5 nm. The diameter of the nanotubes did not change with gas pressure. The length of the nanotubes decreased with increase in arc current and CF_4 gas pressure. This is explained by

the fact that dissociation of the CF_4 molecule increases with increase in operating current. Increased dissociation leads to termination of the carbon bonding thus decreasing the length of the nanotube. The optimum pressure for the formation of nanotubes is between 50-100 torr with an arc current of 20 to 40 A.

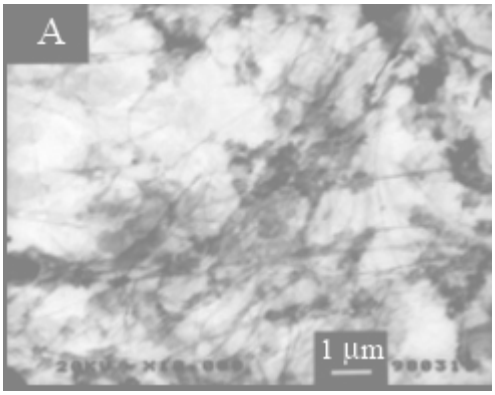

Figure 3.20 MWNTs synthesized in CF_4 gas [61].

E) Polycyclic aromatic hydrocarbons

Lai *et al*. [62] successfully synthesized MWNTs up to 20 µm in length using polycyclic aromatic hydrocarbons (PAHs) as the carbon source. PAHs serve as building blocks for the nanotube formation. The anode and cathode were graphite (10 mm in diameter), and the cathode is coated with PAH precursor xylene. An arc is struck between anode and cathode in a chamber filled with helium at 300-600 mmHg pressure. Constant flow rate of 10 l/min of helium is maintained during discharge. MWNTs up to 20 µm in length are produced in 1 minute as shown in Figure 3.21. The average length of the nanotubes decreased to 5 µm with increase in arc time. Columns of MWNTs were also synthesized using pyrene as the precursor material. The columns were 0.7 to 1.1 mm in height and made of MWNTs which are about 10-50 µm in length.

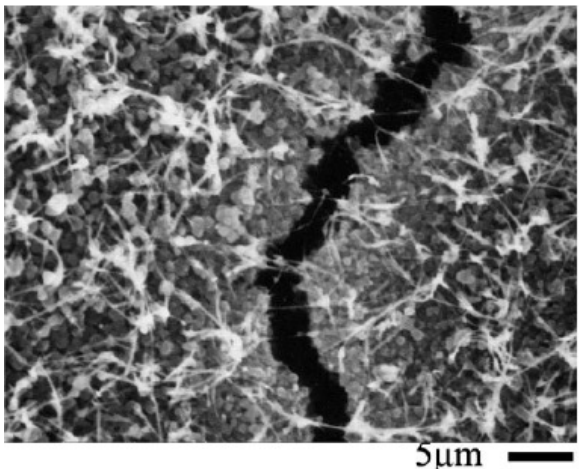

Figure 3.21 SEM micrograph of MWNTs formed from pyrene [62].

Shimotani *et al.* [63] studied the synthesis of nanotubes in acetone, ethanol, and hexane atmosphere using the arc-discharge apparatus. The yield of the nanotubes increases in organic atmosphere, with increase in the number of carbon atoms, as shown in Figure 3.22. Using pure graphite rods as anode and cathode, a stable arc was generated for 2 mins at 100 A current and 20 Volts. The yield of the deposit increased with increase in pressure, maximum yield was obtained at 500 torr of acetone. A 2.1 g MWNTs containing deposit was formed. This can be explained by the fact that in acetone, ethanol, and hexane atmosphere the number of carbon atoms increased with increase in pressure.

Shimotani *et al.* [63] also synthesized MWNTs by arc-discharge between tungsten electrodes in acetone atmosphere proving that organic atmosphere acts as a carbon source for the CNT synthesis. Since the ionization energy of organic molecules is ~ 10 eV, the ionization bond energies of C-C and C-H bond are ~ 9 eV and ~5eV respectively, and the arc-discharge is operated with at least 20 V leading to a kinetic energy of at least 20 eV. Thus the organic molecules decompose into hydrogen and carbon leading to higher number of carbon atoms in the arc-discharge.

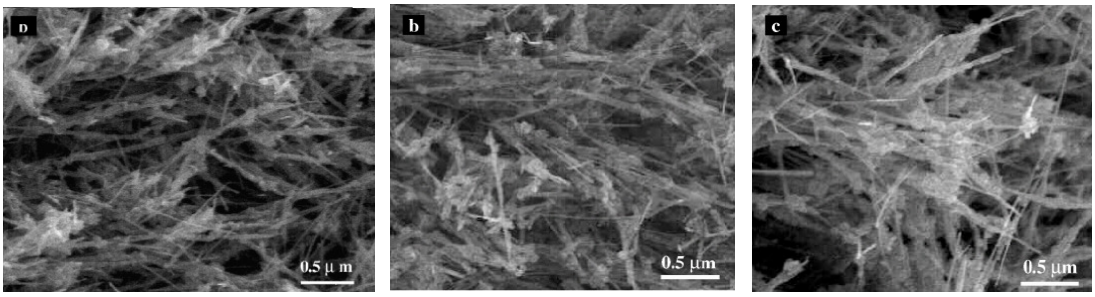

Figure 3.22 SEM micrographs of MWNTs synthesized in (a) acetone, (b) Ethanol at 500 torr and (c) Hexane atmosphere at 400 torr [63].

From the above it can be seen that MWNTs can be synthesized in a variety of atmospheres, such as helium, hydrogen, liquid nitrogen, CF_4, Polycyclic aromatic hydrocarbons, and organic molecular atmosphere. The maximum yield is obtained in helium atmosphere at ~ 500 torr. The MWNTs obtained in hydrogen atmosphere is very clean thus reducing the total purification time, but the yield is lesser than in helium atmosphere. Moreover, the use of hydrogen makes the apparatus extremely complex because of its explosive nature and complex handling system. Use of water in the arc-discharge apparatus makes the apparatus very simple even thought the yield is low.

3.4 Purification of MWNTs

In the DC arc-discharge method the as-grown MWNTs exist with carbon nanoparticles and amorphous carbon, with the nanoparticles composing at least one third of the sample. To purify the sample, the physical bonds between the individual nanotubes and nanoparticles have to be broken followed by oxidation where the nanoparticles are burnt leaving pure sample of nanotubes.

Tsang *et al.* [64] and Ajayan *et al.* [65] independently reported opening of the nanotube ends by heating them in presence of air. Due to differences in the oxidation rates

between cylindrical surface and nanotube caps the caps are destroyed first leaving nanotubes with open ends. The geometry of nanoparticles closely resembles the nanotube caps. So, by heating the as-produced nanotubes in presence of air, the nanoparticles are destroyed first leaving pure nanotubes. By heating the nanotube sample in presence of air at 750^0C for 30 mins, the nanoparticles are burnt off leaving a sample of pure nanotubes. In this process 99% of the material was destroyed leaving only 1% of pure tubes [65]. In the samples oxidized up to 85%, no change in the ratio of the nanoparticles and tubes was observed.

Ebbesen *et al.* [66] further developed the optimum time and temperature using different oxidizing agents, i.e. air, pure oxygen, steam, and carbon dioxide. It can be recognized that the time required for purifying decreases with increase in temperature and increase in the concentration of oxygen atoms.

3.4.1 Air

The optimum heating time is 20-60 mins when the temperature is 700^0 C, 5 to 30 mins at 850^0 C, and 1 to 20 mins at 1000^0 C. From the above, it is known that the oxidation time decreases with increase in temperature. Figure 3.23b shows the TEM micrograph of the samples purified in air.

3.4.2 Oxygen

The optimum heating times are 20 to 60 mins at 600^0 C, 5 to 30 mins at 750^0 C, 1 to 10 mins at 900^0 C, and 0.5 to 5 mins at 1000^0 C. The heating time and temperature decreases in oxygen due to presence of more oxygen atoms during the reaction. Figure 3.23c shows the TEM micrograph of the samples purified in oxygen.

3.4.3 Steam

The rate of oxidation is low and the samples were to be heated at 900^0 C for 12 hours to purify the sample. Figure 3.23d shows the TEM micrograph of samples purified in air.

3.4.4 Carbon dioxide

The oxidation rate is very low and the samples have to be heated at 900^0 C for 36 hours to purify the sample, as seen in Figure 3.23e.

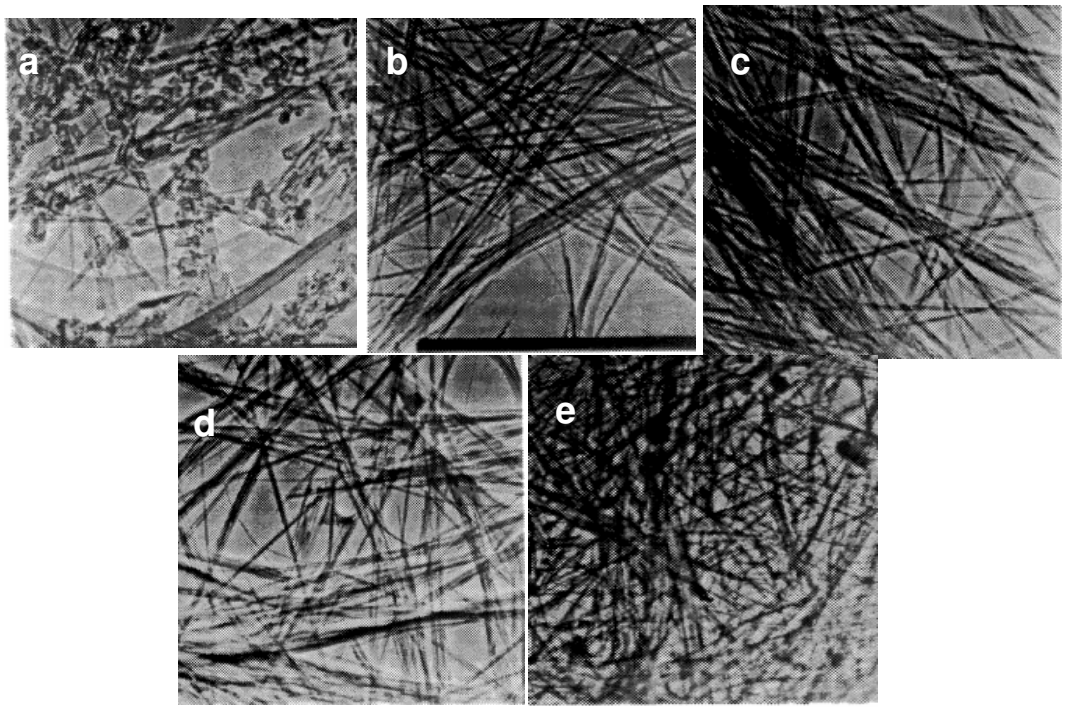

Figure 3.23 TEM images of the samples [66]; a) Crude sample before purification, b) Oxidation in air at 850^0 C for 15 mins, c) Oxidation in oxygen at 750^0 C for 15 mins, d) Oxidation in steam at 900^0 C for 12 hours, e) Oxidation in CO_2 at 900^0 C for 36 hours.

Uchida *et al.* [67] developed a process to isolate the nanotubes from graphitic particles by mechanical separation. The as-prepared MWNTs sample is pulverized in ethanol using a media agitating mill using high toughness zirconia balls as grinding media. The average particle size decreased to 0.2-0.6 μm. This process helps to break the physical bonds between amorphous carbon and nanotubes. The pulverized product is dispersed in water with

the help of a surfactant and ultrasonic waves. This step helps to obtain a stable dispersion and prevents the recombination of nanotubes and nanoparticles. The dispersed particles is centrifuged to precipitate the heavy graphitic particles. This step almost 70-80% of the particles are removed leaving nanotube rich material above the sediments. The supernatant is filtered and the filtrate is heated at 750^0C to burn off the remaining graphitic and carbon nanoparticles. A total of 18 mg of nanotubes is obtained from 721 mg of starting material. In this process the purity of the nanotubes is high but the nanotubes are greatly damaged in the media agitating mill.

Park *et al*. [68] developed an apparatus for improving the efficiency of the purification process as shown in Figure 3.24. The apparatus consist of two quartz tubes. The raw sample is placed in the inner tube and is rotated at 30 rpm by the outer tube using a stepper motor. Air is blown from one end to continuously supply oxygen. This helps the samples to be exposed to hot air uniformly. The amorphous carbon and nanotube caps undergo oxidation at a higher rate than the cylindrical portion of the tube. By carefully controlling the temperature and time, the process is optimized. At temperatures above 760^0 C, the samples were destroyed quickly. Below 700^0 C the samples took too long with considerable damage to the nanotubes. So, a temperature of 760^0 C is chosen as the desirable condition (Fig. 3.25). In 10 mins, the sample is reduced to 40% of the original quantity. From the SEM (Fig. 3.25b) it is calculated that the treated sample contains ~80% nanotubes with diameter of 50 nm and 5 μm in length. The improvement in purification is obtained by even exposure of amorphous carbon to hot air.

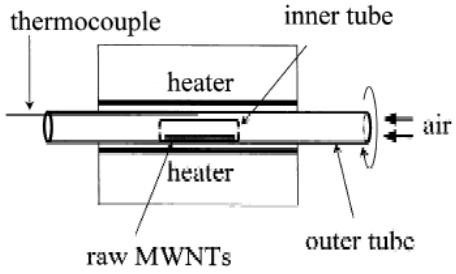

Figure 3.24 Schematic of the apparatus used for purification of MWNTs [68].

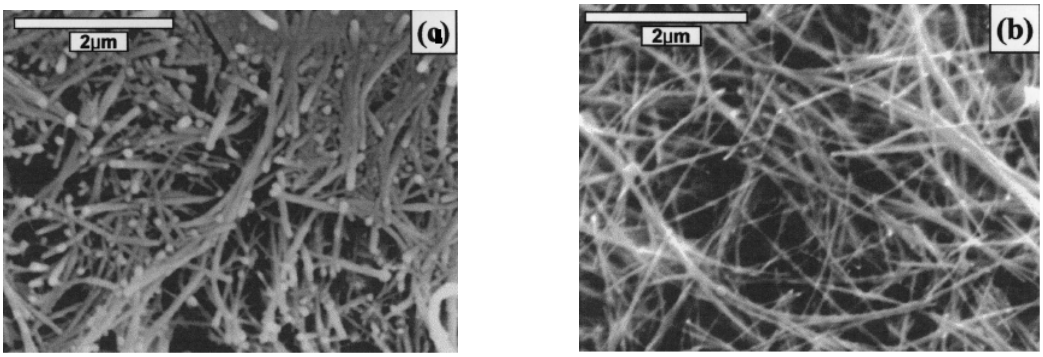

Figure 3.25 SEM image of MWNTs a) Annealed at 760^0 C for 40 mins without air flow, b) Annealed for 10 mins at 760^0 C with air flow [68].

The degree of purification is also characterized using Raman spectroscopy as shown in Figure 3.26, which shows the effect of annealing. The Raman spectra of both raw and purified sample show the peak centered at 1583 cm^{-1} (G-line), indicating the presence of well graphitized carbon nanotubes. The peak at 1285 cm^{-1} (D-line) is attributed to the defects, such as pentagons and heptagons in the graphite and amorphous carbon. The sample after purification shows a decrease in the D peak and a steep increase in the G peak, thus suggesting that the amorphous carbon is oxidized during purification.

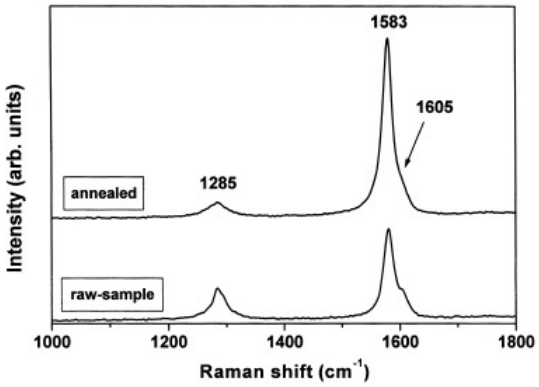

Figure 3.26 Raman spectra of raw and annealed multi-walled carbon nanotubes [68].

The main advantage of this process is that it is very simple to construct the apparatus, the yield is ~40% which is higher than the 1% yield reported by Ebbesen *et al.* [66]. The length and surfaces of the tubes do not undergo any mechanical damage.

3.5 Singlewalled carbon nanotube

3.5.1 Effect of metal catalyst

Iijima and Ichihashi of NEC, Japan discovered the SWNTs in arc-discharge using a metal catalyst [3]. The iron catalyst in the form of filings was placed on the cathode and vaporized in a gas atmosphere of argon and methane. During discharge, carbon and iron from the anode vaporizes and forms iron carbide above the cathode. SWNTs with diameter between 0.7 nm and 1.6 nm and length up to 700 nm were found in the soot-like deposit formed on the chamber walls. The tubes were found in the form of bundles and some were isolated.

Bethune *et al.* [4] from IBM in U.S. discovered SWNTs using an anode filled with ~2% Fe, Ni or Co [4]. The anode was vaporized in 100-500 torr of helium, SWNTs were found in a web-like material formed on the cathode walls which are relatively cold. SWNTs

with diameter ~ 1.2 nm were found along with fullerene soot, the SWNTs exist as bundles along with some isolated nanotubes.

Seraphin *et al.* [69] used a 6 mm diameter anode with 3 mm center hole filled with catalyst powder. Experiments were conducted at 550 torr of helium. Fe, Ni, Co and their mixture were used as catalyst to obtain a web-like material on the chamber walls. This material consist of bundles of SWNTs with diameters 0.9 to 3.1 nm and lengths up to 5 μm, along with metal particles 5-30 nm in diameter. SWNTs containing web-like deposit was formed using a mixture of catalysts Fe/Ni and Co/Ni. Low density SWNTs was observed in the soot by using Fe or Ni catalyst, with clean and straight tubes with nickel.

Saito *et al*. [70] studied the effect of Fe, Co, Ni and their mixtures in helium and argon atmospheres. In the case of iron alone, no nanotubes were observed in helium atmosphere. Low density nanotubes with diameters 1-1.1 nm were observed in methane/argon atmosphere. With nickel catalyst nanotubes with diameter 1.1-1.2 nm was observed in the collar deposit using helium atmosphere between 300 to 600 torr. Large amount of nanotubes were observed in the chamber soot using a Co catalyst in helium atmosphere. The tubes produced with cobalt catalyst were 1.3-1.4 nm in diameter. The yield of nanotubes increased using mixed catalyst. Maximum amount of nanotubes were obtained in Fe/Ni (1/1) in helium at 100 atmospheres. Saito *et al.* [70] also measured the temperature distribution and found that the temperature sharply decreased from 7000 K in the plasma region to 1400 K at a point 1.5 cm from the plasma region. Thus, vapor of carbon and metal were rapidly cooled and the nucleation of clusters took place in the gas phase.

The major breakthrough to produce SWNTs in large amounts was achieved by Journet *et al.* [26] of France using graphite anode with Ni, Y and carbon in the ratio 4.2:1:94.8. They observed that large amounts of SWNTs in the form of bundles were formed in the region around the cathode deposit in the form of black porous free standing material, called, collar deposit. The collar deposit was formed at 660 mbar of helium with 100 A current for 2 mins. Figure 3.27 shows that the bundles are10-20 nm in diameter, with individual tubes of 1.4 nm average diameter. The bundles of nanotubes were homogenously distributed in the collar region.

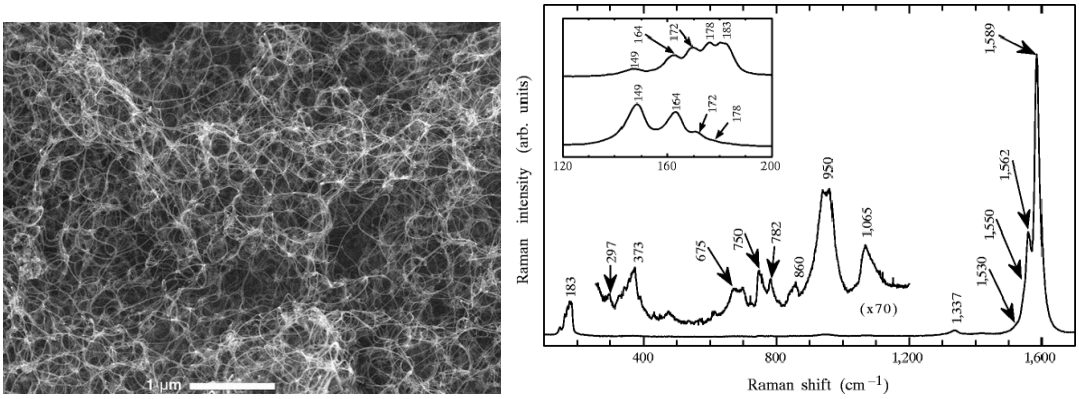

Figure 3.27 a) SEM image of collar deposit showing bundles of SWNTs, b) Raman spectrum of SWNTs showing radial breathing mode and 1589 G peak [26].

Saito *et al.* [71] studied the effect of platinum group metal mixtures. The anode was drilled and mixed with catalyst and graphite powder. SWNTs were found in the collar deposit, the yield strongly depending on the helium pressure and mixture ratio. Highest yield was obtained in a 1:1 mixture of Rh: Pt, as shown in Figure 3.28. The tubes are in the form of bundles entangled with each other. The individual tube diameters is between 1.21-1.33 nm and length up to 10 μm along with spherical particles 10-20 nm in diameter. The diameter of the tubes decreased to 0.7-1.3 nm with decrease in helium pressure to 50 torr. The use of

platinum group metal mixtures helped in producing tubes which are free of magnetic particles, although the cost of platinum group metals is very high compared to Ni, Fe or Co.

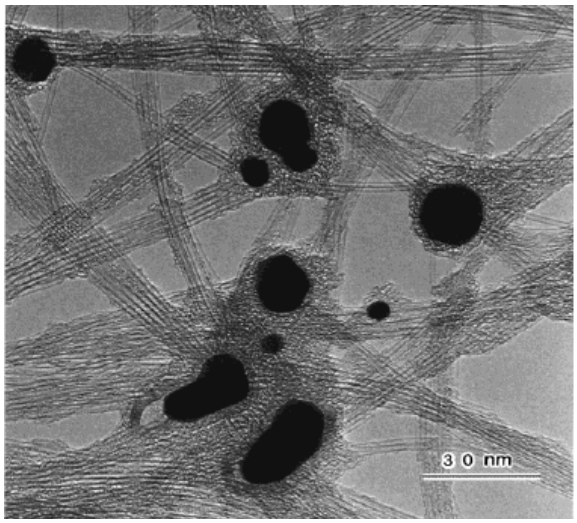

Figure 3.28 TEM image of SWNT bundles grown in the collar region using Rh-Pt catalyst at 600 torr of helium [71].

Wang *et al*. [72] studied the effect of catalyst concentration on the yield and diameter distribution of the SWNTs. The following concentrations of the catalyst and graphite (Y: Ni: C in atomic percentage) were studied, 0.25:1:98.75, 0.75:3:96.25, 1:4:95 and 1.5:6:92.5. The arc was generated in helium at 500 torr with 90 A D.C. to produce a dark deposit on the chamber walls. Maximum yield was obtained for Y: Ni: C = 1: 4: 95 indicating that yield depends on the catalyst concentration. The diameter of SWNTs is between 1.2-1.6 nm with 1.43 nm diameter in majority. Takizawa *et al*. [73] studied the effect of the catalyst ratio on the synthesis of soot and SWNTs. Addition of Y increases the generation of carbon soot but it is not effective for the synthesis of nanotubes. The addition of Ni results in the formation of SWNTs. Thus the combination of Y and Ni helps in increasing the formation of nanotubes. Maximum yield of SWNTs was obtained at ~ 0.6 % Ni and ~ 0.1% Y. The mean diameter

increases with increase in Y concentration and the diameter distribution changes with Y concentration.

Lv *et al*. [74] studied the effect of NiO and Y_2O_3 with Ni: Y at 4.2:1%. The SWNTs are found in the web-like material formed on the chamber walls. The use of Ni and Y compounds instead of metal Ni-Y increases the quality and yield with a significant decrease in the cost of catalyst. Most research groups have focused on optimizing the process using Ni-Y (4:1) catalyst, by varying pressure, buffer gas, and temperature.

3.5.2 Effect of temperature

Takizawa *et al*. [75] studied the effect of chamber temperature on yield of SWNTs. The composite anode was prepared with Ni, Y each at 0.6% in graphite. The experiments were conducted in a 300 mm long, 50 mm diameter quartz tube surrounded by a tube furnace as shown in Figure 3.29. The arc-discharge was carried out in 500 torr helium flowing at 100 sccm by maintaining the arc gap of ~ 1mm for 10 seconds using 100 A arcing current. The soot was collected from the walls of the chamber and the cathode. The temperature is controlled by chromel-almel thermocouple attached to the outer wall of the quartz tube. The yield of SWNTs increases with increase in chamber temperature, reaching a maximum at temperatures between 400 and 600^0 C. At 600^0 C the yield reaches > 70 wt %, while the yield remains 30-40 wt% at room temperature.

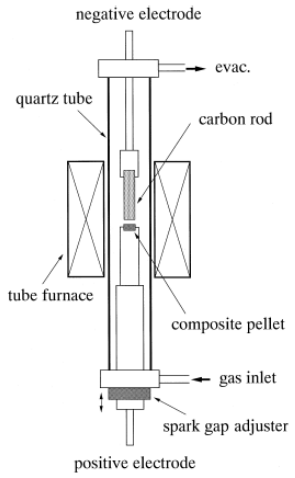

Figure 3.29 Schematic of high-temperature arc vaporization apparatus for synthesizing SWNTs [75].

Liu *et al.* [76] studied the effect of temperature during mass synthesis of SWNTs containing material. A heater is mounted outside the Ø 300 × 400 mm^2 vacuum chamber and the temperature of the chamber is controled during synthesis. Six Ø6 x 100 mm^2 graphite anodes drilled with Φ4 x 60 mm^2 hole are filled with 19:1 (weight ratio) of Fe-Ni-Mg (2:1:2 wt%) powders. The six anodes are mounted at equal distance on a wheel so that it can be rotated to change the active anode, as shown in Figure 3.30.

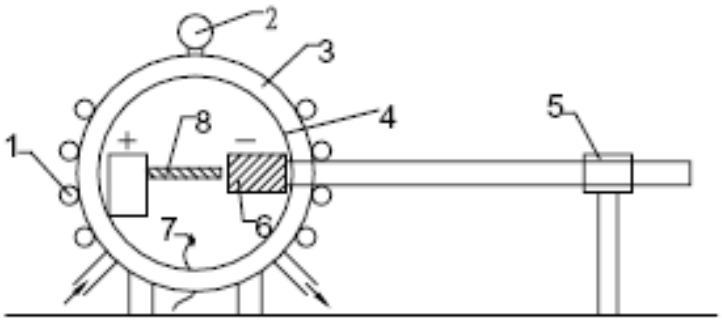

Figure 3.30 Schematic of temperature controlled arc-discharge apparatus. 1- Water cooling system, 2- pressure gauge, 3- vacuum chamber, 4-temperature controlled apparatus, 5-electrode feed mechanism, 6-moving cathode, 7-thermocouple, 8-fixed and rotating anode [76].

The experiments were conducted with 60 A current at 400 torr helium atmosphere. An inter electrode gap of 2 mm is maintained by continuously feeding the cathode during the arcing process. In 5 mins, 5.3 grams of SWNTs containing soot is formed on the walls of the chamber. The chamber temperature strongly affects the yield, the purity, and the bundle diameter distribution with maximum yield at 600 ^{0}C.

Table 3.3 Effect of temperature on the production of SWNTs [76].

Temperature (°C)	Diameters of SWNT bundles (nm)	*Purity (%)	Yield (g/h)
25	10–50	20	25.9
300	20–40	30	33.2
400	20–30	40	39.9
500	10–30	50	58.3
600	7–20	70	64.7
700	7–30	50	43.2

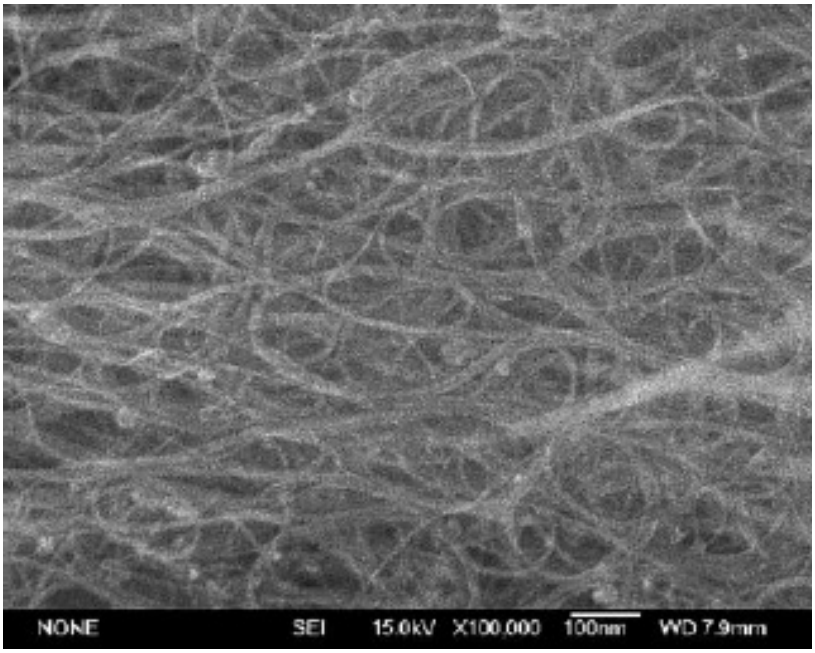

Figure 3.31 SEM micrograph of purified SWNT bundle produced at 600^0 C.

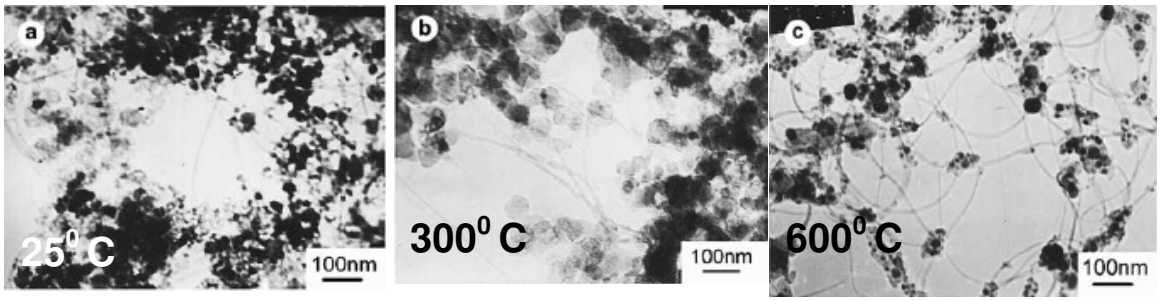

Figure 3.32 TEM image of as-grown SWNTs bundles, a) 25 ^{0}C, b) 300 ^{0}C, c) 600 ^{0}C [76]

The temperature of the environment preheats the catalyst thus reducing the time to activate and form nanotubes. Also, the catalytic activity increases with increase in temperature. At temperatures above 700 ^{0}C, the yield decreases due to thermal decomposition of nanotubes. The increase in purity is attributed to the fact amorphous carbon decomposes at temperatures above 500 ^{0}C, thus increasing the nanotube to nanoparticle ratio. Maximum yield of 64.7 g/h as-produced single walled nanotube (AP-SWNT) material is obtained at 600 ^{0}C. The SWNTs exist as bundles of 7-20 nm in diameter with average tube diameter of 1.24 nm.

3.5.3 Effect of buffer gas

The buffer gas plays an important role in the synthesis of SWNTs because the formation of nanotubes depends extensively on the thermal conductivity of the gas. It has been observed that purity, tube diameter, bundle diameter, and yield can be controlled by changing the buffer gas [77].

Farhat *et al.* [77] studied the effect of argon in the chamber. In a 6 mm diameter graphite anode 3 mm diameter hole was drilled and filled with Ni, Y metal catalyst such that the final molar ratio of C/Ni/Y is 94.8:4.2:1. The cathode, the anode and the chamber is water

cooled. The arc was generated using 100 A current maintaining 3 mm gap during discharge. The water cooled cathode helps in achieving high quench rates and high levels of super saturated vapor with nanotube formation. For pure helium, the largest amount of collaret is formed at pressures ~660 mbar, the optimum pressure decreases to 100 mbar for pure argon. The effect of argon was studied by conducting the experiments in pure helium, 20, 40, 60, 80, and 100% argon atmosphere at pressures between 100 and 660 mbar. The spongy black collaret formed around the cathode was analyzed because maximum amount of SWNTs are found. The use of argon produces nanotubes that are smaller in diameter compared to helium. Varying the gas mixture of helium to argon changes the diameter distribution to lower values. The average tube diameter decreases linearly as a function of the percentage of argon going from ~ 1.4 nm to ~1.2 nm. A 0.2 Å diameter decrease is noticed for 10% increase in argon-helium ratio, as shown in Figure 3.33.

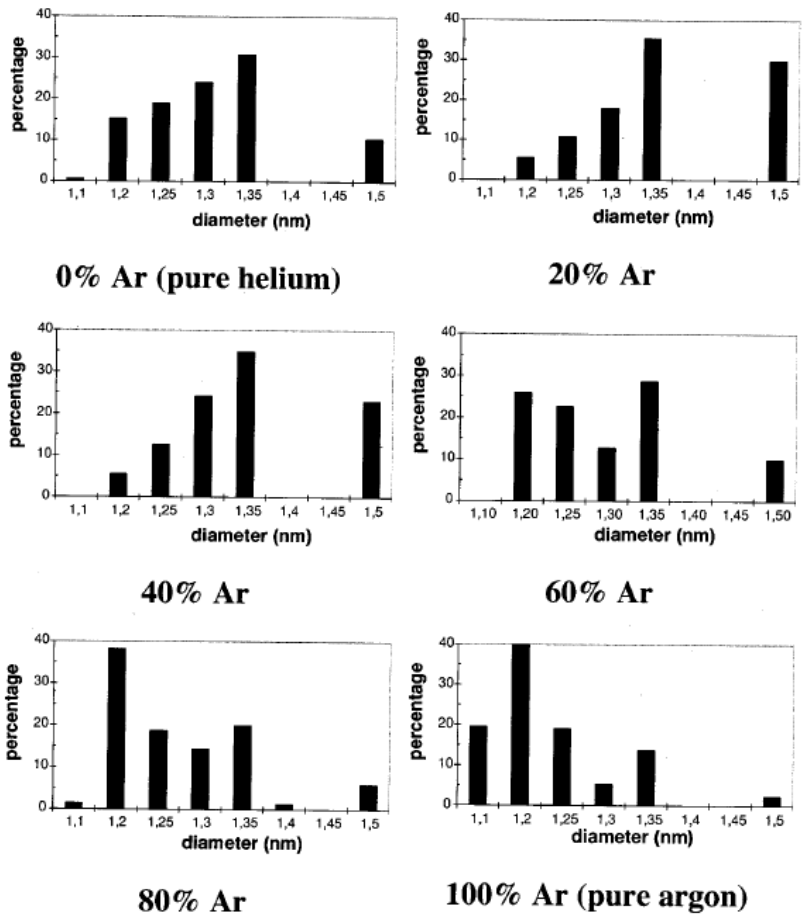

Figure 3.33 Frequency of SWNTs at different diameter for mixture of helium and argon, diameter measured using Raman spectroscopy [77].

This is attributed to the fact that thermal conductivity of argon is about 8 smaller than helium. Thus varying the argon-helium gas ratio alters the heat transfer between anode and cathode. The low thermal conductivity of argon decreases the thermal conductivity of the gas mixture.

Zhao *et al.* [78] studied the effect of hydrogen-argon gas mixture during arc-discharge. A macroscopic oriented web of SWNTs was prepared as shown Figure 3.34. Iron catalyst at 1 at% Fe in graphite is used. An arc is formed in 40% H_2, 60%Ar gas mixture at a pressure of 200 torr. The arc plasma was created by applying 30-70 A current and maintaining ~ 2mm arc distance. The SWNTs web was produced at the rate of 7.7 mg/min.

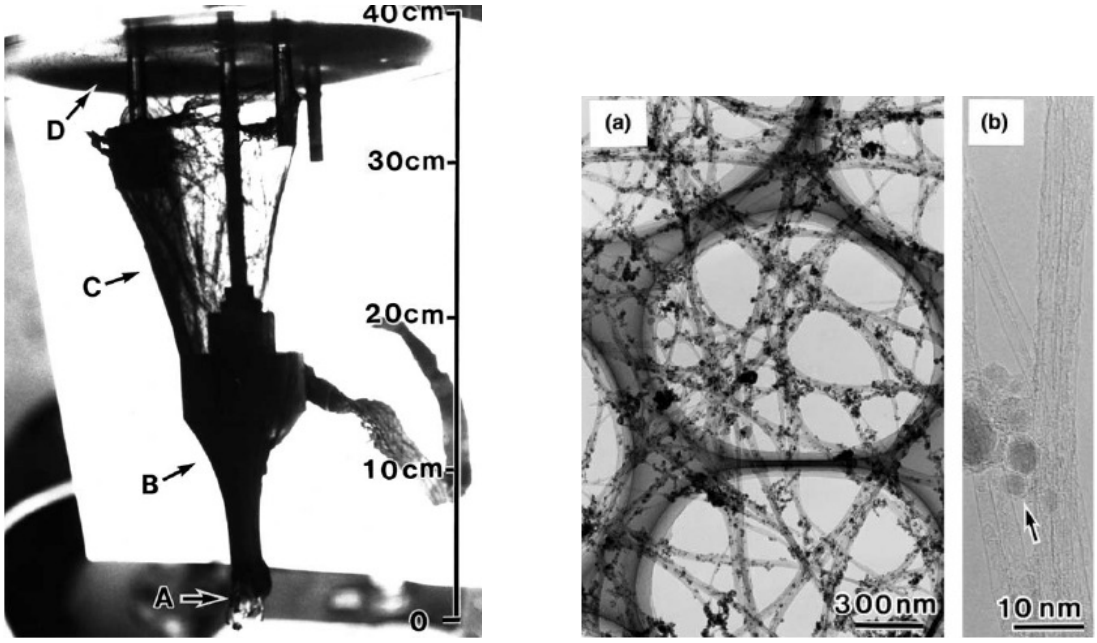

Figure 3.34 Macroscopic oriented web of SWNTs. TEM image of as grown SWNTs, HRTEM of as grown SWNTs [78].

SEM analysis shows that the purity of web material is more than 70%. Atomic hydrogen in the H_2-Ar arc-discharge promotes vaporization of carbon anode and keeps the Fe catalyst active. Hydrogen also hinders the fullerene formation and selectively etches the amorphous carbon attached to the nanotubes thus serving as an *in situ* purification process and improves the purity of SWNTs. The same role is played by hydrogen in the synthesis of MWNTs. The SWNTs exhibit high crystalline nature and clean surface. The presence of argon helps to stabilize the arc. SWNTs cannot be prepared with Fe catalyst in pure argon or helium atmosphere because the high solubility of Fe in graphite causing self deactivation which hampers SWNTs formation.

Ando *et al.* [79] studied the effect of hydrogen-nitrogen mixture in the arc-discharge chamber. Anode containing 1 at% Fe was used in a H_2-N_2 buffer gas at 200 torr. A constant flow of 2000 sccm (H_2-N_2) mixture was maintained to introduce new hydrogen atoms. The

dc arc-discharge was generated by applying current of 40-70 A. Maximum yield of 76 mg of the web-like material was obtained in 60% H_2, 40% N_2 at the rate of 13 mg/min as shown in Figure 3.35. The purity of the web-like material is estimated to be 70%.

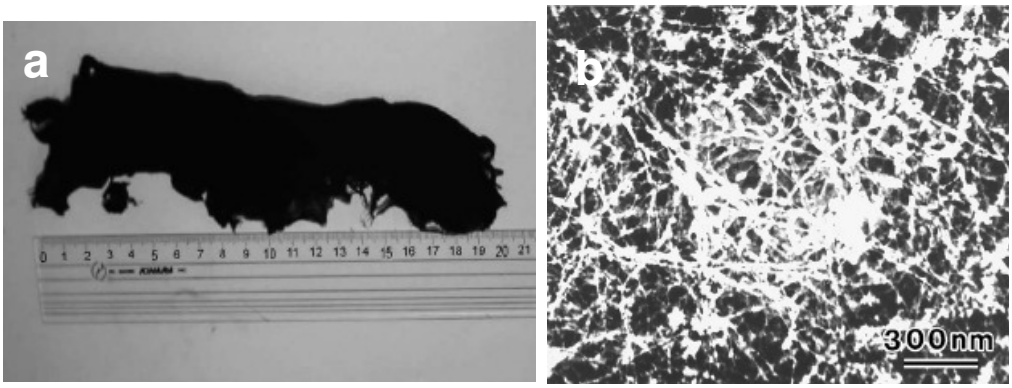

Figure 3.35 a) SWNT web, b) SEM image of as grown SWNT [79].

The presence of atomic hydrogen selectively etches the amorphous carbon attached on the surface of Fe particles by forming hydrocarbons. The H_2-N_2 arc possesses higher enthalpy than of H_2-Ar arc plasma, thereby promoting evaporation of C-Fe electrode and increasing the yield. The as-grown SWNTs have a diameter distribution of 0.8 to 1.31 nm which is lower that H_2-Ar arc-discharge. This is attributed to the fact that nitrogen has a thermal conductivity of 243 W/m K which is higher than 162 W/m K of argon. The diameter distribution can also be controlled by changing H_2-N_2 mixture ratio. The advantage of using hydrogen in the buffer gas is that purity of the as-produced material is higher and inexpensive metal catalyst, such as iron can be used which can be removed easily. The disadvantage of introducing hydrogen is that it makes the system unsafe due to its explosive nature.

Guo *et al*. [80] performed spectroscopy studies on the effect of buffer gas in SWNTs synthesis using Fe catalyst. In pure Ar atmosphere, Fe is predominantly observed and C_2

spectrum is weak and SWNTs are less in quantity. In H_2 gas, strong C_2 is observed but Fe spectrum is very weak with less SWNTs. In the case of H_2-Ar gas, the emission spectra for Fe atoms and C_2 are observed. The spectroscopic analysis showed that H_2-Ar provides the best conditions and quenching rates for the formation of SWNTs.

3.5.4 Effect of gas pressure

Waldorff *et al*. [81] studied the effect of helium pressure on the diameter of the SWNTs and the anode ablation rate. Anode filled with metal catalyst in the ratio C:Y:Ni in a 13:1:4 at% ratio was used in the study. The DC discharge was run at 78.5 A current at 120 V. The helium pressure was varied from 100-1000 torr. Web-like material containing SWNTs bundle was found in the side of the cathode deposit after 3 mins of ablation. The ablation rate was determined from the initial and final weight of the anode. From TEM and Raman spectroscopy, the diameter distribution is calculated. They reported that the nanotube diameter did not vary significantly with pressure. The relative concentration of nanotubes reached maximum level at 200 to 300 torr of helium. With increase in the chamber pressure, the heat flux to anode increases leading to an increase in the surface temperature of the anode and accelerating the ablation rate. Thus the optimum pressure is found to be between 200 and 300 torr.

Shi *et al.* [82] studied the effect of high pressure helium atmosphere on the formation of SWNTs. Graphite electrodes filled with Y-Ni alloy in metal/C atomic ratio of 3:10 was used as anode. The arc was generated in 2 atmosphere of helium using ~ 40 A current to produce cloth-like soot on the chamber walls. It contained SWNTs in the form of bundles (~25 nm) and length up to 10 μm. The individual nanotubes have diameter ranging from 1.1

to 1.4 nm, as shown in Figure 3.36. SWNTs containing soot is produced at the rate of 2.5 grams per hour. High chamber pressure leads to high temperature gradients from the center of the arc to the water cooled chamber walls leading to the formation of SWNTs.

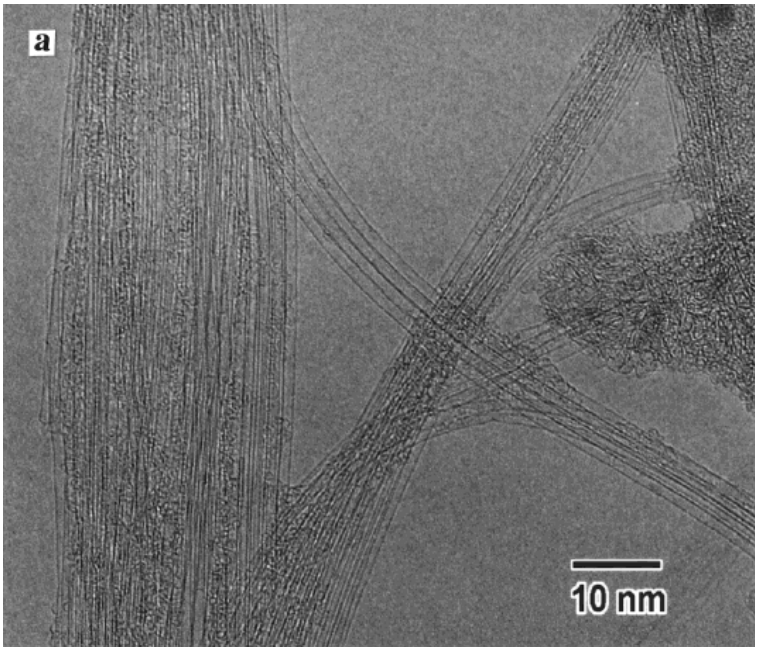

Figure 3.36 HRTEM image of SWNTs produced with Ni-Y catalyst in high pressure [82].

Park *et al*. [83] studied the effect of helium pressure on the yield of SWNTs using nickel and iron mixture as a catalyst. Anode containing 5% catalyst (Ni:Fe = 1:1) was vaporized in helium atmosphere at 100 to 500 torr using 60-80 A current. The collar deposit formed around the cathode, known to contain the highest amount of SWNTs, was analyzed [26]. SWNTs are formed in the form of bundles with diameter 10-20 nm, with carbon particles attached to the crossed junction. The ratio of SWNTs to particles decreased with decrease in helium pressure, as shown in Figure 3.37. This can be attributed to the fact that arcing temperature increases with decrease in gas pressure. The anode consumption rate increases with decrease in pressure due to increase in arc temperature.

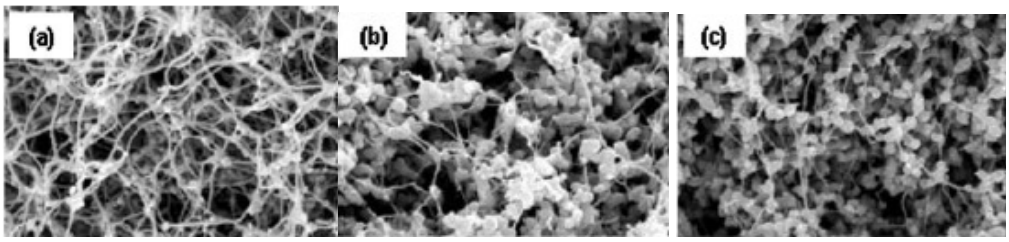

Figure 3.37 SEM images of SWNTs grown at a) 100 torr; b) 300 torr; c) 500 torr [83].

Addition of sulfur increases the evaporation rate by broadening the arching temperature. The use of FeS instead of Fe increases the yield of SWNTs. The addition of sulfur increases the bundle diameter and also increases the ratio of SWNTs to particle as shown in Figure 3.38a. The amorphous carbon is formed during the cooling process, where the transition metals are not active and do not play the role of a catalyst.

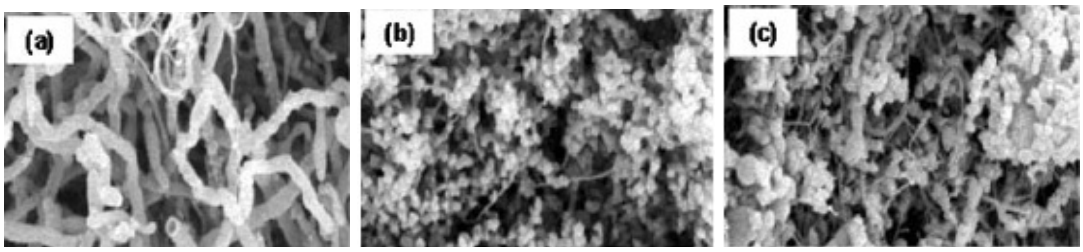

Figure 3.38a SEM images of SWNTs grown using Ni and FeS catalyst at a) 100 torr; b) 300 torr; c) 500 torr [83].

Hinkov *et al.* [84] studied the effect of argon and helium pressure on the synthesis of SWNTs using C: Ni: Y = 94.8: 4.2: 1 at% electrodes. The arc was created using 100 A current by maintaining a distance of 3 mm between the electrodes. The pressure was varied between 100 and 800 mbar. The collar deposit formed around the cathode deposit was analyzed. It was evaluated using the Brunauer-Emmett-Teller coulter by measuring the surface area of the samples. The BET surface area of the sample was determined by nitrogen adsorption at 77 K. At this temperature nitrogen is physically adsorbed on the surface of the sample. The adsorption isotherms are recorded as specific volume (cm^3/g) of gas at standard

temperature and pressure. The presence of SWNTs shows very high BET surface area of ~ 1315 m^2/g, as shown in Figure 3.38b.

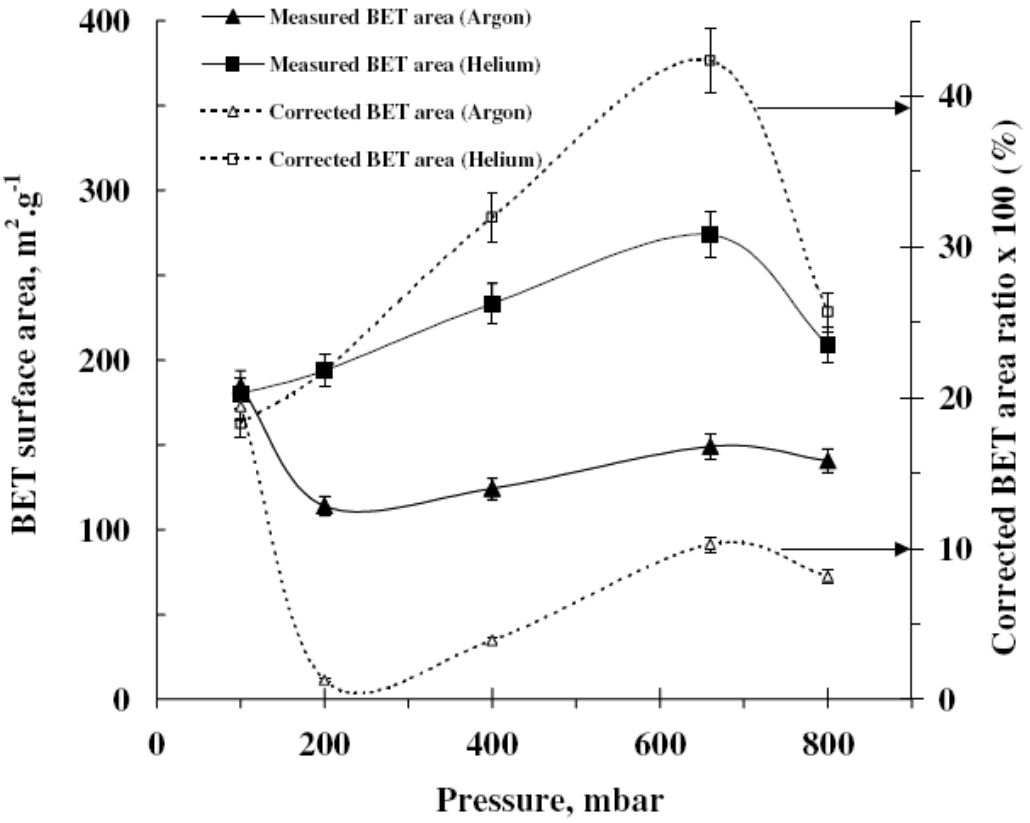

Figure 3.38b Measured BET surface area versus total pressure for argon and helium [84].

Samples produced with helium show higher BET surface area compared to argon samples thus suggesting that helium is more efficient than argon to vaporize the anode. The observation is also confirmed with SEM analysis which shows that nanotube density decreases drastically with argon instead of helium. Thus, helium is more efficient than argon to produce nanotubes. Nanotube growth rate is about three times faster when helium is used and optimal pressure is found to be about 600 mbar for helium and 100 mbar for argon. This can be explained by the lower thermal conductivity of argon compared to helium, leading to less efficient heat transfer in the inter electrode gap.

3.6 Mechanism of MWNTs

Only in the electric arc technique, MWNTs are formed without the presence of catalyst particles. Many growth models have been proposed but there is still no agreement on the experimental data or theoretical simulations. Several research groups have worked on the growth mechanism to understand the critical parameters to determine the kinetics of open ended tube growth. A growth mechanism has to explain many questions such as, the following:

a) Which process parameters are crucial for the CNT formation?

b) Why does the nanotube growth terminate after a period?

c) What causes the capping of the tubes since nanotubes are always found to be closed?

d) Can the proposed mechanism be verified by molecular dynamics (MD) simulations?

The arc plasma formed in the inter electrode gap is a mixture of carbon ions and helium atoms from the buffer gas. The temperature in the arc plasma region reaches ~ 3000 K. The high temperature favors formation of straight tubes. During the arc-discharge the anode is vaporized and deposited on the cathode to form a cathode deposit which contains soft core material made of nanotubes surrounded by hard shell, as shown in Fig 3.39. The straight walls of the nanotube consist of fused 6-member carbon rings forming hexagonal graphitic lattice which is wrapped into a cylinder. The formation of pentagonal defect leads to tapering of the wall and finally closure of the tube [85, 86].

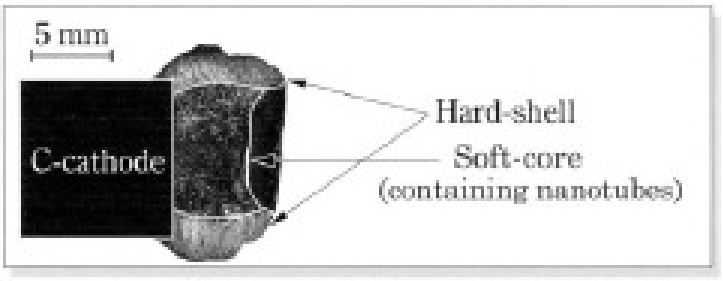

Figure 3.39 Cathode deposit containing nanotubes [24]

Iijima *et al.* [85] proposed the first growth model for MWNTs, called, the open ended growth model i.e. the growing tubes remain open at the ends during growth. Nanotubes consist of hexagonal network along its length and pentagons at the tips. The nucleation of pentagons at the periphery of open ends results in the termination of the growth process by the formation of cone shaped structure. The formation of heptagons aids the growth of tubes by inducing negative curvature which compensates cone shaped formation. Starting with the nucleus (O) various tube morphologies are produced depending on the formation and stability of hexagonal, pentagonal, and heptagonal rings at the open end, as shown in Fig. 3.40. Cylindrical tube walls are generated by the addition of hexagons to the growing end. Tube thickening is caused by island nucleation and layer by layer growth on the outer surface of the growing tubes. Pentagons and heptagons on the tube surface act as nucleation sites for layer growth of graphitic planes. The helicity on the cylindrical surface is controlled by the distribution of pentagons at the tip. It has also been observed that presence of symmetric tip tubes do not show any helixity. This model fails to explain the formation of nucleus for tube growth, or five, six and seven- member rings.

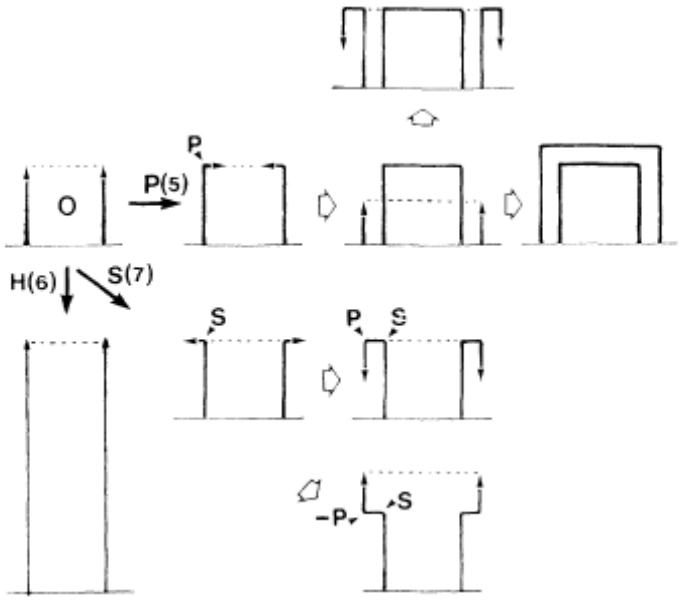

Figure 3.40 Schematic showing the various growth probabilities starting from nucleus O [85].

Addition of only hexagons H (6) to the periphery of an open tube leads to growth along the axis with no defects. Tube thickening is caused by island growth of fresh layers of graphite basal planes. Successive addition of pentagons P (5) causes tube closure, The addition of single pentagon (P or –P) can change the growth direction by 90^0, leading to cap formation or formation of successive cylindrical layers. Heptagons S (7) lead to opening of tube ends for further growth.

Crespi [86] studied the ends of the tubes which terminate the growth process. Each blunt cap contains five additional pentagonal rings. The nanotube cap formation is governed by relative stability of pentagons and hexagons during the growth process. Pentagons minimizes the number of dangling bonds and the hexagons minimize the distortions in the bond angles. The stability of hexagons decreases with decrease in tube diameter leading to unstable or shorter tubes. During the growth process many polygons are added to increase the

length of nanotubes, the cap is formed due to thermal fluctuation in the plasma zone as shown in Figure 3.41.

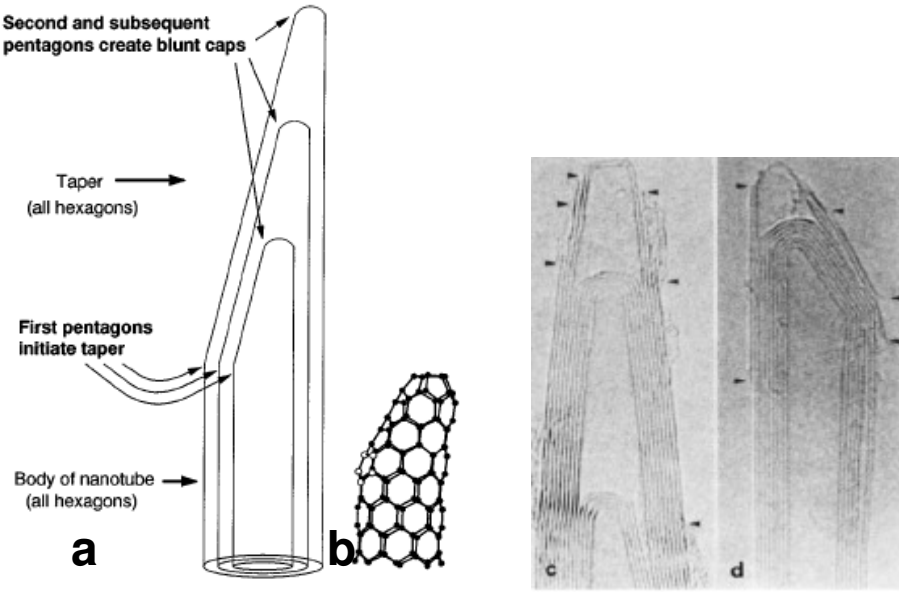

Figure 3.41a, b) Schematic of capped multi-walled nanotube c, d)HRTEM image of conical ended tubes [86].

Smalley and Colbert [87] analyzed the growth of nanotubes based on electric field in the plasma region. Nanotubes grow in the cathode region where the electric field concentrates which indicate that it may play a vital role in the growth process. The electric field in the arc plasma stabilizes open tip structure against closure which was confirmed by heating nanotubes. The nanotubes tips remain open when heated to ~ 3000^0 C in an electric field and closes in the absence of electric field. The tubes grow along the axis when the tips remain open, thus accounting the role played by the electric field to keep the tip open during growth.

Gamaly and Ebbesen [88] proposed a bimodal velocity distribution of carbon ions for the formation of MWNTs. The growth of nanotubes is governed by the attachment

probabilities of carbon atoms, ions and clusters of various shapes and dimensions controlled by a set of space-time dependent parameters in the arc plasma. In the region close to the cathode surface the density of evaporated vapor is maximum (~ 10^{18} cm^{-3}). The nanotubes grow in this region due to competitive input from two groups of carbon species having different velocity distribution. An isotropic Maxwellian velocity distribution corresponding to 4000 K leads to the formation of carbon clusters, such as nanoparticles. A directed ion current due to charged carbon ions accelerate in the anode-cathode region by the potential drop leads to the formation of elongated structures. The carbon species having Maxwellian velocity distribution helps in the thickening of the tubes normal to the growth axis. The radial growth is about 200 times less effective compared to axial growth leading to high aspect ratio of the tubes. Termination of the tubes is explained by the local instabilities in the arc which disrupts the directed carbon-ion current. This model explains the formation of tubes by thermodynamic approach and physical parameters of the arc. Experiments and simulations have shown that electric field is not necessary and sufficient conditions for the growth of nanotubes along the axis [92].

Guo *et al.* [89] put forward a hypothesis that presence of carbon adatoms play a key role by bridging between adjacent edges of growing multilayered graphite sheets thus extending the life time of the open structure. Tight binding calculations confirm that a bridging site is more energetically preferred by 0.5-1.5 eV per adatom over any chemisorption site directly on one layer, as shown in Figure 3.42. This has been confirmed by Charlier *et al*. [90] by MD simulations. Calculations show that the growth along the axis is stabilized by adding atoms bridging the dangling bonds between layers.

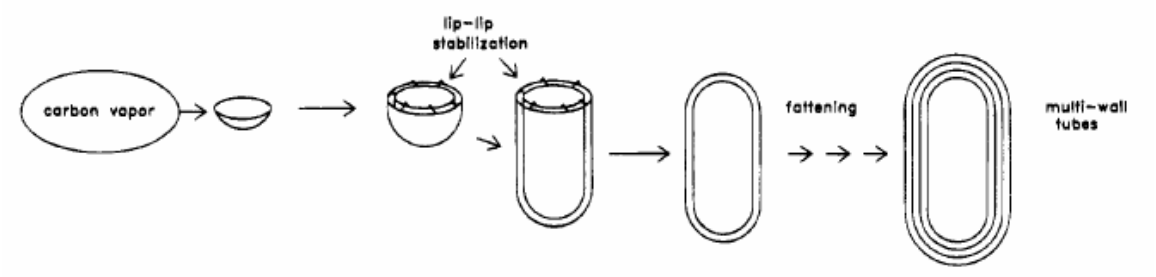

Figure 3.42 Growth of MWNTs by lip-lip stabilization [89].

Charlier *et al*. [90] studied the microscopic growth mechanism by performing first principles MD simulations of double-walled nanotubes. The forces acting on the atoms are derived from the instantaneous electronic ground state which is described within the density functional theory. During the growth process open end bilayer structure was trapped into a metastable energy minimum by formation of bridging bonds between the edges of adjacent tubes. This "lip-lip" interaction prevented the dome formation which terminates the growth process. At ~ 3000 K, the bridging bonds connecting the inner and outer tubes are continuously broken and re-formed. This fluctuating lip-lip bond provides the active sites for rapid incorporation of C fragments and growth, as shown in Fig. 3.43c.

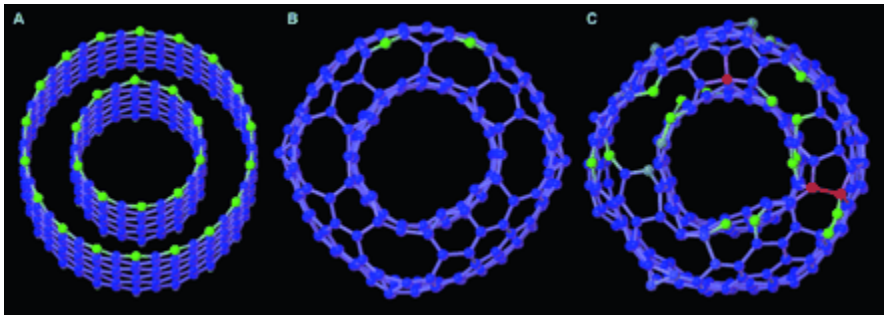

Figure 3.43 Stabilization of double-walled C nanotube edge by "lip-lip" interactions. (**a**) Top view of the open-end starting bilayer system at 0 K (b) Top view of the lip-lip interacting concentric shells at ~300 K. (**c**) Lip-lip interaction after 2.8 ps of simulation at ~3000 K [90].

Thus it can be identified that collision of carbon fragments like chains and rings with seed structures, such as half fullerene domes in a carrier gas favors the growth of nanotubes.

The presence of directed velocity of carbon species will increase the growth rate. This can be confirmed using low current (or current density) in the arc (low carbon vapor density), nanotubes are not formed. So, the role played by current in arc-discharge is to vaporize the anode so that it forms high density directed carbon plasma in the anode-cathode region.

Robertson *et al.* [91] performed MD simulations by integrating Newton's law of motion with an accurate high order Nordsieck predictor correction method. The initial conditions are generated by assuming that the velocity of individual atoms in a relaxed carbon ribbon is distributed according to Boltzmann distribution with arbitrary directions in 3D space. The dynamics of isolated ribbons were followed at constant energy to simulate their motion in carbon vapor between collisions. The simulations were conducted in 250-ps length which is an order magnitude less than the collision time. Figure 3.44 shows the snapshots of the trajectory, the carbon ribbon starts in a planar configuration, and increases curvature until it forms a closed structure at ~ 70 ps. The fusion of ribbon ends is confirmed by the increase in temperature at ~ 70 ps.

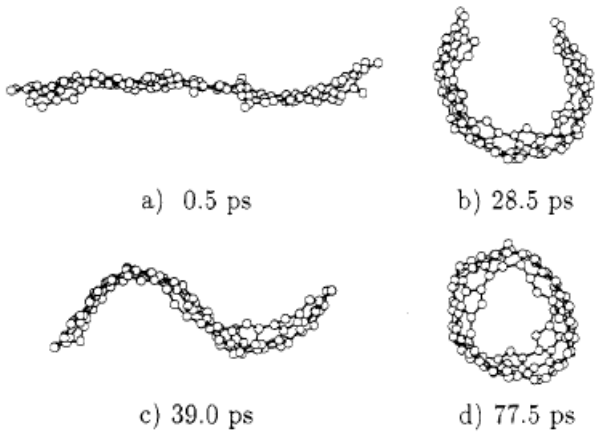

Figure 3.44 Snapshots of the curling and closure of 108 carbon atom ribbon at (a) 0.5 ps, (b) 28.5 ps, (c) 39 ps and (d) 77.5 ps started at 1150 K [91].

Maiti *et al.* [92] studied the growth energetics of carbon nanotubes during arc-discharge. *Ab initio* molecular dynamics (MD) calculations showed that electric field plays a limited role in the growth of open ended tubes. The tube closure is initiated by the formation of pentagon structures. Tube closure is energetically favorable for tubes narrower than critical diameter ~ 3 nm. For larger diameter tubes, the addition of atoms and small clusters to the tube edge leads to the formation of hexagonal structures that favor growth along the tube axis. Isolated pentagons or heptagons at the tube edges are converted back to hexagons by bond switching and migration thus continuing the axial growth process, as shown in Figure 3.45. The formation of large number of pentagons leads to the formation of highly curved structures and ultimately tube closure.

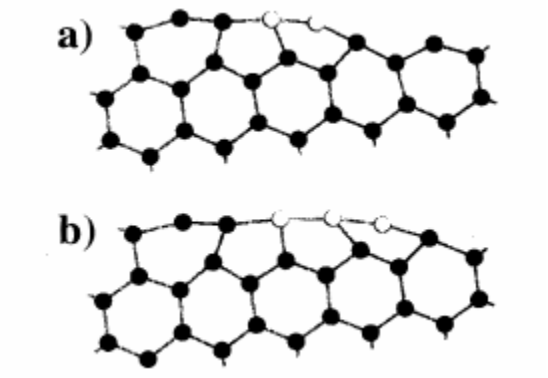

Figure 3.45 Low energy structures formed at edges: a) 5-5 pair, b) 5-5-5 containing pentagons [92].

Kwon *et al*. [93] used MD simulations to analyze the growth process in double walled nanotube. They showed that tube growth is a highly exothermic process driven by the energy gain when carbon from atmosphere adsorbs at the growing tips. The formation of hemispherical dome is less favorable energetically and the lip-lip bonds have to be disrupted completely. Since the edge energy is higher for closing dome than continuous growth of tubes, the natural termination of tube growth is less likely to occur.

3.7 Mechanism of single-walled nanotube growth

A metal catalyst has to be used for the synthesis of SWNTs. The metal catalyst, buffer gas, gas pressure, gas flow rate, chamber temperature, temperature gradient and chamber design play an important role in the formation of SWNTs. SWNTs are formed in the region around the cathode deposit and on the chamber walls. No SWNTs are found in the cathode deposit. Many growth models have been proposed and supported with MD simulations.

Shi *et al.* [94] proposed that the driving force for the formation of single-walled nanotubes is the thermal gradient that exists between the side walls and the core of the plasma. As the metal-yttrium doped anode is brought near the cathode, plasma is formed between the two electrodes.

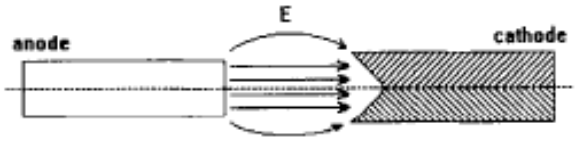

Figure 3.46 Vertical section of cathode, electric field and equip-temperature surface [94].

The metal-carbon vapor generated from the anode bombards the cathode surface to form cathode deposit. In Figure 3.46, the loudspeaker like mouth on the cathode represents the equip-temperature surface. The key step in the growth of nanotubes is nucleation and the driving force for further growth is the thermal gradient. Yttrium carbide along with carbon vapor reaches the cathode surface and condenses to form nanometer sized nuclei. Carbon atoms around the nuclei then condenses to form small clusters. The moving equip-temperature causes the clusters around nanometer sized nuclei to grow into tubes along the

equip-temperature surface. The growth process stops when the cathode surface reaches a uniform temperature and thermal gradient is absent. Yield depends on the number of nuclei formed, diameter of SWNTs is controlled by the size of the nuclei, and the length depends on carbon vapor density and thermal gradient.

Saito *et al*. [102] studied the effect of rare earth elements such as Sc, Y, La, Ce, and Pr on SWNT growth. They observed that vapor pressure of the catalyst metal plays an important role in the formation of SWNTs. Saito *et al*. [101] also proposed that use of Y in graphite anode decreases the melting point of carbon by alloying. The decrease in melting point causes an increase in the vaporization rate of graphite leading to an increase in the yield of SWNTs.

Shi *et al*. [95] further supported the theory of thermal gradient using a Y-Ni alloy composite electrodes and varying the helium atmosphere. Shi *et al*. [95] observed that no SWNTs are formed below 300 torr. The amount of SWNTs in soot increases with helium pressure and does not change with changes in electric current. Increase in helium pressure increases the thermal gradient between the chamber walls and electrodes thus leading to increase in yield. The presence of yttrium or scandium helps to form metallofullerenes in higher yield which acts as nucleation sites for the formation of SWNTs. They also observed that increase in helium pressure causes a decrease in the metal vapor pressure which is in agreement with the observation of Saito *et al*. [70].

Shi *et al*. [96] postulated that rare earth elements play a key role in the growth of SWNTs due to their acetylide properties. Rare earth metals form chemical bonds with C_2^{-2} in the plasma. Metals, such as nickel and carbon nuclei of fullerene consist of conjugation π

bonds. During the growth process, the acetylide metal ion stays in the open cap end of the nanotube and at the same time draws nickel ions to the open area of the nanotubes. When the growing nanotube moves out of the high temperature region, the open cap closes and metal ions leave the end of the nanotubes. Thus, the acetylide metal plays a linkage role in the formation of SWNTs with nickel acting as the true catalyst.

Saito *et al*. [112] described the segregation of carbon from nanoparticles to form SWNTs. This laid the foundation for the segregation growth mechanism. Kanzow *et al.* [97] proposed the formation of SWNT bundles by a four stage growth process. The starting point for nanotube formation is a liquid metal particle that is saturated with carbon atoms. The saturation of carbon leads to segregation of carbon atoms to form graphene layer on the surface of the metal particle, as shown in Figure 3.47. At high temperatures, the kinetic energy per area at the particle interface is high enough to overcome the work of adhesion. The graphene plane detaches from the metal surface to form a fullerene cap. Addition of carbon atoms to the cap allows growth of the tube. Tube diameter depends on the diameter of fullerene cap, temperature and work of adhesion of the catalytic particles. As the metal particle cools down to solidify, large amounts of carbon atoms segregate from the metal particle to form caps that closes the tip and also encapsulates the metal particle thus making it inactive.

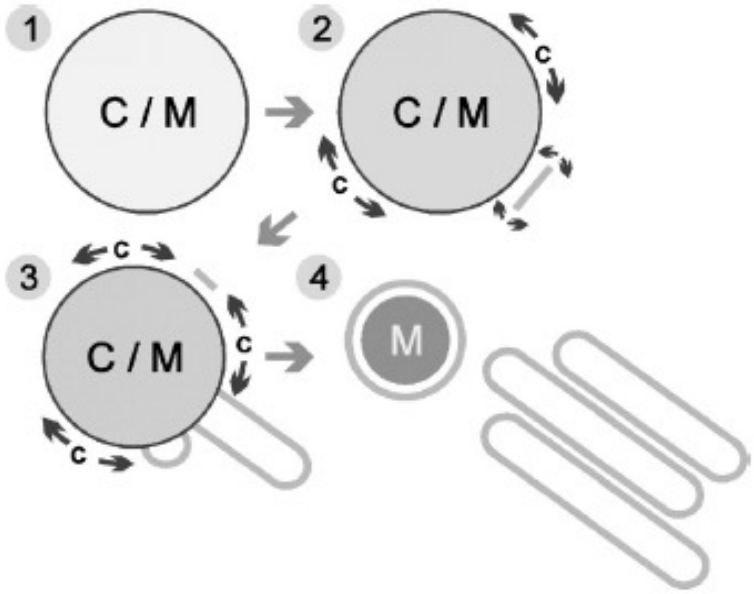

Figure 3.47 Growth model for ropes of SWNTs [97].

Kanzow *et al.* [97] also explained the formation of fullerene cap from highly symmetric flat graphite sheet (C_{48}) surrounded by metal atoms. When the bonding between metal atoms bound to two carbon atoms are removed, six pentagons are created at the border of the sheet, as shown in Figure 3.48b. Fullerene caps are formed when two pentagons from the edge diffuses into the center by two in-plane switches of C_2 units as shown in Figure 3.48 d. This transformation is called Stone-Wales arrangement and was used to explain isomerization reaction of fullerenes in 1986[110].

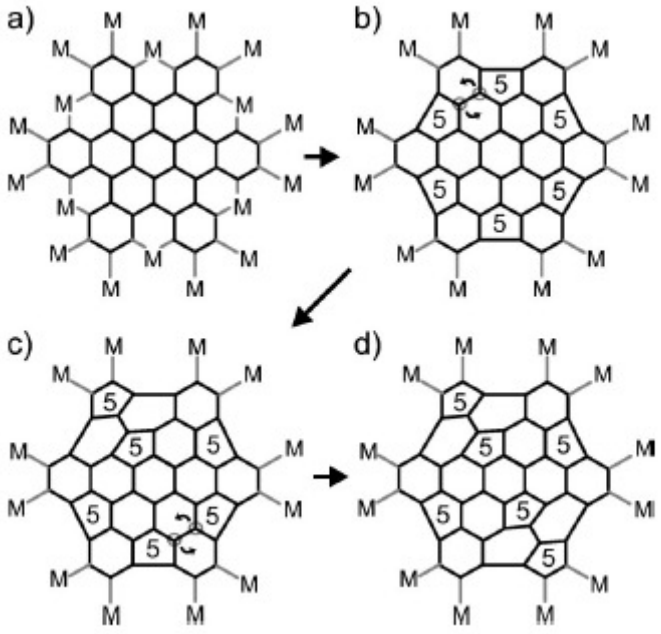

Figure 3.48 Formation of fullerene caps from flat graphite sheets by Stone-Wales rearrangement [97, 110].

Gavillet *et al*. [98] explained the formation of SWNTs bundles based on the work of Saito *et al.* [102] and extended the vapor-liquid-solid model to explain the growth of silicon whiskers. The formation of nanotubes can be divided into two stages namely, nucleation and growth.

During nucleation liquid nanoparticle of metal supersaturated with carbon is formed from condensation of metal plasma/vapor in the moderate temperature zone. The size of the nanoparticle is controlled by the gas pressure and the thermal gradient. The amount of carbon in the nanoparticle depends on the temperature and size of the particle. As the particle moves to colder region, the solubility of carbon decreases and carbon starts to segregate. Since carbon has very low surface tension compared to transition metal catalyst such as Ni, Co, or Fe segregation of carbon occurs through diffusion towards the particle surface. The segregation of carbon to the surface has been confirmed by MD simulations of metal carbon

clusters cooled from 2000 K to 1500 K at the rate of 100 K/ps. Simulations show that most of carbon atoms (~ 80%) segregate to the surface of the cluster while Co atoms migrate to the center of the cluster as shown in Figure 3.49. Further simulations show that carbon atoms at the surface form a network connected by linear chains and aromatic rings which play a crucial role in the growth process.

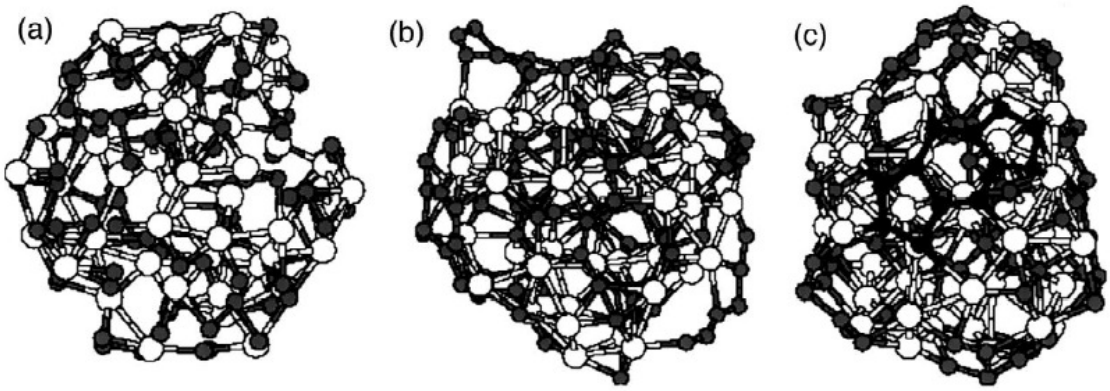

Figure 3.49 Segregation process of carbon (dark spheres) from cobalt (white spheres) [98].

Carbon crystallizes at the surface of a particle according to two competing transformation paths leading to the formation of graphitic sheets around the nanoparticle and nucleation of SWNTs. The formation SWNTs depends mainly on the segregation velocity. When the segregation velocity is high, carbon flux is very rapid and leads to the formation of islands or nucleation of tubes as shown in Figure 3.50c. At low segregation velocity carbon is progressively extruded and carbon gets organized by surface and bulk diffusion in the most stable configuration of graphene sheet, as shown in Fig 3.50b.

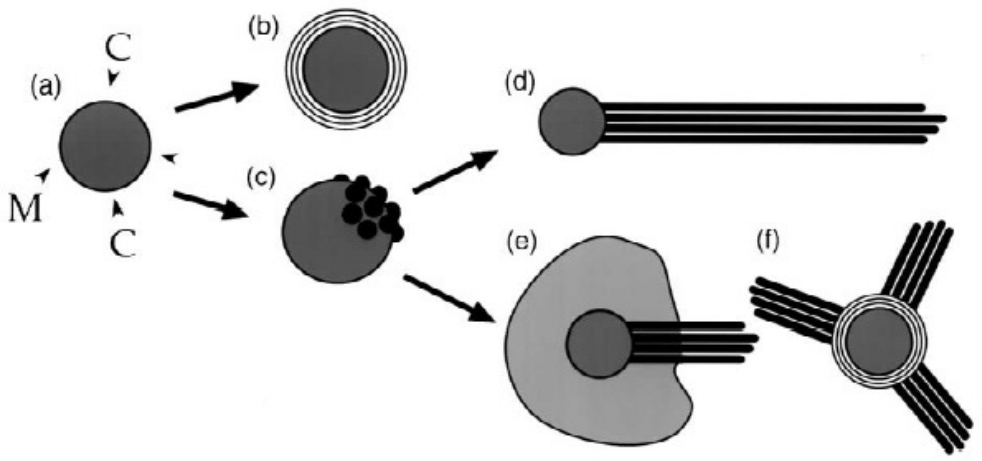

Figure 3.50, V-L-S model for nucleation and growth of SWNT ropes [98].

MD simulations show that SWNTs are formed by the root growth mechanism because the growth proceeds through further incorporation of carbon atoms at the root. During the growth process, the role of catalyst is to provide fluctuating Co-C bonds so that new carbon atoms are introduced continuously thus increasing tube length. Since carbon atoms present in the nanoparticle are not sufficient to produce SWNT bundles, carbon has to be supplied continuously from the vapor phase and should diffuse into the particle. The root growth mechanism continues until the local temperatures are too low leading to freezing of nanoparticles. For the formation of long bundles, the catalyst particle has to be active by maintaining the temperature and carbon atoms have to be supplied continuously. Rapid cooling of catalyst particles or lack of carbon atoms leads to the formation of baby ropes (3.50e, f) which is intermediate between nuclei and long bundle.

The above mentioned model has been confirmed by Ando *et al.* [48] using a modified arc plasma jet method where a low temperature gradient causes longer flight time in the high temperature region. Although V-L-S model helps to explain the nucleation and root growth mechanism, it fails to explain the optimum particle size.

Zhou *et al.* [99] explained the formation of SWNTs growing radially from YC_2 particles based on a two step process. During the first step, yttrium carbide particle is saturated with large amounts of carbon. The super saturation occurs at high temperature in the carbon rich region of the plasma. As the particle moves out of the plasma region, bundles of single-walled tubes grow from nucleation sites in all directions through interfacial reactions. The carbon atoms for the growth are supplied from gas phase.

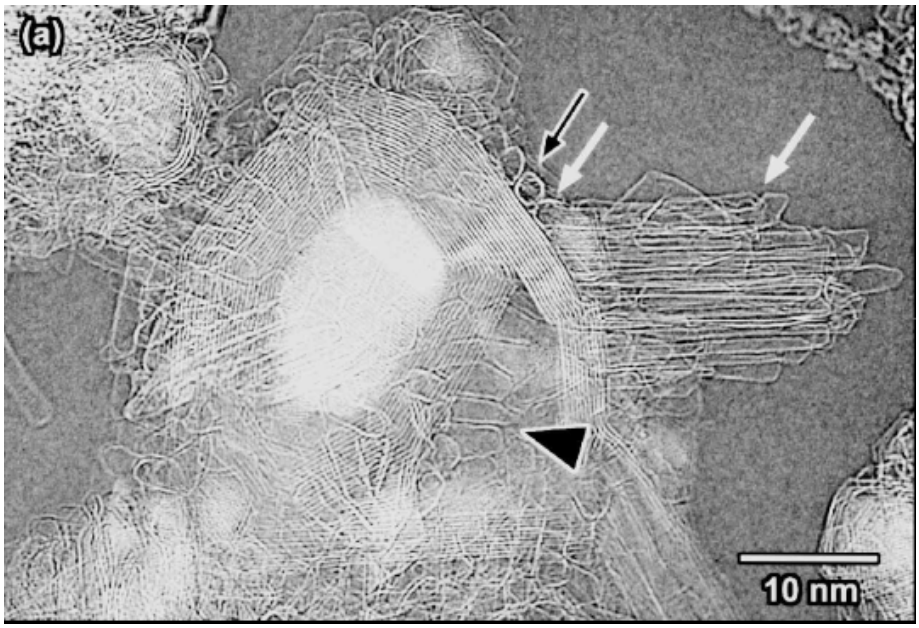

Figure 3.51 Formation of graphitic cages encapsulating metal carbide [99].

When the particle temperature falls below 2415^0 C, the segregation of supersaturated carbon atoms from the particle interior is favored. The segregation of carbon atoms leads to the formation of graphite layers at the particle surface thus making it catalytically inactive. The growth of nanotubes terminates once few graphitic layers are formed on the particle. Further segregation of carbon atoms causes the formation of successive graphite layers on the particle and also reduces the particle size. The segregation stops when pure yttrium carbide phase and graphitic cages are formed at the surface, as shown in Figure 3.51. The number of

graphitic layers appear to depend on the size of the particle, because larger the particle, thicker the cage. This can be explained by the fact that number of supersaturated carbon atoms increases with particle size. It is interesting to note that according to this model SWNTs grow initially before the segregation of carbon atoms which is contrary to models proposed by Gavillet *et al.* [98], Kanzow *et al.* [97] and Shi *et al.* [94,95,96].

Itkis *et al*. [100] studied the effect of Ni-Y catalyst percentage using solution phase near-infrared spectroscopy. When the nickel percentage is decreased below 4 at%, it does not alter the rate of soot production but it decreases the SWNT content in soot. This is explained by the fact that a decrease in nickel content causes lesser nucleation sites, thus decreasing the yield. An increase in nickel percentage suppresses the formation of SWNTs due to the fact that higher nickel content increases the nanoparticle size. Thus maximum yield of nanotubes is obtained with 94.8% Carbon, 4.2% Nickel and 1% Yttrium, as shown in Figure 3.52.

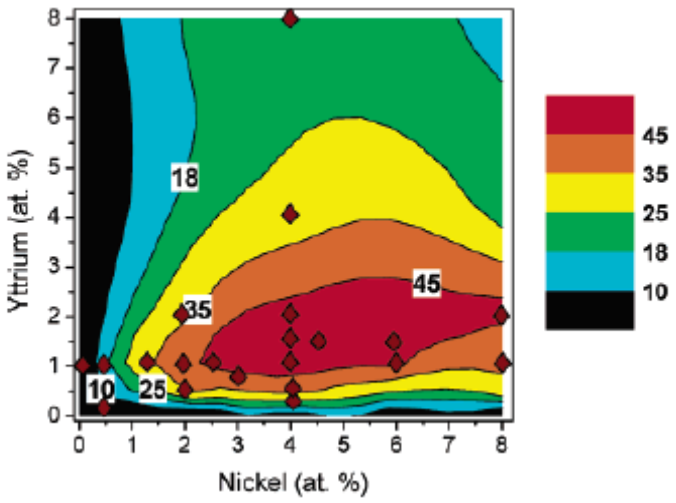

Figure 3.52 Contour plot of the relative purity of AP-SWNT soot as a function of Ni-Y composition [100].

Although a number of growth mechanisms have been proposed and explained theoretically, there is a lack of clear understanding of the growth process for both multi-

walled and single-walled nanotubes. The study of mechanism is hindered by the fact that there is no clear data on the arc temperature, temperature distribution, reaction rate, role played by the catalyst, buffer gas, and electric field.

3.8 Other forms of carbon

In the arc-discharge apparatus, apart from nanotubes other interesting forms of carbon has been observed and reported. These include carbon nanofibers, nano-onions giant fullerene particles.

3.8.1 Carbon nanofibers

Ugarte [103] reported the formation of graphite sheets during the study of C_{60} preparation in the arc-discharge apparatus. The use of amorphous carbon electrodes instead of graphite electrodes resulted in the formation of graphite sheet structures along with polyhedral particles. These particles have basal planes that are curved at the end and turning an angle of 360^0 and rejoining another sheet on the surface thus forming a folded sheet as shown in Figure 3.53.

Baker *et al.* [104] observed a very similar structure and classified them as carbon nanofibers. These nanofibers were found to vary from 5 μm to 100 μm in length and are 5-100 nm in diameter. The potential applications of these particles include energy storage devices and adsorption devices taking advantage of its high surface area and adsorption properties.

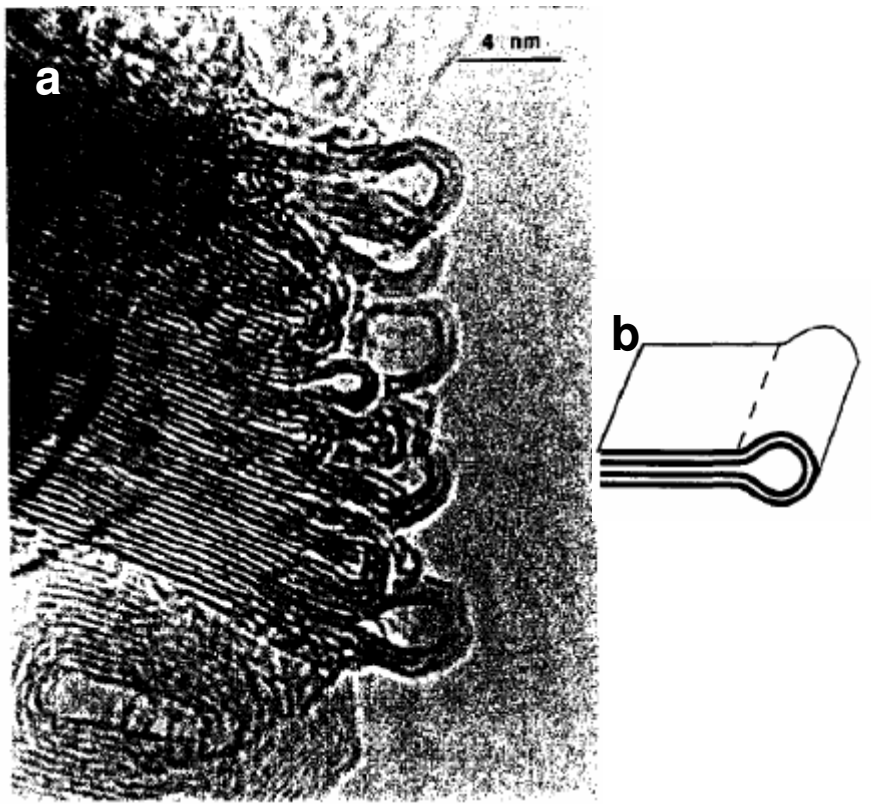

Figure 3.53 a) HRTEM image of a graphite particle produced by arc-discharge in helium atmosphere. The surface of basal planes are bent 360^0 to join another plane of the surface. b) the schematic of the basal planes [103].

3.8.2 Carbon nano onions

Ugarte [105] published a series of HRTEM images showing the transformation of carbon nanoparticles into an onion-like structure, as shown in Figure 3.54a. The particle begins with a hexagon shaped particle. The partial collapse of the structure leads to the elimination of the hollow cavity present at the center. The particle becomes more ellipsoidal due to graphitization of the surface layers. The particle evolves into a sphere with concentric shell structure becoming perfect. The hexagonal nanoparticles have also been reported by Saito [114] using rare earth elements as catalyst in the arc-discharge. Saito [114] observed that the particles are made up of concentric graphite sheets as shown in Figure 3.54b. The

hexagonal shaped particle which acts as initial source was initially reported by Graham *et al*. in 1961 [107] and Marsh *et al*. [108] in 1971.

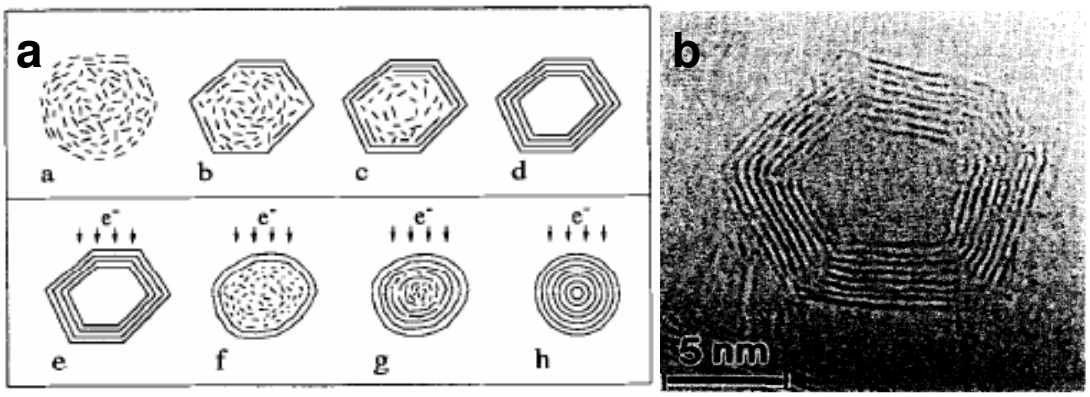

Figure 3.54 a) Schematic illustration of Ugarte's proposed mechanism of onion-like carbon structure formation [106], b) Polyhedral nanoparicle [114].

CHAPTER 4

PROBLEM STATEMENT

Commercial applications of CNT-based composites and flat panel displays can be realized only if nanotubes are grown on a large scale, economically. Thus there is an increasing interest in the large scale synthesis of carbon nanotubes. Methods such as laser ablation, plasma assisted CVD and high pressure carbon monoxide (HiPCO) process can synthesize CNTs only on the order of few grams per day. The DC arc-discharge method is a simple and inexpensive method to grow nanotubes on a large scale to the high vaporization rate of graphite electrode. The same apparatus can be used to grow SWNTs by introducing metal catalyst in the anode.

The objective of the present investigation is to construct an arc-discharge apparatus using a welding equipment to synthesize multiwalled and singlewalled CNTs on a large scale. The first part of the study is aimed at finding the ideal conditions for the synthesis and purification of MWNTs. The second part of the study is aimed at finding the optimal conditions for the synthesis of SWNTs as well as understanding the growth mechanism. The study involves the analysis of yield by varying the process parameters such as process gas, chamber pressure, anode-cathode distance, effect of catalyst, purification time, and temperature.

CHAPTER 5

EXPERIMENTAL SETUP AND METHODOLOGY

5.1 EXPERIMENTAL SETUP

A D.C. arc-discharge apparatus in the vertical configuration was constructed to synthesize CNTs using an arc welder as shown in Figure 5.1. A Pyrex bell jar (12.5" OD, 3/16"thick and 18" high) was used as the chamber. It was inverted to place the open end at the top. A silicone gasket was fixed on the chamber wall to seal the bell jar. Sand was used to fill the spherical bottom part of the bell jar to a height of ~ 4 in. A copper cathode holder was used to firmly fix the 2" diameter graphite cathode. The cathode holder with the graphite rod was placed on the top surface of sand. The presence of sand greatly reduces the heat transfer from the cathode to the glass walls thus reducing thermal stresses. The bell jar was placed inside a steel cage to protect the operator from any damage. A steel framework was built around the steel cage and placed on a wooden cart to move the equipment as needed. Figure 5.2 shows the schematic of the experimental set-up.

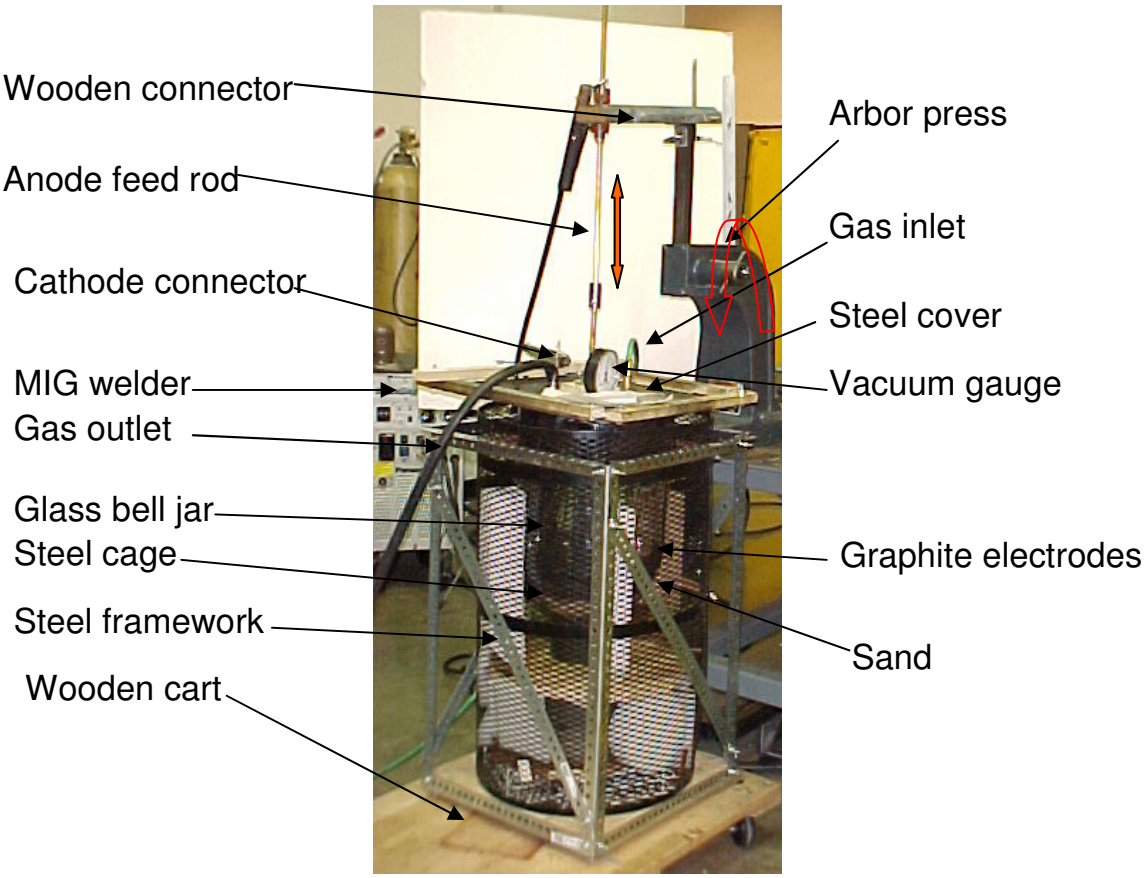

Figure 5.1 Photograph of D.C. arc-discharge set-up for the synthesis of CNTs

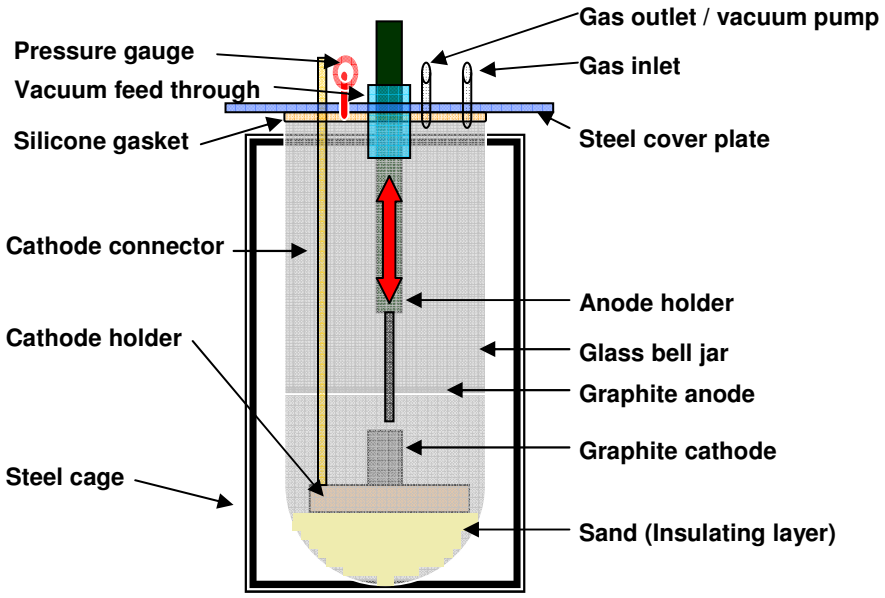

Figure 5.2 Schematic of D.C. arc-discharge setup

A steel plate 0.25” thick, 14” x 14” was used to cover the bell jar as shown in Figure 5.3. On the steel cover plate the following connectors were fixed, namely, a vacuum gauge, a vacuum feed through, a cathode connector, gas inlet and gas outlet. A vacuum gauge (0 to -30”) was used to continuously monitor the chamber pressure. Brass ¼ NPT connectors were used to supply the desired gas and to evacuate the chamber to the desired pressure. The gas inlet was connected to the desired gas cylinder and the gas outlet was connected to domestic vacuum pump. A 0.6” rubber cork with a 0.2” copper rod was fixed on the steel plate to connect the cathode to the welding machine. A vacuum feed through was designed and constructed to continuously feed the anode towards the cathode. To protect the gaskets in the vacuum feed through, a 0.40” diameter brass rod with mirror like finish was permanently fixed in the vacuum feed through. The graphite anode was firmly fixed to the permanent brass rod during the experiments. Four wooden blocks were fixed on the edges of the cover plate, to clamp the cover plate with the steel support as shown in Figure 5.3. The chamber was tested for leaks before conducting the experiments, minor leaks in the junctions were sealed using high vacuum grease.

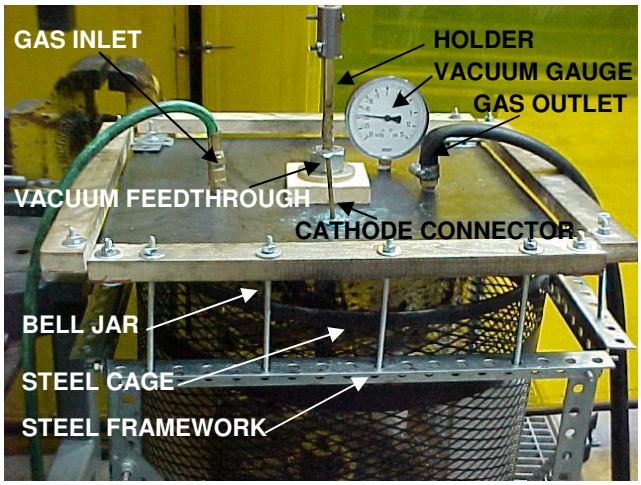

Figure 5.3 Top plate of chamber with the accessories.

An arbor press was used to continuously feed the anode during the experiment. A wood holder was used to connect the arbor press to the anode holder. The anode is moved along its axis by rotating the arbor press handle. The DC arc welding apparatus was used to supply current to the anode. The exact arrangement of the apparatus is shown in Figures 5.1 to 5.3. Figure 5.4a shows the apparatus during the experiment, the bright region seen is due to the formation of high temperature arc. Figure 5.4b and Figure 5.4c shows the anode and cathode before and during the experiment.

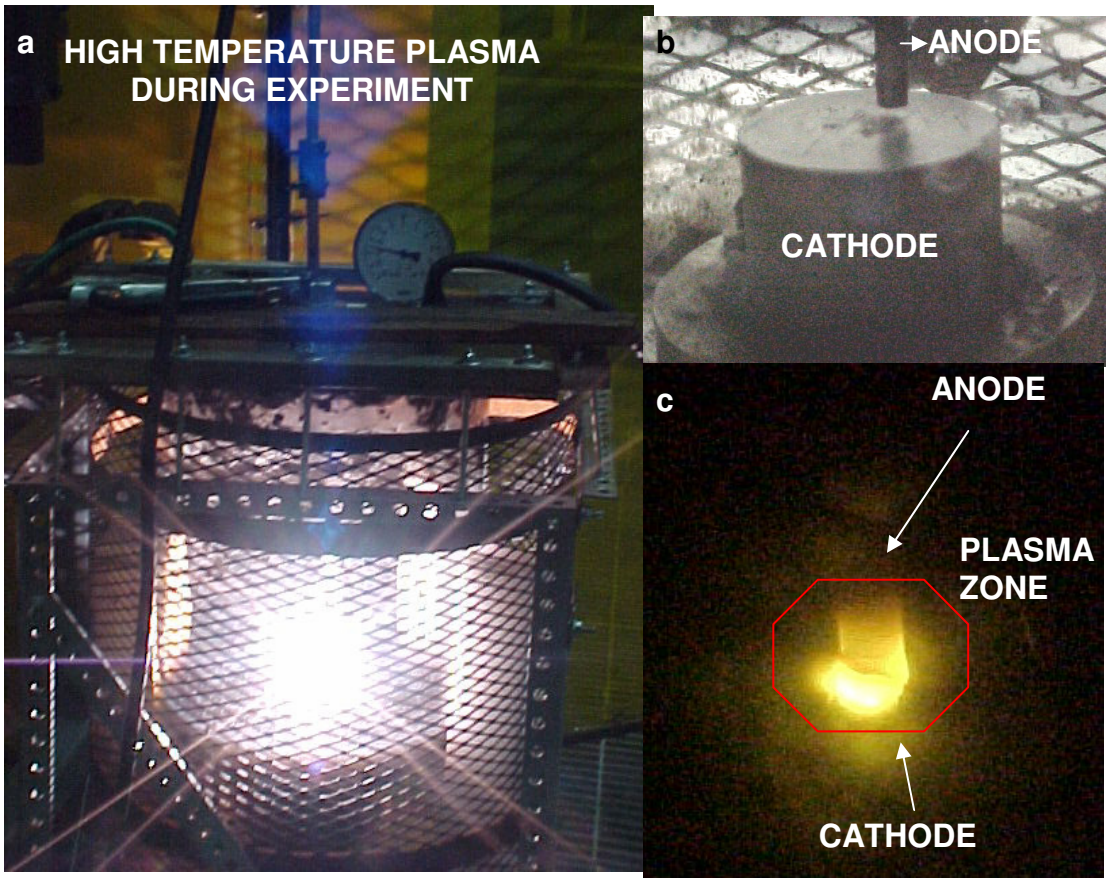

Figure 5.4 High temperature arc formed during the experiment.

5.2 Methodology

5.2.1 Anode preparation

For the synthesis of MWNTs, the as received 0.25" diameter graphite rod was used. For the synthesis of SWNTs, the graphite rod is filled with the desired catalyst with the desired composition. The metal particles should be evenly distributed so that the carbon-metal nanoparticles are even in composition during the experiment. Calculations show that 0.125" diameter hole for 1" long, needs 0.2846 g of nickel, 0.1369 g of Y_2O_3 and 0.2757 g of graphite. The desired metal mixture is mixed thoroughly and filled into the anode in steps of 100 mg. The graphite-metal mixture is compressed regularly using a drill bit to obtain maximum density and uniform distribution of metal particles in the anode. Usually the anodes are prepared in batches of five to save time and maintain uniformity.

5.2.2 Experimental procedure

a) The anode is fixed to the anode holder and the 2 in diameter cathode is fixed to the cathode holder.
b) The chamber is sealed using a steel plate and gaskets with the help of clamps. The chamber now is pumped down to ~ 50 torr and helium is let into the chamber until it reaches 700 torr. This process of evacuating and refilling is repeated three times to remove trace amounts of atmospheric gases. The helium pressure is set at the desired operating value.

c) The anode holder is connected to the negative terminal and cathode to the positive terminal of the welding machine. Then the welding machine is turned on with the desired current.

d) The anode is slowly brought in contact with the cathode to strike an arc. The anode is moved back so that a continuous arc is formed.

e) The anode is continuously fed towards the cathode so that the anode-cathode gap is maintained constant during the experiment. The arc is continuously observed and monitored using a welding mask.

f) After the experiment, the welding machine is turned off and the whole system is allowed to cool for 15 mins.

g) After 15 mins the chamber is evacuated to ~ 100 torr and refilled with helium. This step eliminates any harmful gas that is produced during the experiment. The process of evacuation and refilling is done twice in SWNT experiments.

h) The cathode, cathode deposit, and soot on the chamber walls are removed and used for analysis.

5.2.3 Precautions

It should be remembered that this process uses very high current, produces very high temperatures, and intense plasma zone. The following safety measures should be followed, apart from the safety precautions normally followed during welding.

1. Only non-combustible gases should be used in the chamber. This chamber is not designed for gases such as methane, acetylene or hydrogen.
2. The plasma zone should not be viewed without the welding mask to protect eyes.

3. The operator should not touch any part of the chamber including the cage once the welding machine is turned on.
4. The evacuation procedure should be followed to protect the operator from any harmful gases that may be produced during the experiment.
5. The arc current should not exceed 150 A to protect the vacuum feed through gaskets.
6. The experiment time should not exceed 15 mins, because the gaskets in the vacuum feed through has a melting point of 350^{0} C.
7. The vacuum feed through should be greased at regular intervals,
8. After the experiment the cathode should be allowed to cool for at least 15 min before further handling. The cathode should always be handled with welding gloves since it could be very hot.

CHAPTER 6

RESULTS

6.1 Introduction

Experiments on the growth of multi-walled and single-walled carbon nanotubes were conducted under different process conditions. They were varied to study their effects on the growth of nanotubes and were mainly focused on obtaining maximum yield of the carbon nanotube raw material. The key process parameters investigated are process gases, gas flow rate, chamber pressure, and effect of catalyst. Additionally, the effect of time, temperature and air flow have been investigated in the purification of MWNTs.

Once the experiments were conducted, the cathode containing CNTs were characterized using a scanning electro microscope. Carbon or gold-palladium coating was used for SWNT samples. Transmission electron microscope (TEM) was used to study the tube morphology, tube tips, and effect of purification. These techniques were used to understand the growth mechanism of SWNTs.

6.2 Arc stability

Arc stability or the noise produced during the experiment plays a very important role in the synthesis of MWNTs. A stable arc was found to be a necessary condition for continuous synthesis of MWNTs containing black core material. With extensive experiments it was established that a stable arc produces minimum noise, minimum amount of outer hard shell, and maximum amount of black core material. The arc stability can be increased by maintaining constant anode-cathode distance, and decreasing the anode-cathode distance, the current density, gas pressure and the gas flow rate. An unstable arc produces a cathode deposit that is made of number of circular plate-like structures stacked on one another with no hollow core as shown in Fig. 6.1. A stable arc produces a cathode deposit that is lustrous at the outer surface and is hollow in the inner region as show in Fig 6.1. Similar observations were made by Ebbesen *et al*. [24].

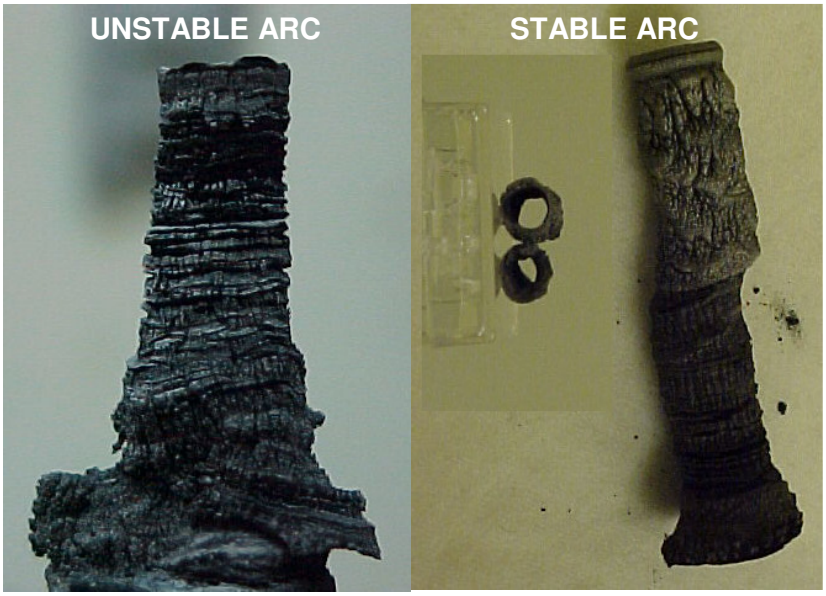

Figure 6.1 Cathode deposit produced by an unstable arc and stable arc.

6.3 Effect of buffer gas

Initial experiments were performed with argon and helium gases in the chamber. Argon generated an arc that was extremely unstable and noisy. It was also difficult to control the anode-cathode distance. Apart from the unstable arc, the chamber pressure during argon experiments increased by at least 150 torr during the experiment. For example when the chamber pressure was set at 420 torr, the pressure increased to 570 torr during the experiment. The chamber pressure decreased back to 420 torr slowly after the experiment. No such variation in chamber pressure was noticed in the case of helium. In the case of argon the arc was stabilized by reducing the chamber pressure or by decreasing the anode-cathode distance. The cathode deposit formed in argon gas was mainly made of hard shell along with MWNTs. The arc in the case of helium was stable and it was easy to control the anode-cathode distance. Table 6.1 shows the amount of graphite anode consumed, cathode deposit formed and MWNTs containing material with helium and argon. The experiments were conducted using 75 A direct current for 5 mins. Figure 6.2 shows the SEM image of the MWNTs formed using argon and helium gas.

Table 6.1 Effect of buffer gas on MWNTs yield

S.No	Gas	Gas pressure (Torr)	Anode consumed (g)	Cathode deposit (g)	MWNTs material (g)
1	Argon	330 (Initial)	0.7081	0.4473	0.05
2	Argon	440 (Initial)	0.5879	0.3752	0.08
3	Helium	340	1.5252	0.9714	0.137
4	Helium	430	1.0178	0.6215	0.10

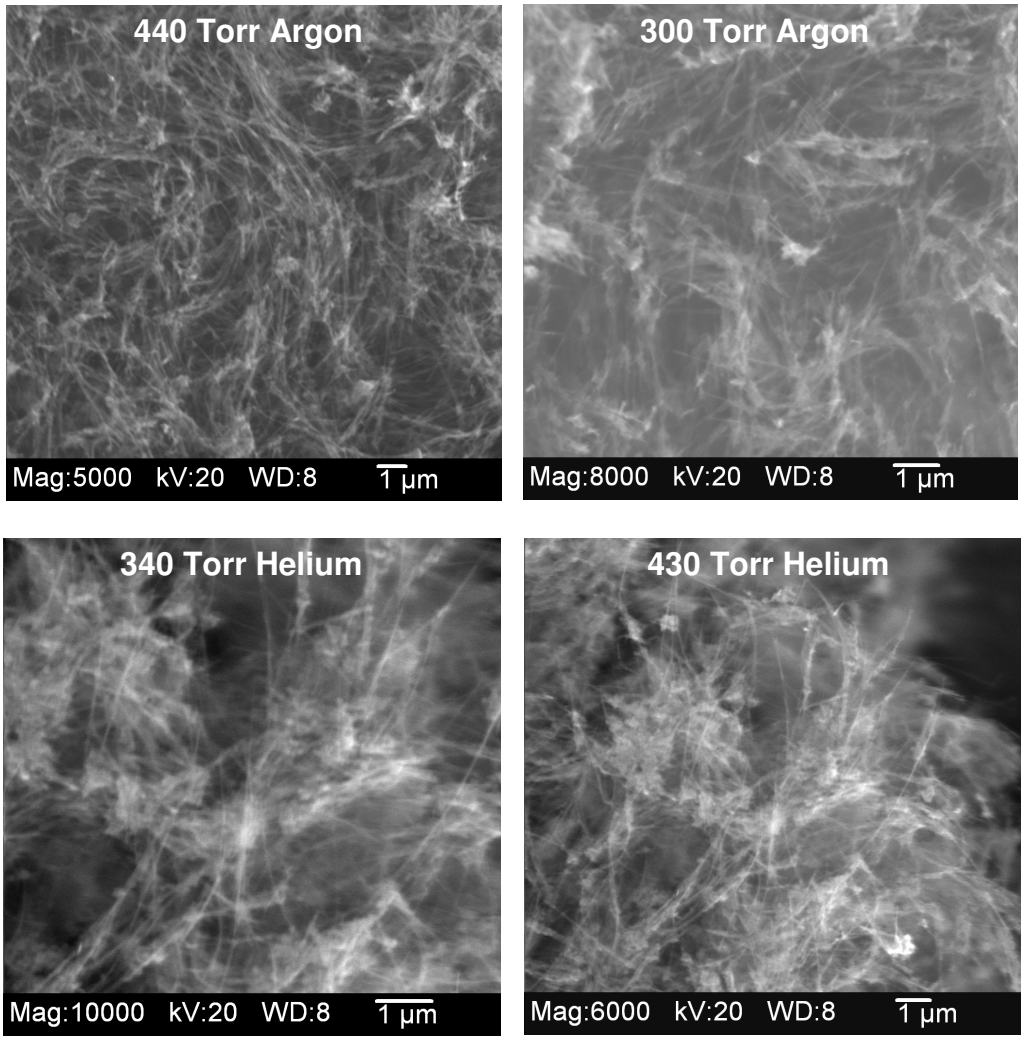

Figure 6.2 SEM micrographs of MWNTs grown in argon and helium.

With both gases, the MWNTs are formed along with amorphous carbon and are randomly oriented. Due to the synthesis of large amount of MWNTs, no conclusion can be drawn regarding the effect of gas on length, diameter or the purity of tubes produced. In both gases the tubes are a few micrometers in length and have almost a uniform diameter. Considering mainly the chamber pressure and arc stability in addition to the vaporization rate, cathode deposit and MWNTs containing material produced, helium was used for further study.

6.4 Effect of helium pressure

Since chamber pressure during the experiment determines the anode evaporation rate and quantity of cathode deposit [51], this was studied systematically. The aim is to find the optimum helium pressure for the synthesis of maximum amount of cathode deposit. The current was maintained constant at 75 A, and anode-cathode distance ~ 2 mm throughout the experiment and helium gas pressure was varied. All experiments were conducted under identical conditions for 5 mins. Table 6.2 gives details of the process parameters, evaporation rate, and deposition rate for different helium gas pressures. The fibrous core material was used for further analysis in the SEM, and TEM and used for further purification studies. From Table 6.2, it can be observed that there is a difference between mass of anode consumed and cathode deposit. This is accounted by formation of collar deposit on the cathode surface as shown in Figure 6.3. The collar deposit was observed at all helium pressures. At helium pressure above 650 torr, the arc was very unstable and led to the formation of a cathode deposit with many circular plate-like structures, as show in Figure 6.1 with very sparse growth of MWNTs. With decrease in helium pressure, the arc stability increased and the cathode deposit formed with MWNTs contained fibrous core. The arc became very stable and noiseless at pressures of 253 torr and below.

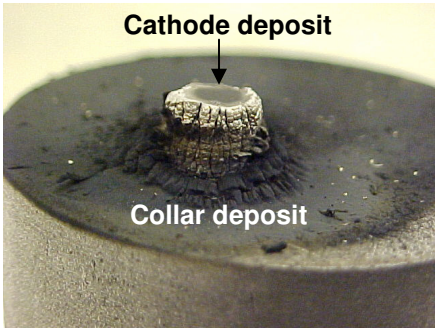

Figure 6.3 Cathode and collar deposit.

Table 6.2 Effect of helium pressure on cathode deposit

S. No	Helium pressure (Torr)	Anode consumed (grams)	Cathode deposit (grams)
1	545	0.7516	0.5464
2	506	0.8218	0.5338
3	470	0.9105	0.6122
4	430	1.0178	0.6215
5	374	0.9556	0.6127
6	365	1.0591	0.7412
7	355	1.417	0.9969
8	340	1.5252	0.9714
9	315	1.4981	1.0997
10	291	0.8402	0.5922
11	253	0.795	0.5241
12	190	0.6103	0.3936
13	150	0.7185	0.4648
14	140	0.8264	0.5548
15	120	0.7772	0.5241
16	110	0.6877	0.4294

Figure 6.4 shows photographs of the cathode deposit, the scale is included to estimate the variation of deposit length with pressure. The length of the cathode deposit increased with decrease in pressure and reached a maximum of 15 mm at a helium pressure of 315 torr. Any further decrease in helium pressure led to a decrease in length of the cathode deposit. The diameter of the cathode deposit remained between 8 to 10 mm at all pressures.

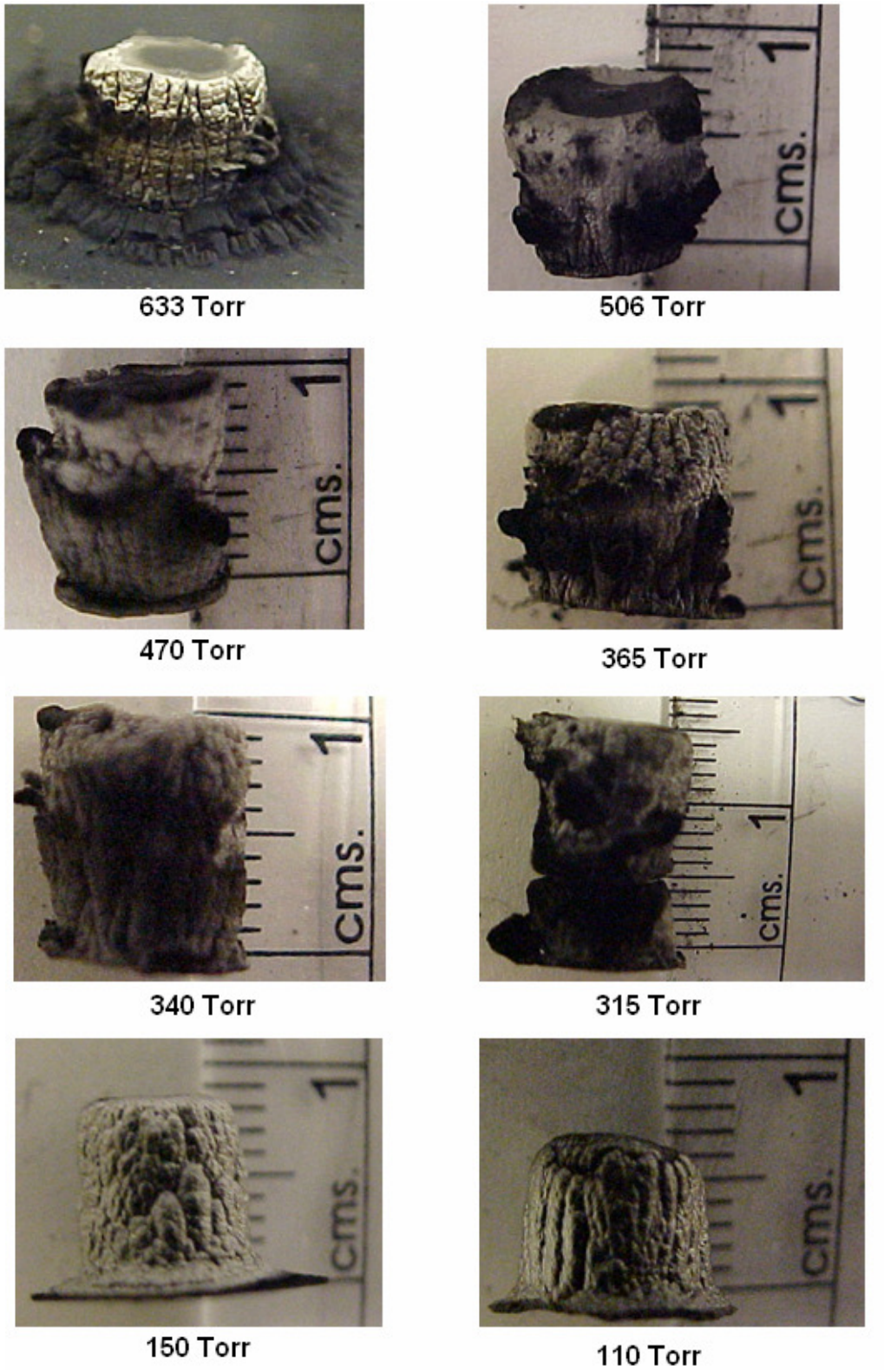

Figure 6.4 Photographs of the cathode deposits formed at different helium pressures.

6.4.1 Anode consumption

The variation of anode consumption with pressure is shown in Figure 6.5. The anode consumption rate was found to be a function of the helium pressure. At pressures above 650 torr the arc was very unstable and the consumption rate was found to be ~1.1 g in 5 mins. Even though the consumption rate was high, MWNTs containing core material was not formed.

With decrease in pressure to 633 torr, a stable arc was generated with inner fibrous core. In the pressure range of 370 to 540 torr, the anode consumption increased very gradually from 0.75 to 0.95g. With further decrease in helium pressure below 370 torr, the anode consumption increased very rapidly and reached a maximum value of 1.52 g at a pressure of 342 torr. Any further decrease in helium pressure below 316 torr decreased the anode consumption and it always remained below 1 g.

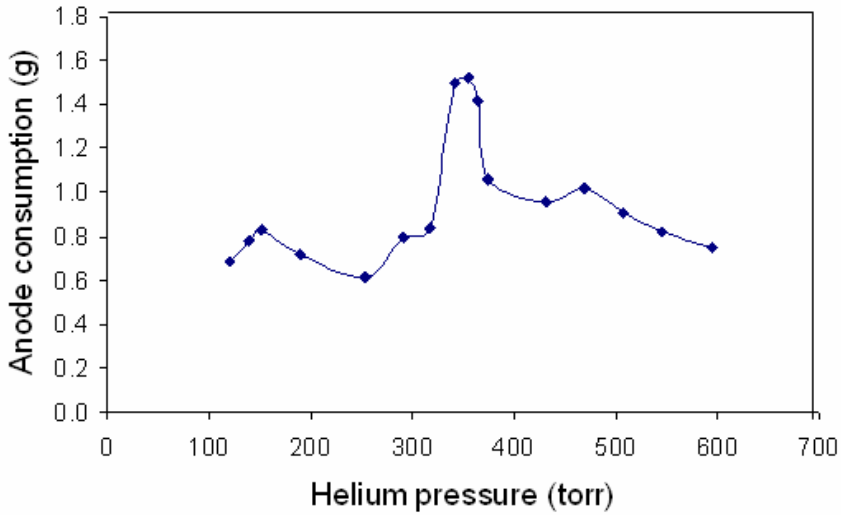

Figure 6.5 Variation of anode consumption with pressure

6.4.2 Cathode deposit

Figure 6.6 shows that cathode deposit varies with helium pressure. The mass of the cathode deposit was found to be function of helium pressure similar to anode consumption. At pressures above 650 torr, the cathode deposit formed was less because of unstable arc. The cathode deposit with fibrous core was formed at all pressures below 633 torr. . A collar deposit was also formed around the cathode deposit. This accounts for the difference in the mass of vaporized anode and cathode deposit.

The quantity of the cathode deposit remained in the range of 0.54 to 0.67 g for pressures between 374 to 545 torr. At pressures below 374 torr, there was a steep increase in the cathode deposit reaching a maximum of 1.09g at 316 torr. Below 300 torr the cathode deposit remained less than 0.6 g. It was also noted that the arc was extremely stable at pressures below 250 torr. The arc became self staining at these low pressures i.e. the rate of evaporation was equivalent to the rate of deposition on the cathode. This completely eliminated the need of manual feed for anode towards the cathode.

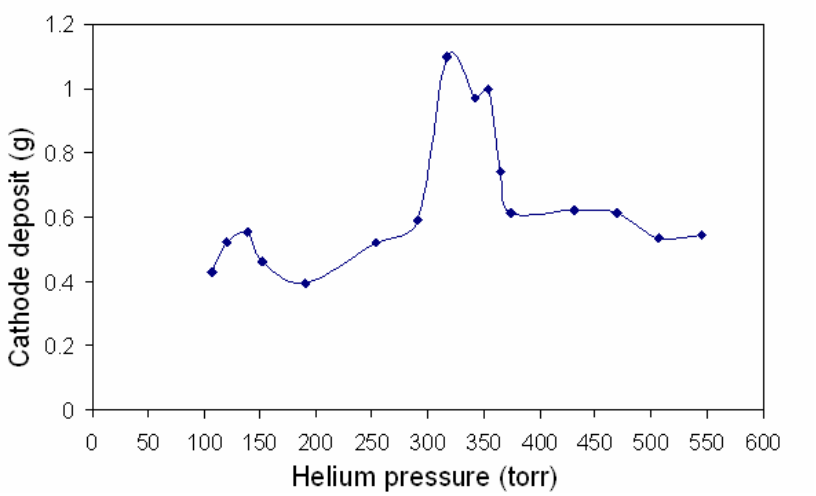

Figure 6.6 Variation of cathode deposit with pressure

When the chamber pressure was maintained between 315 to 355 torr, ~70% of the evaporated anode material was deposited on the cathode as cathode deposit. This pressure range was found to be optimum for the synthesis of MWNTs. The cathode deposit formed at 340 torr was split open and dispersed in 50 ml of acetone, using an ultrasonic bath (Cole Parmer 80 W, 56 KHz) for 30 mins. The hard shell pieces was filtered out and dried for 48 hours in air. The weight of the shell was measured to calculate the mass of the core. The difference in weight of the cathode deposit and shell was found to be 137 mg. Since this is formed in 5 mins, the rate of production is calculated to be 27.4 mg/min. This yield is higher than the yield reported, 24 mg/min by Cadek *et al.* [111] or Zhang *et al.* [51].

6.4.3 SEM analysis of cathode deposit

SEM was used to study the morphology of the cathode deposit and MWNTs. The cathode deposit was found to be made up of large number of needle-like material, as shown in Figure 6.7a. The length of the needle-like material ranges from 1 to 5 mm and ~5μm in diameter.

The needle-like material consists of bundles of randomly oriented MWNTs covered with an outer layer of amorphous carbon as shown in Fig. 6.7b. The individual MWNTs in a bundle are a few micrometers long and are held together by amorphous carbon. This fibrous core material was produced at all pressures below 633 torr of helium but the quantity of the core varied as a function of pressure, as discussed earlier.

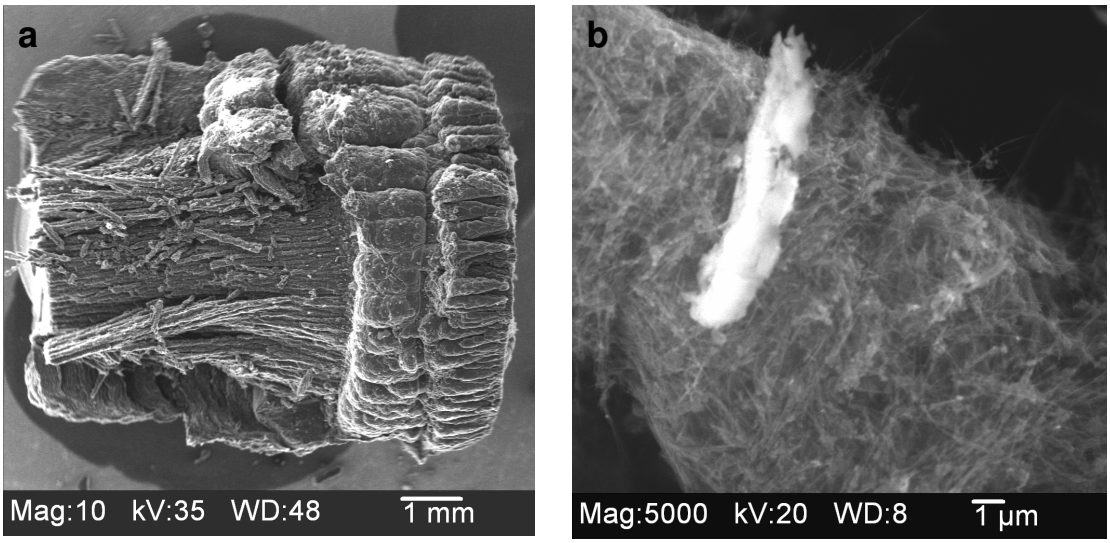

Figure 6.7 SEM micrographs of (a) cathode deposit (b) Fibrous core

The SEM micrographs of nanotubes grown at different helium pressures are shown in Figures 6.8. From the micrographs it is not possible to conclude the variation of MWNTs diameter, length or purity because a large amount of MWNTs containing material is formed. Therefore the focus here is the variation of cathode deposit and the purification of MWNTs produced at different pressures.

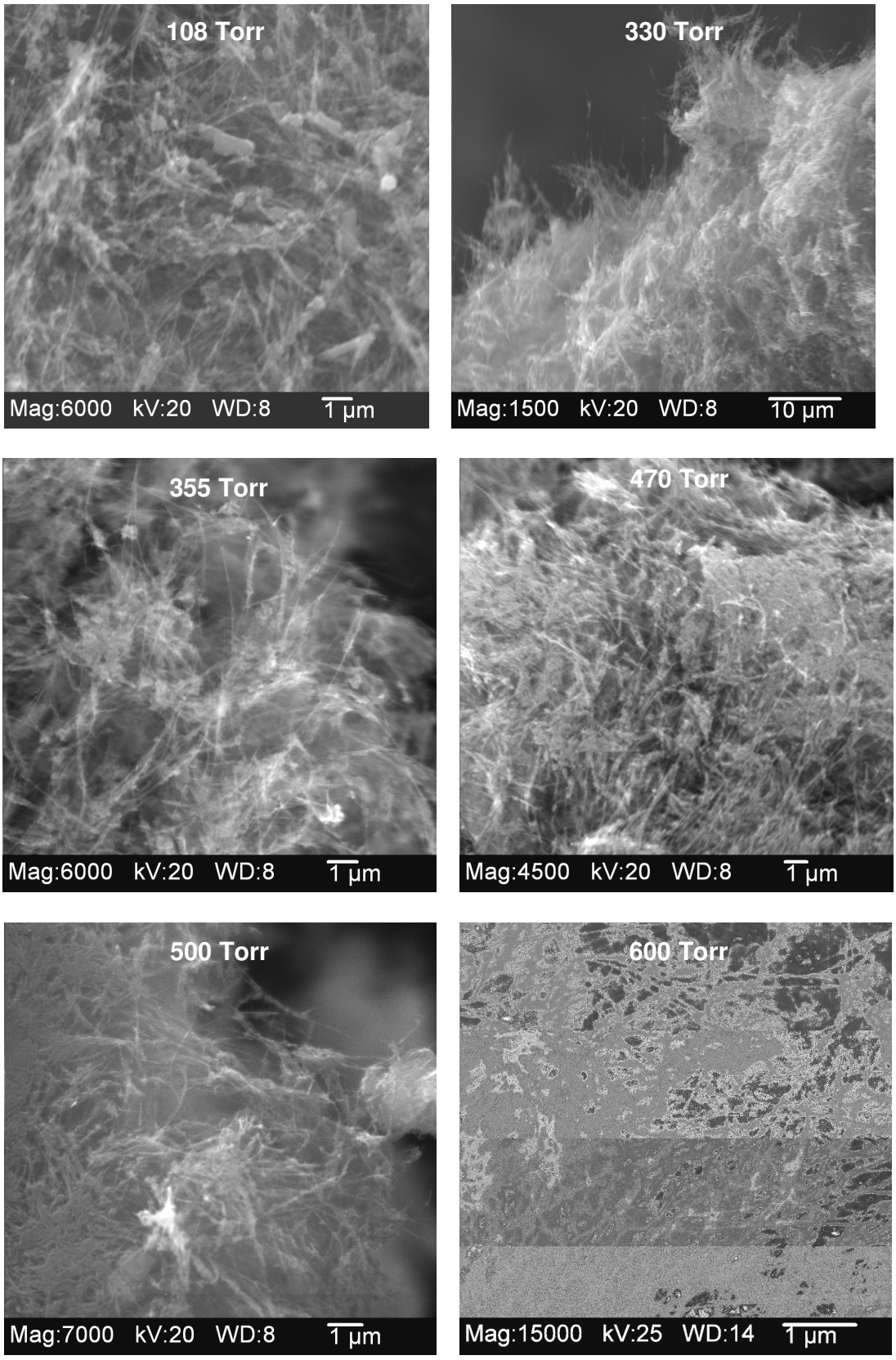

Figure 6.8 SEM micrographs of MWNTs produced at different pressures

6.5 Purification of MWNTs

Purification of arc-produced MWNTs was studied systematically by varying time, temperature, and air flow. The as-produced MWNTs co-exist along with amorphous carbon and carbon nanoparticles as seen in the TEM micrograph in Figure 6.9. Most of the MWNTs are heavily covered with carbon nanoparticles along the cylindrical surface and at the tube ends. They appear to bond together at the ends by amorphous carbon as seen in Figure 6.8.

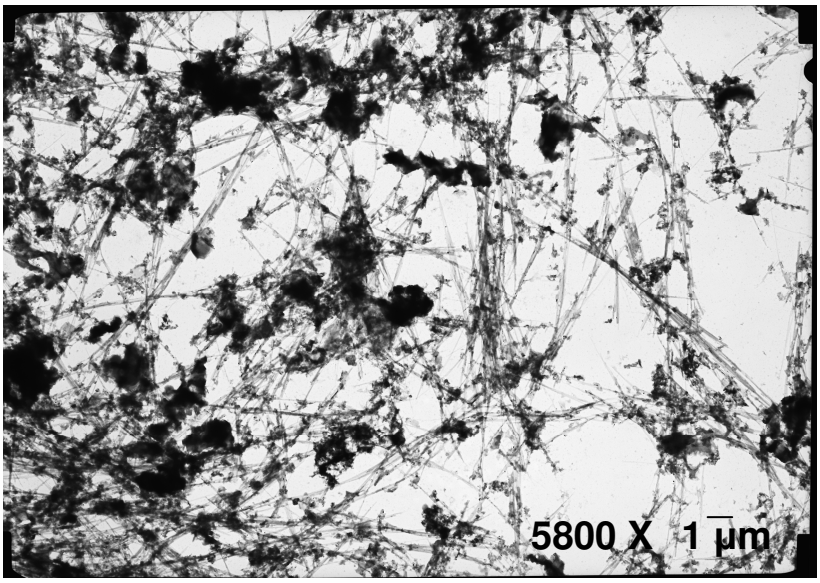

Figure 6.9 TEM micrograph of as-produced MWNTs

The ideal purification process must remove the carbon nanoparticles and amorphous carbon without causing any damage to the nanotube tips, length, or diameter. One way to remove amorphous carbon and carbon nanoparticles is by oxidation in air at temperatures of 700^0 C or above. It has been reported [65, 66] that amorphous carbon and carbon nanoparticles have a higher oxidation rate and lower oxidation temperature compared to carbon nanotubes [65, 66]. Every purification process exploits this phenomenon to eliminate amorphous carbon. The oxidation conditions must be such that process must be stopped once

the carbon nanotubes begin to oxidize. The main parameters investigated in this study are oxidation temperature, time, and effect of air flow. From the literature [65, 66, 67, 68] and from initial experiments, the ideal oxidation temperature to be in the range of 700^0 C and 760^0 C with a heating time from 5 to 30 mins.

At temperatures below 700^0 C, long amounts of time (> 1 hour) is required to remove the amorphous carbon. Long heating times lead to the oxidation of nanotubes and damage to nanotube surface. This study was aimed at finding the optimum oxidation temperature and time where the amorphous carbon is alone oxidized leaving carbon nanotubes intact. In this study, 16 samples were prepared from the black core material and subjected to different oxidation treatments (temperatures and time).

The first step in the purification process is dispersion. The as-produced nanotube material was dispersed in a non combustible medium, water in this case. An ultrasonic bath was used to accelerate the dispersion process where ultrasonic waves are used to break the physical bonds between amorphous carbon and MWNTs. In this study, 1 gram of as-produced MWNTs containing material was dispersed in 300 ml of water using an ultrasonic bath (Cole Parmer 80 W, 56 KHz) for 2 hours. The 300 ml solution was divided into 16 parts and classified into four batches of four samples each. The dispersed mixture was placed in a 3 in diameter by 0.5 in deep ceramic plate and tested for different conditions. Thermolyne furnace (1488 W) was used to heat the samples in a controlled environment. The furnace was turned on and allowed to reach the desired steady state temperature before conducting the experiments. During the first two batches a fan was used to blow air continuously into the furnace from the top to introduce fresh oxygen molecules. Four samples were placed in the

furnace and the samples were removed one by one after the desired time. Methanol was added to the ceramic container to disperse the sample for further analysis. The dispersed samples were observed in a TEM to analyze the effect of time, temperature and air flow.

6.5.1 Batch 1

Table 6.3 gives details of the variation of oxidation time with temperature maintained at 700 ^{0}C.

Table 6.3 Effect of purification time

S. No	Temperature (^{0} C)	Time (mins)	Air flow	Result
1	700	5	Yes	Amorphous carbon present
2	700	10	Yes	Amorphous carbon reduced
3	700	15	Yes	Amorphous carbon removed
4	700	20	Yes	Tubes oxidized

Figure 6.10 shows the TEM micrographs of the oxidized samples. It can be seen that heating for 5 mins did not cause any change in the amount or particle size of amorphous carbon. Further heating for 10 mins resulted in decrease in the size of amorphous carbon particles due to the oxidation of amorphous carbon. Heating, for 15 mins completely oxidized the amorphous carbon attached to the tube surface and heating further for 20 mins resulted in extensive oxidation of the nanotubes. The damage to the nanotube surface can be observed in S4 where the oxidation has been initiated at 2 or 3 points along the surface.

Closer observation of the TEM micrographs showed that the tubes are closed in the first three samples and are open ended in the fourth sample, as shown in Figure 6.11. This suggests that the tubes are oxidized starting from the tips, then the oxidation proceeds along the axis. The absence of open tips in the 15 min sample suggest that tubes are not destroyed when heated for 15 mins at 700^0 C, as shown in Figure 6.11.

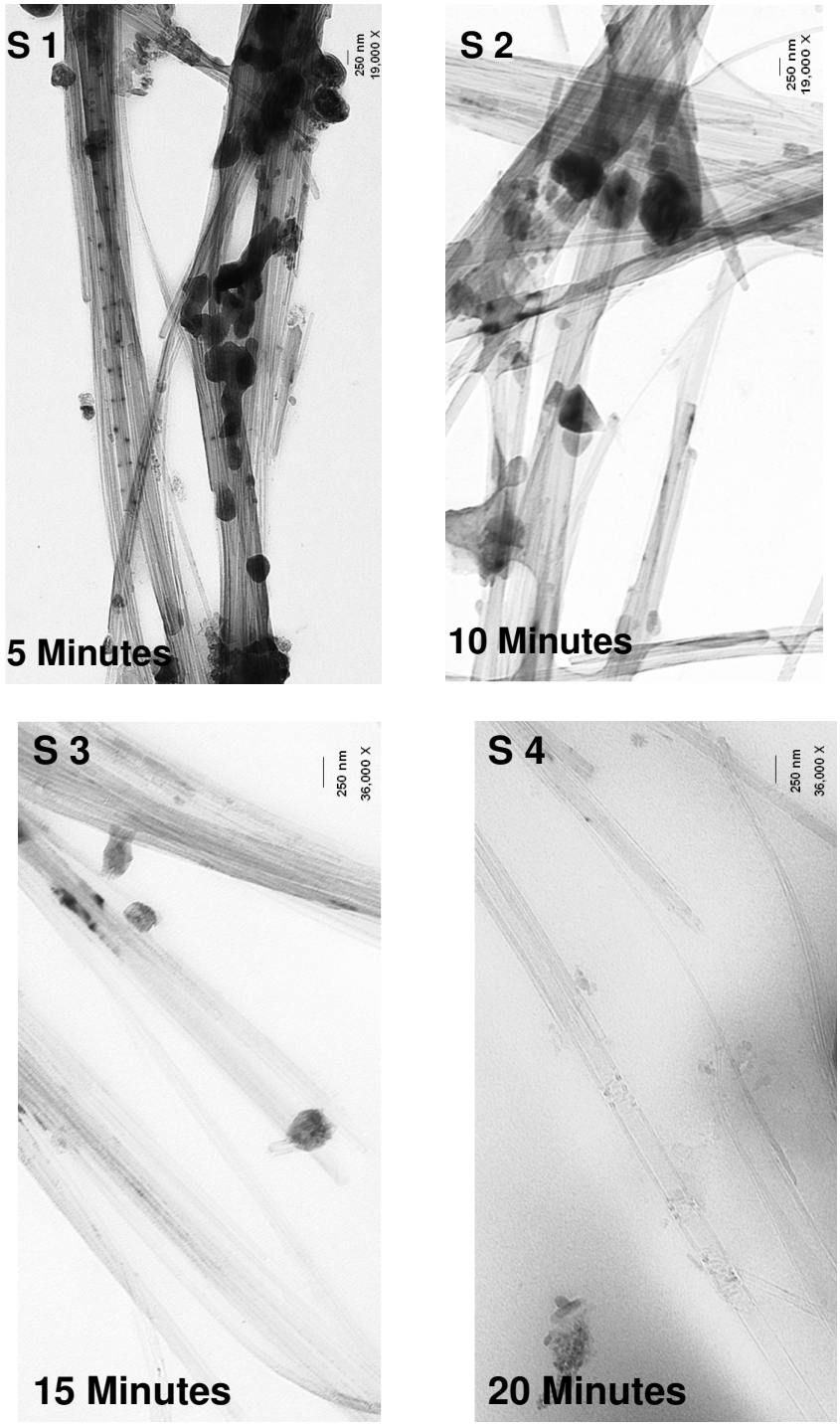

Figure 6.10 Effect of purification time of MWNT samples heated at 700^0 C with air flow

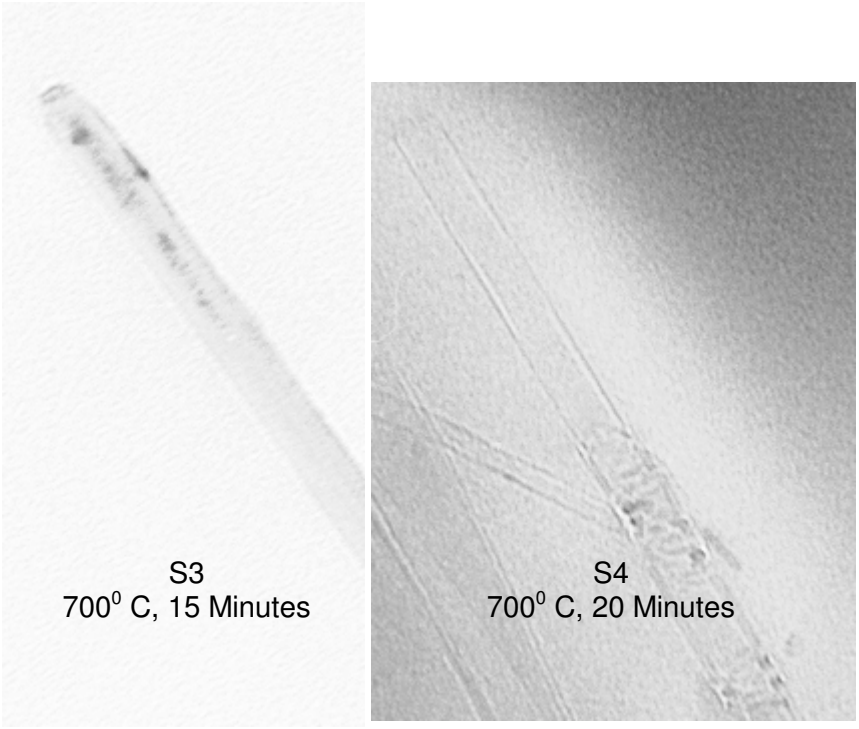

Figure 6.11 Nanotube tip after heating at 700^0 C for 15 and 20 mins

6.5.2 Batch 2

Table 6.4 gives details of the variation of oxidation time with temperature maintained at 750 ^{0}C; air was continuously supplied into the furnace. Figure 6.12 shows the TEM micrographs at various stages of oxidation.

Table 6.4 Effect of purification time

S. No	Temperature (^{0} C)	Time (mins)	Air flow	Result
5	750	5	Yes	Amorphous carbon present
6	750	7	Yes	Amorphous carbon reduced
7	750	9	Yes	Tube surface damaged
8	750	11	Yes	Tubes split into two

From the TEM micrographs in Figure 6.12, it can be seen that heating for 5 mins did not oxidize the amorphous carbon. Heating for 7 mins decreased the amount of amorphous carbon. Heating for 9 and 11 mins reduced the amount of amorphous carbon significantly thus indicating that heating at 750^0 C for 9 to 11 mins is sufficient for the oxidation of amorphous carbon.

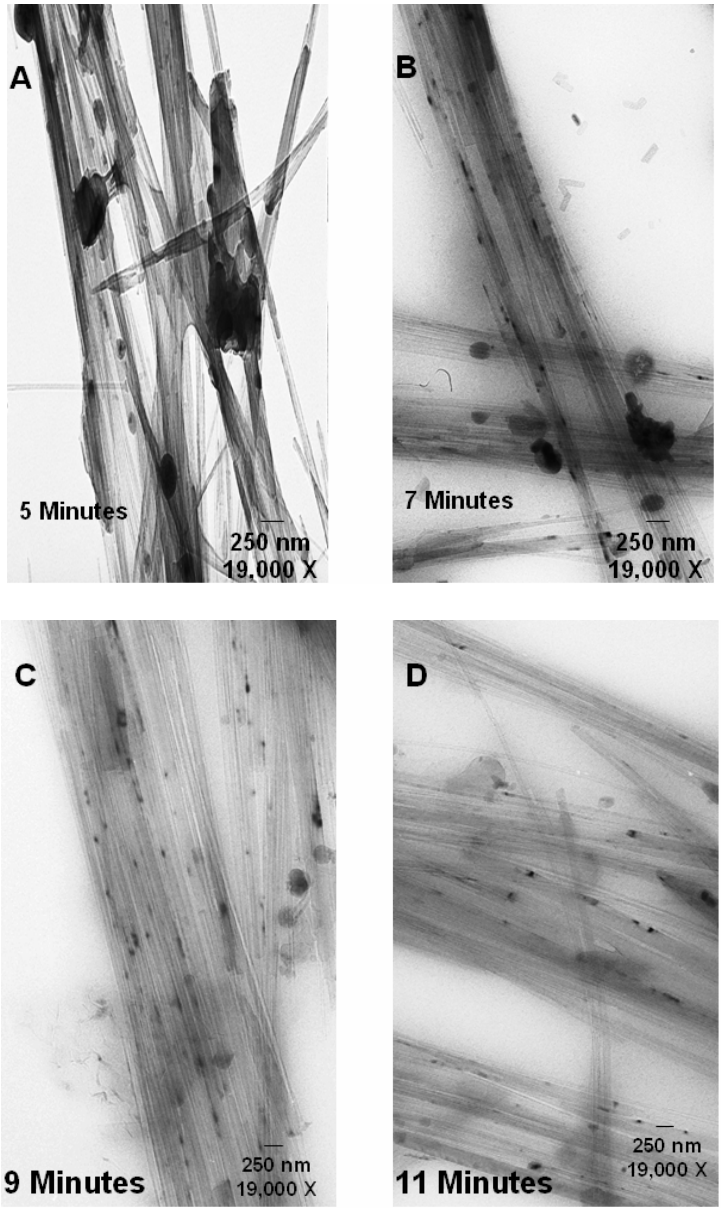

Figure 6.12 Effect of purification time when heated at 750^0 C with air flow

A closer observation of the tube surfaces showed that the tubes are coated with dark particles as shown in Figures 6.13 and 6.14. These particles were formed during purification due to oxidation of the walls, i.e. the tube walls begin to oxidize due to continuous supply of oxygen during the process. Comparing Figure 6.13a and Figure 6.14a, it can be recognized that the number of oxidation sites has increased with time. Figure 6.14 shows the stages that are involved in the destruction of tube along the length. The oxidation process proceeds along the circumference and finally splits the nanotube into two parts as shown in Figure 6.14c. This suggests that continuous supply of oxygen during heating damages the side walls and reduces the yield and length. From these TEM micrographs it can be concluded that supply of air during oxidation at 750^0 C is unfavorable for the purification process due to high and uncontrollable oxidation rates.

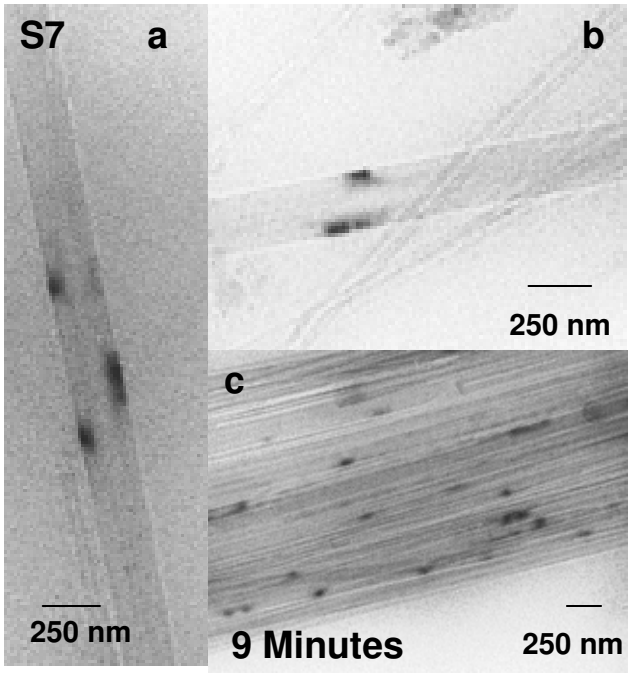

Figure 6.13 TEM micrographs indicating oxidation of nanotube walls

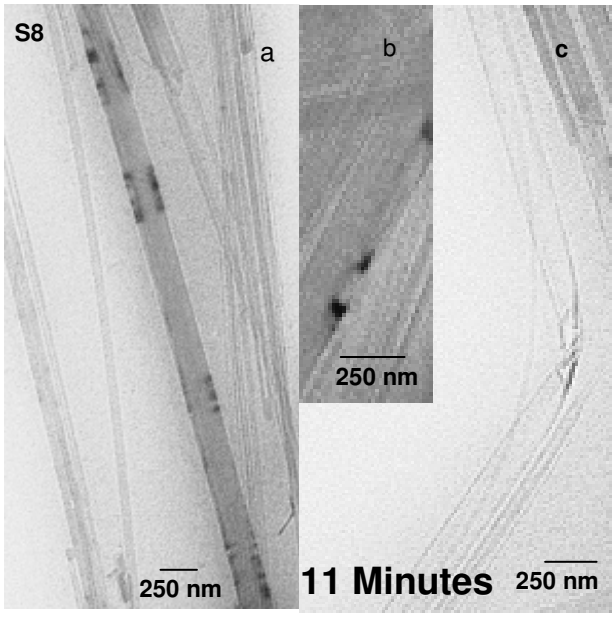

Figure 6.14 TEM micrographs showing stages of nanotube wall oxidation

6.5.3 Batch 3

Table 6.5 shows the effect of test conditions (temperature maintained at 700 ^{0}C) on the purification of MWNTs. The experiments were conducted without continuous supply of air. Figure 6.16 shows the TEM micrographs of the samples 9 to 12.

Table 6.5 Effect of purification time

S. No	Temperature(^{0} C)	Time (mins)	Air flow	Result
9	700	5	No	Amorphous carbon present
10	700	10	No	Amorphous carbon reduced
11	700	15	No	Tubes purified
12	700	20	No	Tubes oxidized

It can be noticed from the TEM micrographs that heating for 5 or 10 mins did not eliminate the amorphous carbon. Heating for 15 mins completely oxidized the amorphous

carbon and any further heating completely destroyed the tubes. It was observed that heating for 15 mins opened the tubes indicating that any further heating will lead to oxidation of the tubes. Heating for 20 mins completely destroyed the tubes leaving only residues of the oxidized tubes.

A closer observation of Sample 11 clearly showed that the tubes walls are clean suggesting that the tube walls are not destroyed or even attacked during the purification process. Some of the tube tips in Sample 11 are open, suggesting that oxidation of the tubes has just started, as shown in Figure 6.15. Thus it can be concluded that heating at 700^0 C for 15 mins is the most favorable condition for the purification of MWNTs.

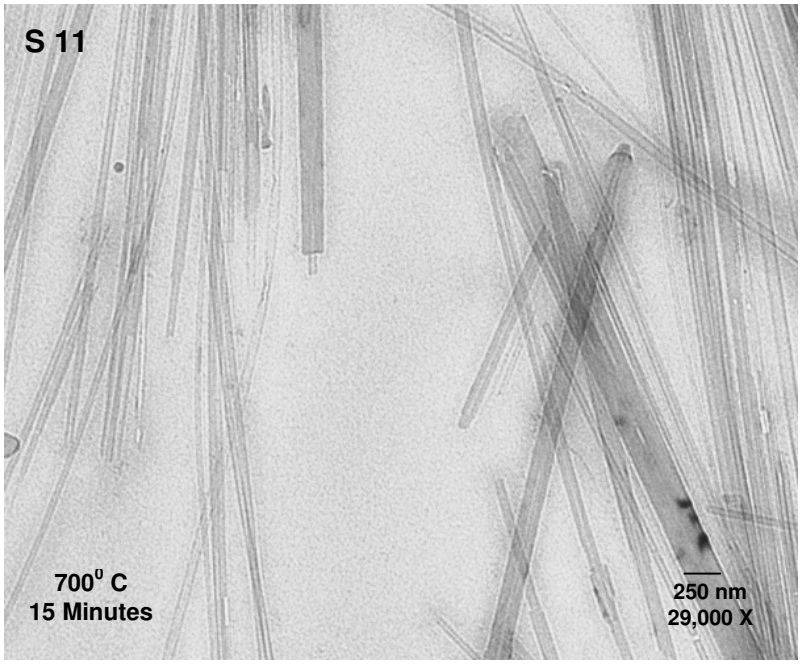

Figure 6.15 TEM micrograph of clean MWNT surfaces.

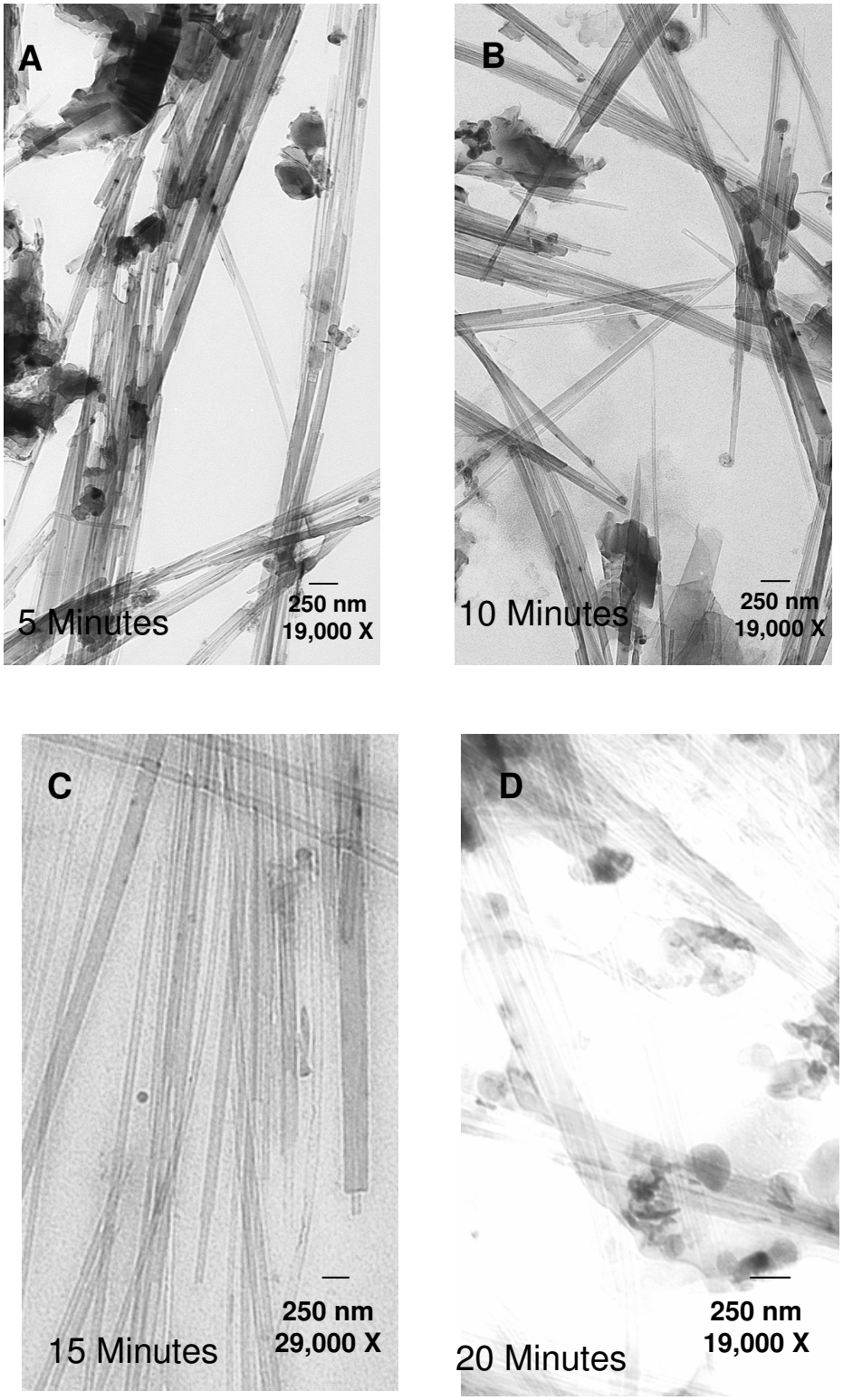

Figure 6.16 Effect of purification time when heated at 700^0 C without air flow

6.5.4 Batch 4

Table 6.6 gives details on the variation of oxidation time (with temperature maintained at 750 ^{0}C) on the purification of MWNTs. Figure 6.17 shows the TEM micrographs of Sample 13 and Sample 14.

Table 6.6 Effect of purification time

S. No	Temperature(^{0} C)	Time (mins)	Air flow	Result
13	750	5	No	Amorphous carbon oxidized
14	750	8	No	Tubes damaged
15	750	10	No	Tubes destroyed
16	750	12	No	Tubes destroyed

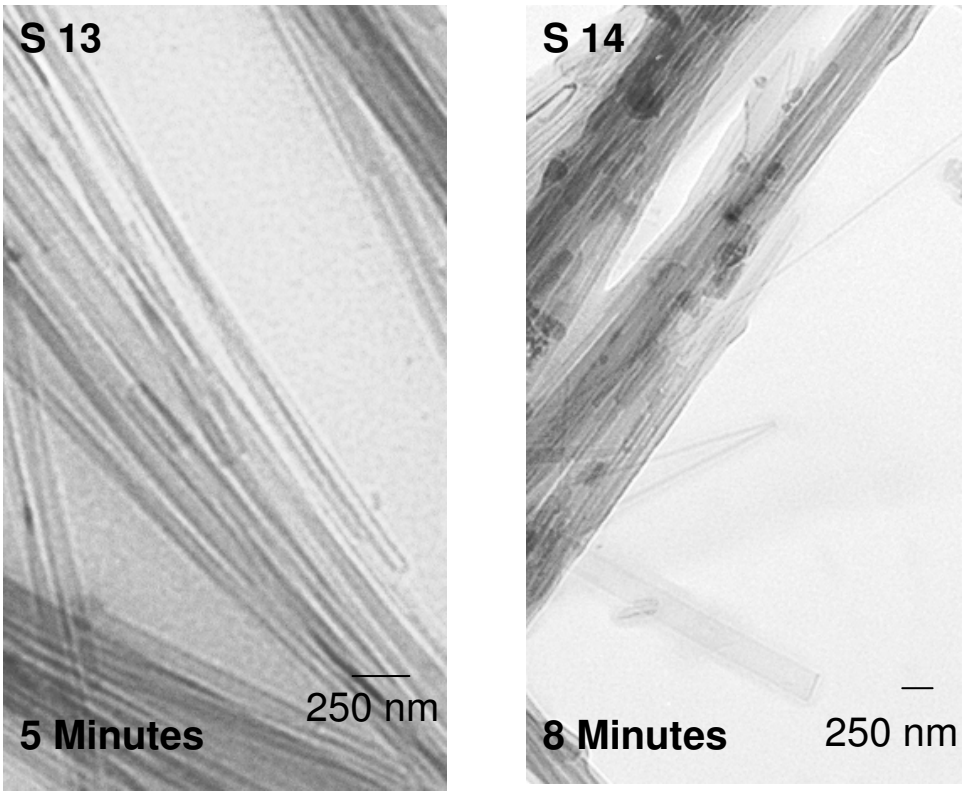

Figure 6.17 TEM micrographs of Sample 13 and Sample 14.

From the TEM micrographs it can be observed that heating for 5 mins at 750^0 C removed most of the amorphous carbon. Some of the tubes Sample 13 are found to be open thus indicating that the oxidation of the tube ends has just started in 5 mins. The tube surfaces are also found to be free of any oxidation sites. Any further heating only oxidized the tubes and decreased the purity due to the formation of residues of oxidized nanotubes as seen in Sample 14. All tubes were oxidized in the 10 and 12 minute samples leaving only residual particles or heavily oxidized tubes.

6.6 Single-walled carbon nanotubes (SWNTs)

The effect of helium pressure and helium flow rate on the synthesis of as-produced single-walled nanotube (AP-SWNT) material was studied systematically. The aim of this study is to find the optimum pressure and flow rate for the synthesis of maximum amount of collar deposits. After the experiments, SEM and TEM analyses were carried out to study the tube morphology and growth mechanism. Graphite anodes containing 4 at% Ni and 1 at% Y was used in the study [26].

6.6.1 Effect of helium pressure

The effect of helium pressure was studied by maintaining a constant helium flow into the chamber. The circulation of helium facilitates in the removal of the gases produced during the experiment and also maintains high purity helium atmosphere around the cathode. The experiments were performed using 75 A D.C. and the time taken for the consumption of 1” long metal filled anode varied between 2 to 5 mins. The anode was continuously moved towards the cathode to maintain a constant distance of ~ 2-3 mm. The arc was extremely

stable and noiseless when metal filled anode was vaporized; the arc started producing noise once the metal filled part was vaporized and the experiment was stopped. Table 6.7 gives the effect of helium pressure on the quantity of collar deposit formed.

Table 6.7 Effect of helium pressure

S. No	Helium pressure (Torr)	Cathode deposit (g)	Collar deposit (mg)
1	760	1.05	45
2	630	0.7	40
3	506	0.65	100
4	380	0.8	45
5	315	0.8	50
6	250	0.34	52

It was found that maximum amount of collar deposit was formed when the helium pressure was ~506 torr. These experiments gave a clear indication that ~500 torr was the most favorable pressure for the formation of maximum amount of collar deposit. The effect of helium pressure on the growth of SWNTs is explained in detail in Section 6.7 which deals on the growth mechanism of SWNTs.

6.6.2 Effect of helium flow rate

In order to increase the yield, the effect of gas flow rate was studied by maintaining the helium pressure at 506 torr. During this study helium was continuously supplied into the chamber at the same time the vacuum pump was operated to remove the gases produced. The chamber pressure was maintained constant during the experiments. Table 6.8 shows the

effect of helium flow rate on the yield of collar deposit. It can be seen that the amount of collar deposit formed depends on the helium flow rate. With decrease in flow rate to 2 l/min, the collar deposit increased to 250 mg, and any further decrease in helium flow rate decreased the collar deposit.

Table 6.8 Effect of helium flow rate.

S. No	He Pressure (Torr)	He flow rate (l/min)	Cathode deposit (g)	Collar deposit (mg)
1	506	10	0.65	100
2	506	2	0.78	250
3	506	0	1.1865	54

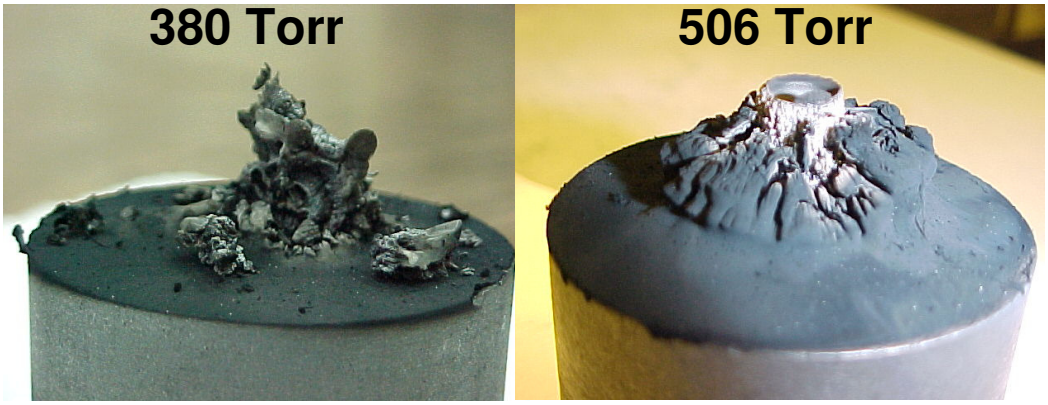

Figure 6.18 Collar deposit formed at 380 torr and 506 torr

After the experiments the collar deposit on the cathode was carefully scrapped, weighed and used for further analysis. Figure 6.18 shows photographs of the collar deposits formed at two helium pressures. We can clearly see that the amount of collar deposit formed is very high at 506 torr of helium. The flow rate of helium is found to be a significant parameter in the formation of collar and cathode deposits. From Table 6.8 it is recognized that with decrease in helium flow rate the cathode deposit increases at the same time increasing the collar deposit.

6.6.3 SEM analysis of collar deposit

SEM analysis showed no tubular structure at 760 torr, instead only spherical particles were formed as shown in Figure 6.19a. These particles were observed to be between 0.2 to 1 μm in diameter. The particles were found to be attached to each other through a chain-like structure as observed in the TEM micrograph in Figure 6.23. The formation of spherical particles has also been reported by Park *et al.* [83]. With decrease in helium pressure to 633 torr, a fine network of particles were formed with no tubular structures.

SWNTs in the form of bundles were observed between 506 and 315 torr in all parts of the collar deposit. The bundles were found to be bright and circular at one end, which was found to be the metal catalyst by TEM analysis. At 506 torr clusters of bundles of bundles were formed at many points in the collar deposit as shown in Figure 6.19c. These clusters were observed only at 506 torr. When the pressure was decreased to 250 torr spherical particles with diameter 0.1 to 1 μm were observed at many points in the collar deposit. Based on SEM analysis, helium pressure between 315 and 506 torr is found to be the most favorable condition for the synthesis of SWNT bundles.

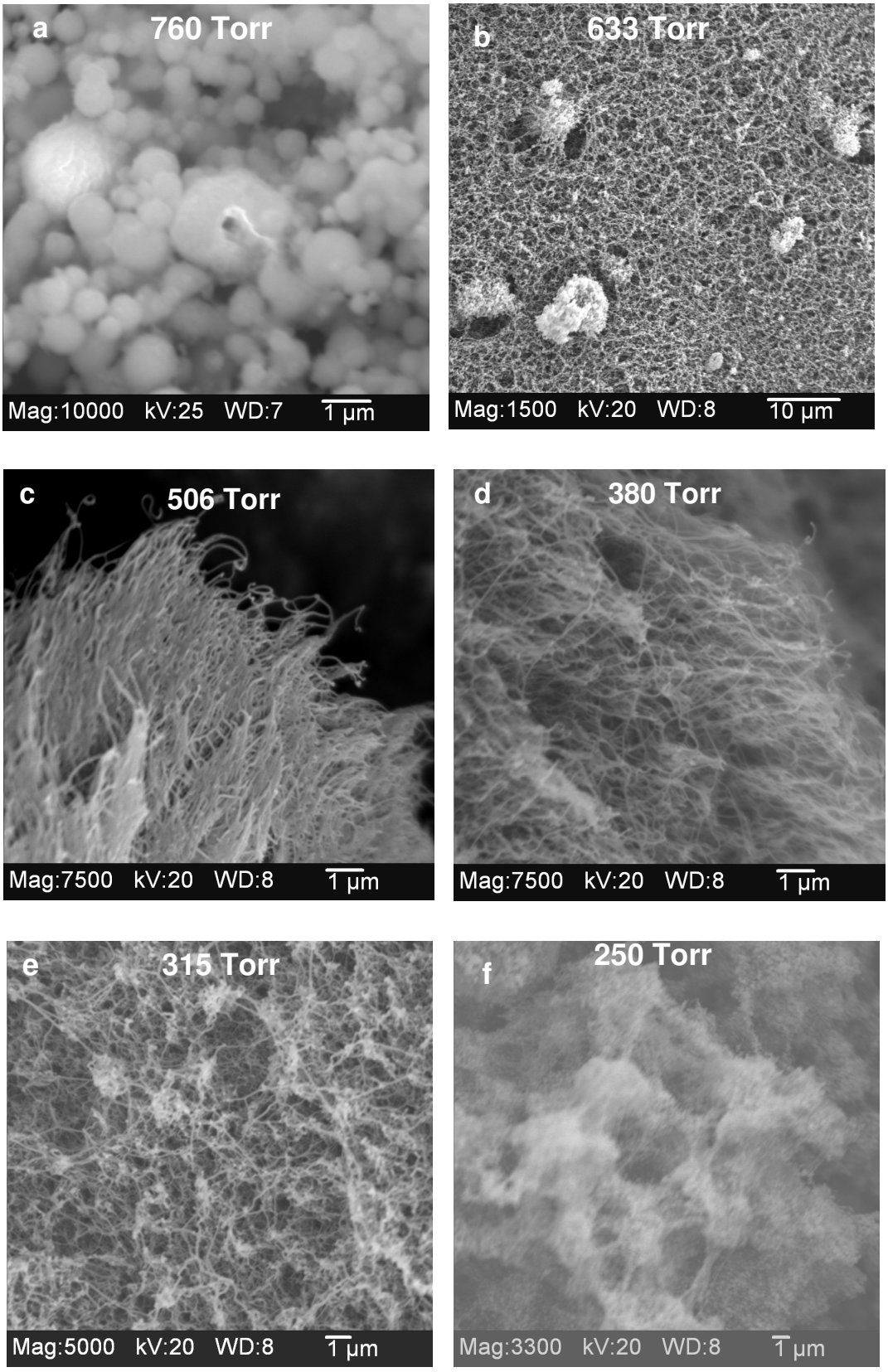

Figure 6.19 SEM micrographs of collar deposit at different helium pressures

SEM analysis showed that SWNTs are found in the form of bundles and there is no relation between the bundle length, diameter, orientation or purity of the tube with pressures. For example, Figures 6.20a and b show SEM images of SWNTs bundles observed at two different location of the same sample. Figure 6.20a shows that the tube bundles are oriented along one direction where as Figure 6.20b shows that bundles form a random network. From these images it is not possible to draw any conclusions on the length, purity, or any possible orientation and the only comparison is the amount of collar deposit that is formed. Hence, this study was focused only on the quantity of collar deposit formed, bundle morphology, and the growth mechanism.

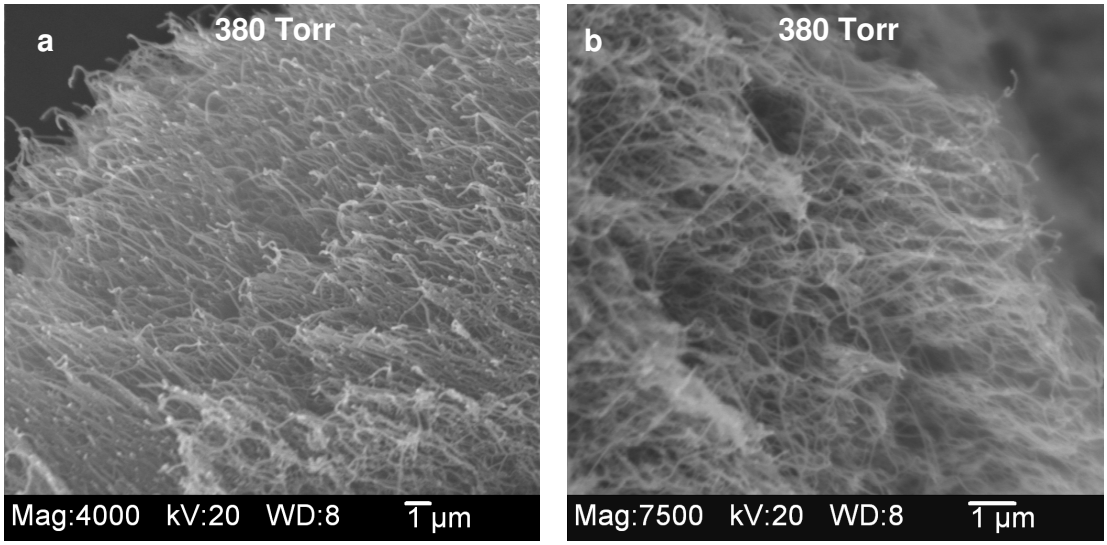

Figure 6.20 SEM micrograph of oriented and random SWNT bundles grown at 380 torr

6.6.4 TEM analysis of collar deposit

TEM analysis was extremely useful in understanding the bundle morphology and growth mechanism of SWNTs. The collar deposit was scrapped and mixed with acetone to form a suspension of SWNTs. The suspension was dispersed using an ultrasonic bath for 30-

60 mins to obtain a uniform dispersion of SWNTs. A drop of dispersed sample was placed on the TEM grid and allowed to dry before analysis. Figures 6.21 and 6.22 are TEM micrographs of the sample formed at 506 torr of helium at the same magnification. Figure 6.21 shows regions of the TEM grid with few bundles and Figure 6.22 show a very dense network of SWNT bundles.

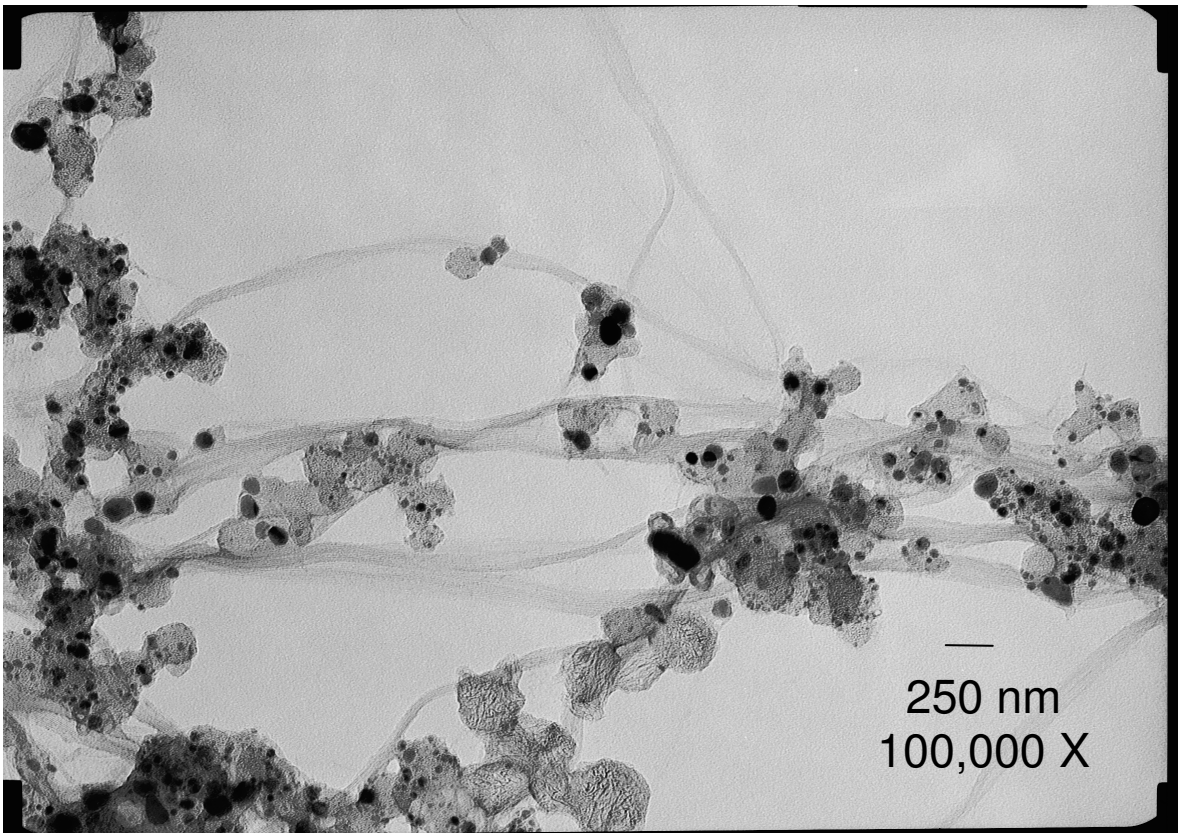

Figure 6.21 SWNT bundles formed at 506 torr

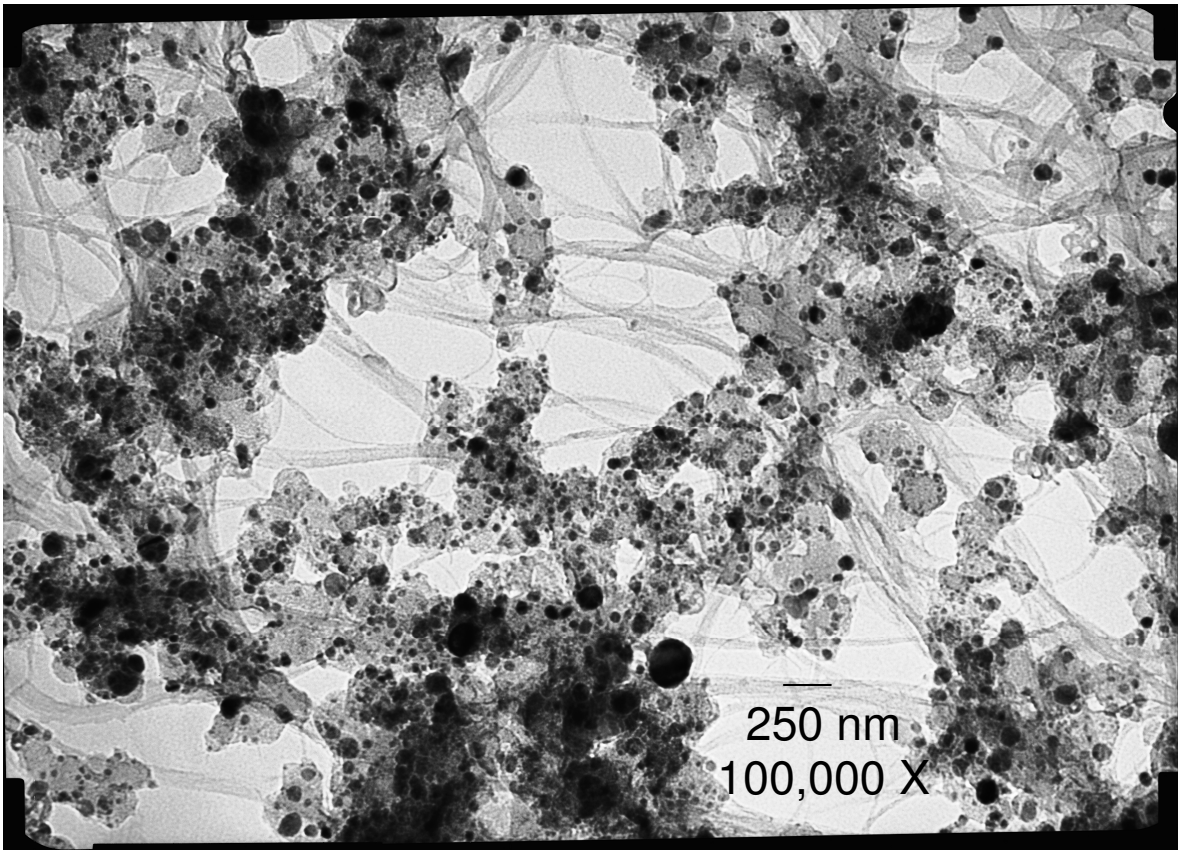

Figure 6.22 SWNT bundles formed at 506 torr

The TEM analysis showed that nanotubes are not formed at 760 torr; only chain-like structures are found at 760 torr as seen in Figure 6.23. These are found along with dark metal particles and amorphous carbon. From the TEM micrograph, the diameter of the chain is found to be ~50 nm. Similar chain-like structure was observed by Saito [114] and was called nanochains. A nanochain comprises of tens of hollow particles that are linearly connected with each other.

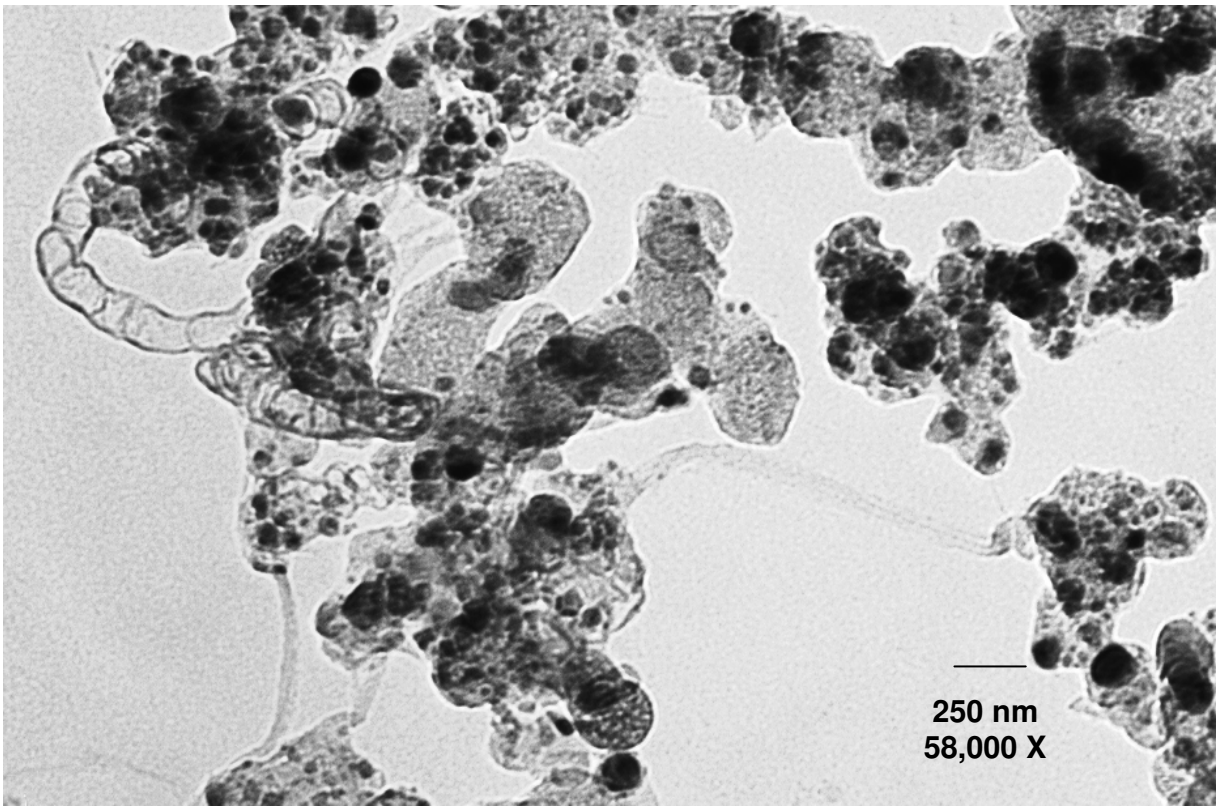

Figure 6.23 Nanochain-like structure at 760 torr.

With decrease in pressure to 506 torr SWNT bundles attached to metal particles are observed initially in the SEM image and further confirmed in the TEM images. Figures 6.24 - 6.26 show SWNT bundles formed at different pressures. Figure 6.24 is a high magnification TEM image showing bundles of CNT's originating from the metal particle. It may be noted that bundles of CNTs are made up of many individual tubes that are formed together and held by Van der Waals forces. Figure 6.24 shows that almost every metal particle is at the head of a bundle. This implies that most of the metal has been utilized in the formation of SWNT bundles. Figures 6.25 and 6.26 show TEM micrograph of the bundles formed at 380 and 315 torr of helium respectively.

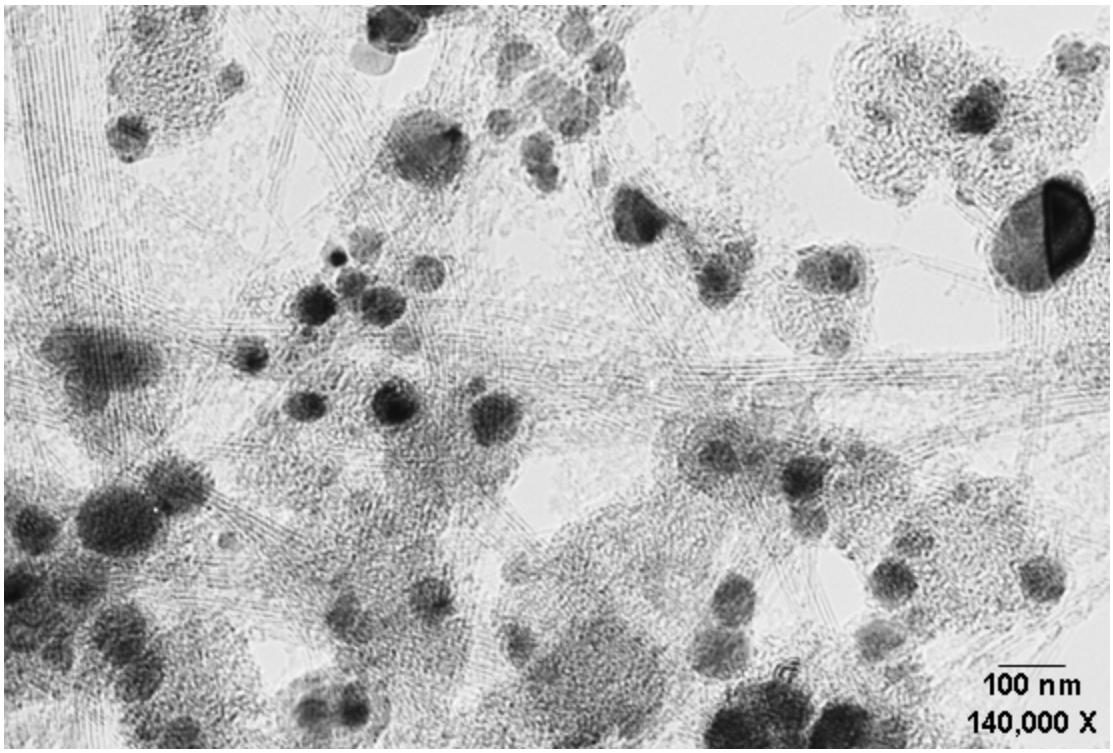

Figure 6.24 TEM micrograph with CNT bundles formed at 506 torr.

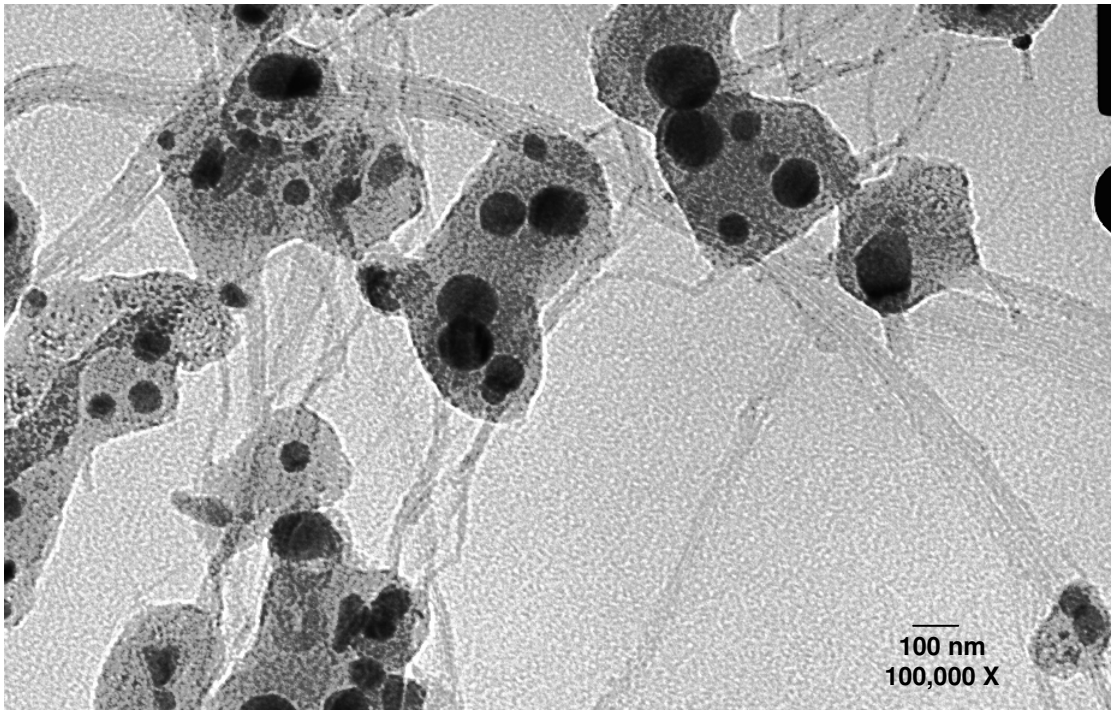

Figure 6.25 TEM micrograph with SWNT bundles formed at 380 torr

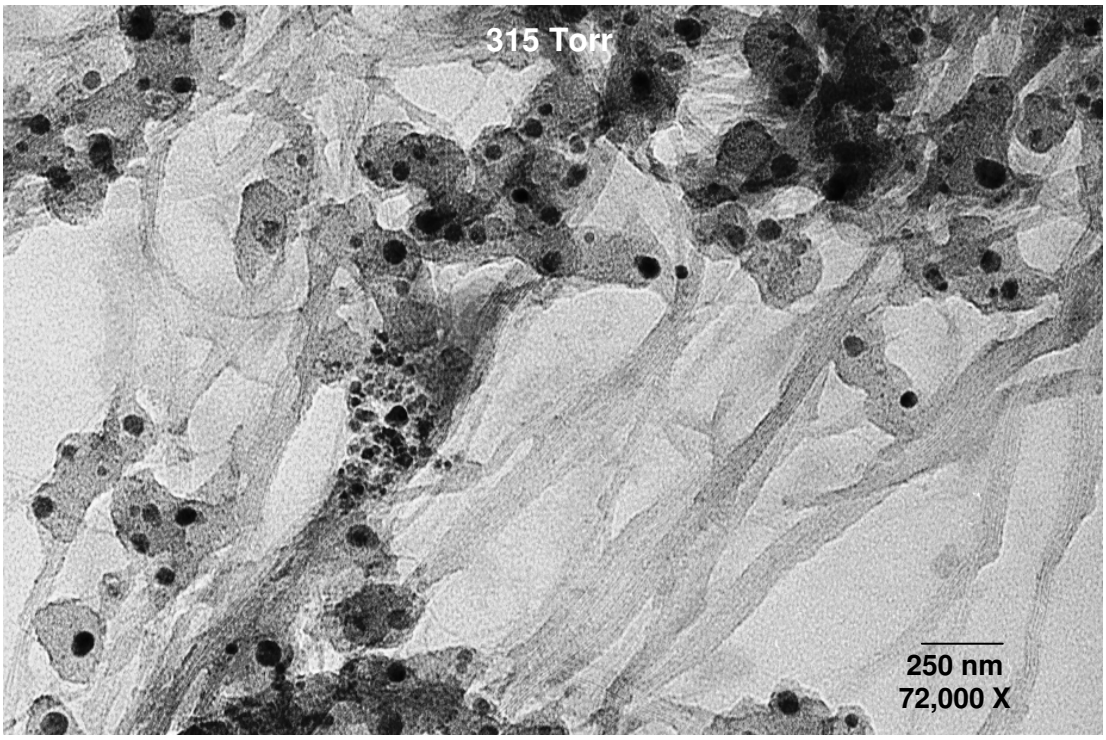

Figure 6.26 TEM micrograph with SWNT bundles formed at 315 torr

6.6.5 Bundle morphology

SEM and TEM analysis was used to investigate the morphology of the SWNT bundles. Features such as bundle length, diameter, and bundle ends were calculated from the images.

From the TEM and SEM images, it was observed that SWNT bundle length is on the order of micrometers. For example Figure 6.27 shows the length of a bundle is at least 3.42 μm. Using TEM, it was observed that SWNTs are of equal length in a bundle. So it can be noted that the individual SWNTs produced here are a few micrometers in length.

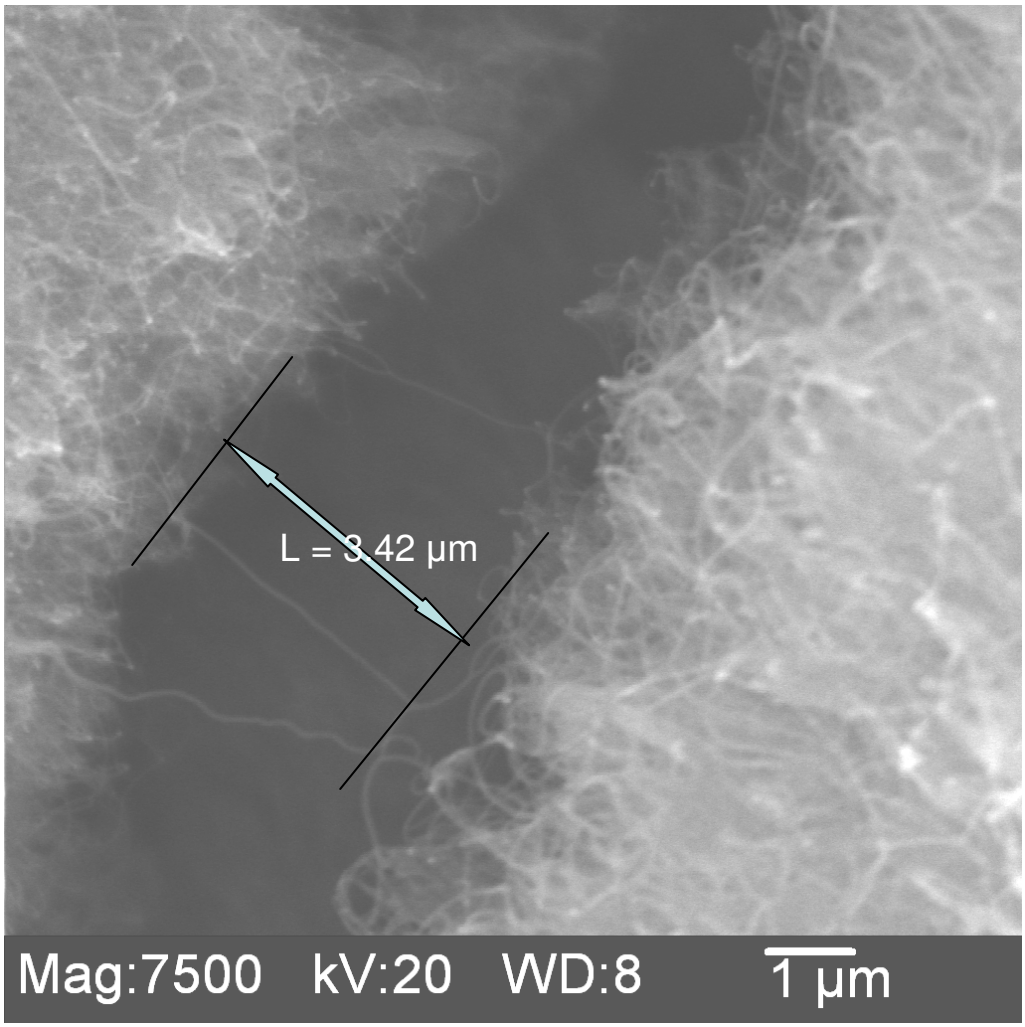

Figure 6.27 Measurement of bundle length

TEM studies showed that the bundles are 40-80 nm in diameter and some of them bonded together along the length to form larger bundles. Also, some of the bundles attach themselves at a point along its length thus cross-linking. From Figure 6.28, it can be seen that individual SWNTs are bonded to each other. This is due to Van der Waal forces. From the TEM images, it is estimated that the individual CNTs is approximately 4 nm, this has been calculated by magnifying the images.

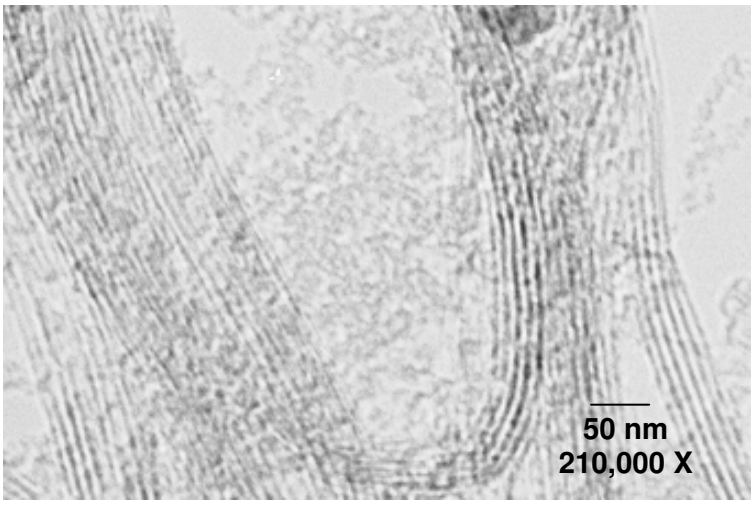

Figure 6.28 Attachment of SWNT bundles

It was observed that the SWNTs are always closed as shown, in Figure 6.29a. The bundle tips show that the individual tubes are of equal length thus suggesting that the growth of SWNTs terminate at the same time in a bundle. It has also been observed that some of the bundles are parallel or inclined to the electron beam thus helping us to view the circular ends as shown in figure 6.29b. These images confirm that one side of the bundle is free from metal catalyst.

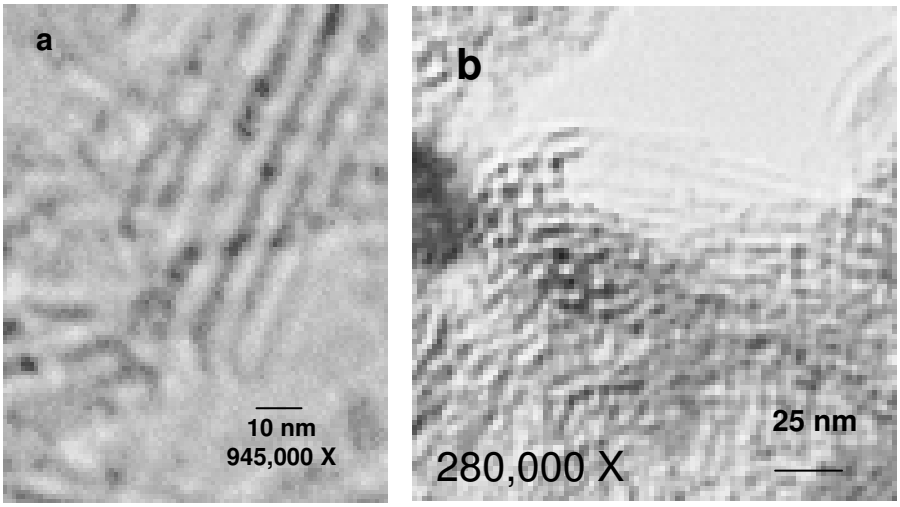

Figure 6.29 TEM micrograph of SWNT ends.

6.7 Growth mechanism of SWNTs

The growth mechanism of SWNTs described in the following comprising of two stages. (1) The formation of SWNTs containing mats and (2) the formation of SWNT bundle. The SEM and TEM analysis of SWNTs were extremely useful to formulate the growth mechanisms involved in their formation.

6.7.1 Mat formation

At a helium pressures of 506 torr, and below the collar deposit was found to be made of large number of mat-like structures stacked over one another as shown in Figure 6.30a. At the top surface of the collar deposit a sparse network of randomly oriented tubes was observed as well as many tubes buried below the surface as shown in Figure 6.30b. For SEM analysis, the collar deposit was usually pierced with the tweezers to study the microstructure of the collar mats.

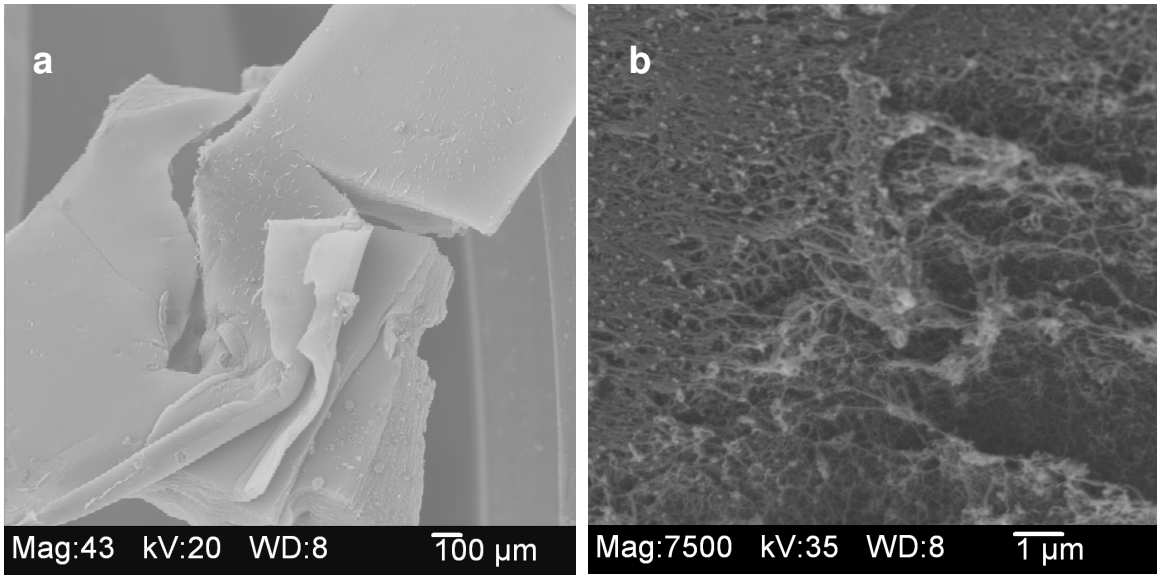

Figure 6.30 SEM micrograph of a) Mat-like deposit in the collar, b) Top surface of the collar mat.

The mats formed in the collar deposit are found to contain majority of SWNTs bundles below the surface of the metal catalyst as seen in Figures 6.31 and 6.32a. The mat cross-section showed that SWNT bundles below the metal catalyst layer to be oriented along a single direction and of same length. This suggests that bundles initiate, grow in length and terminate at the same time thus forming a metal covered mat of uniform thickness on the collar. Figure 6.31a is an SEM micrograph of the collar mat showing the tubular growth below the top surface. Figure 6.31b is SEM micrograph of the cross section of the mat where the tubes are seen along one direction. The top surface of the collar mat showed that the surface is made up of many spherical particles as shown in Figure 6.31b. Similarly oriented SWNT bundles have also been reported by Lv *et al*. [74], Farhat *et al.* [77] and Hinkov *et al.* [84].

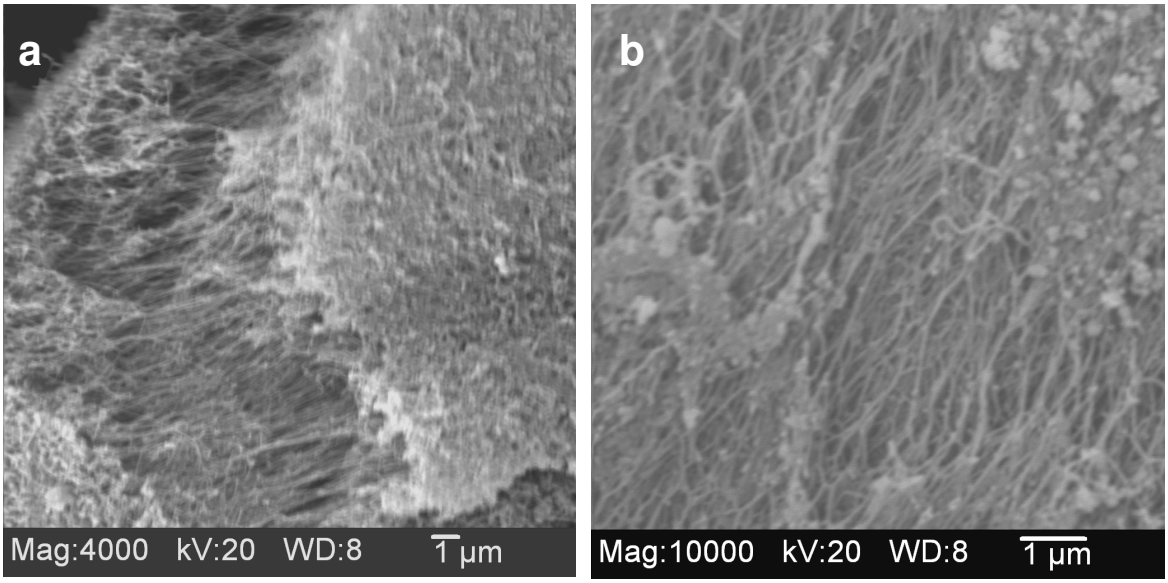

Figure 6.31 SEM micrograph of mat cross section

SEM analysis showed that bundle ends are always bright and circular as shown in Figure 6.32b. These bright spots are metal catalyst particles attached to the ends of tubes; this has been confirmed by TEM analysis. Based on the SEM images it appears that one layer of

collar mat is formed by the growth of SWNT bundles which are of nearly of the same length. When the catalyst particle becomes inactive, the growth of SWNT bundles is terminated and a new bundle begins to grow. When this process is repeated it leads to the formation of mats stacked one over the other to form the collar deposit.

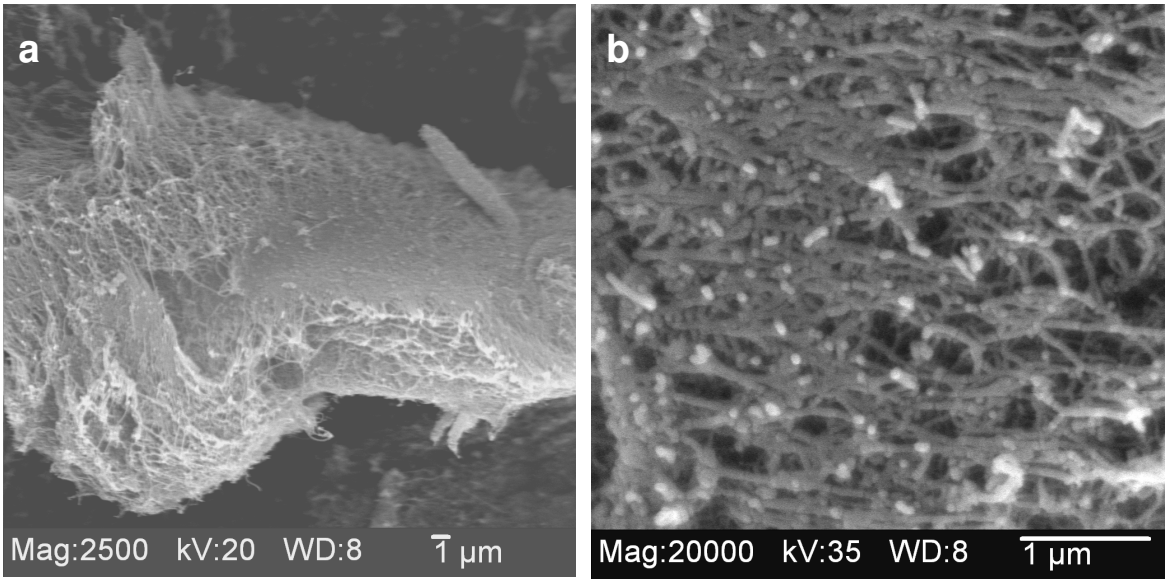

Figure 6.32 SEM micrographs of a) Collar mat with buried bundles, b) Bundles tips with metal catalyst particles.

6.7.2 Bundle formation

The formation of SWNTs in the form of bundles was analyzed using the TEM. Here, the SWNTs bundle formation is described and supported according to the vapor-liquid-solid (V-L-S) model by Saito *et al.* [102, 112], Kanzow *et al*. [97] and Gavillet *et al.* [98]. The formation of bundles is described in two stages, namely, nucleation and growth.

As discussed in Chapter 3, during nucleation, liquid nanoparticles of metal supersaturated with carbon are formed from condensation of metal plasma/vapor in the moderate temperature zone. The presence of nanoparticles was observed in TEM as shown in

Figure 6.33 where the metal is seen as dark particles. As the particle moves to colder region, the solubility of carbon decreases and carbon atoms begin to segregate from the inner regions of the nanoparticles. Once the segregation process starts there are two competing processes that can take place.

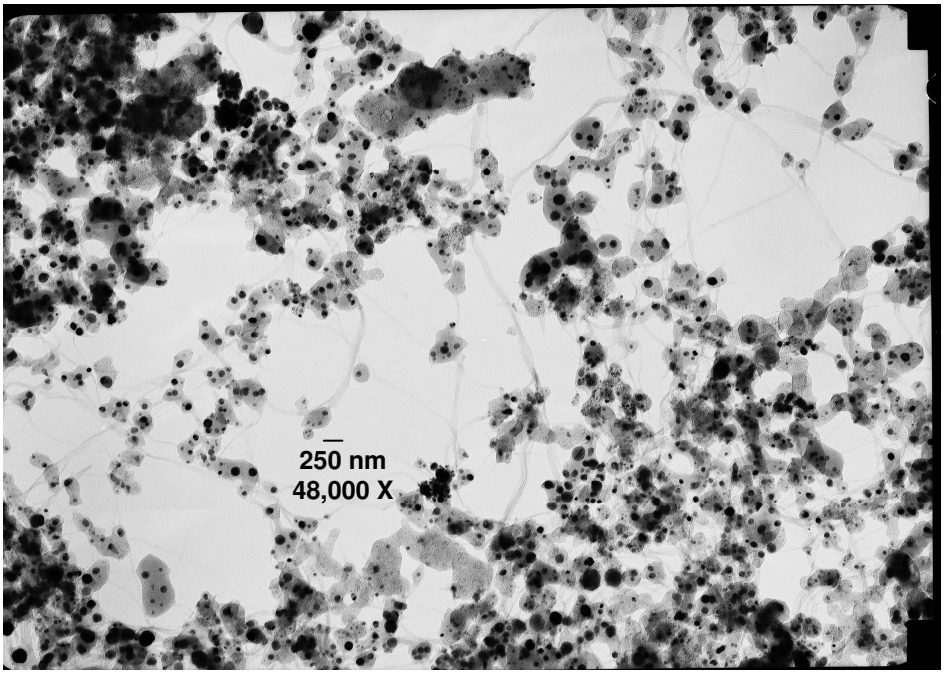

Figure 6.33 TEM micrograph showing presence of metal nanoparticles

Firstly, the carbon atoms can crystallize at the surface of the metal leading to the formation of graphitic shell over the metal particle as shown in Figure 6.34b. This occurs when the segregation velocity is low, carbon atoms are gradually segregated and they get organized into the most stable configuration that is the graphite sheet.

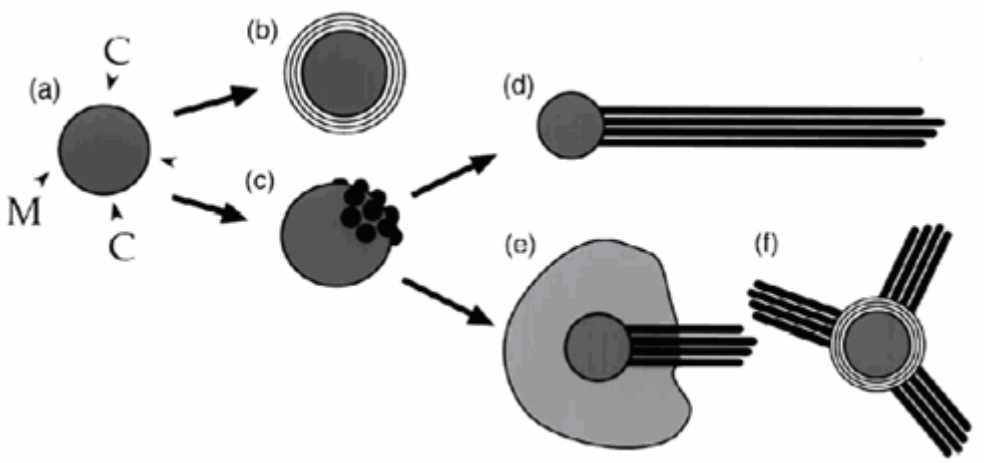

Figure 6.34 V-L-S model for nucleation and growth of SWNTs [98].

The formation of graphite sheets around the metal was observed in TEM as shown in Figure 6.35. It shows the presence of carbon layers on the outer surface of a large metal particle. It should be mentioned here that the SWNTs are not seen from the metal particle. The shell around the metal particle is uniform showing no signs of nucleation. The formation of shell makes the catalyst inactive or death of its catalytic activity. This has also been confirmed using MD simulations by Gavillet *et al.* [98].

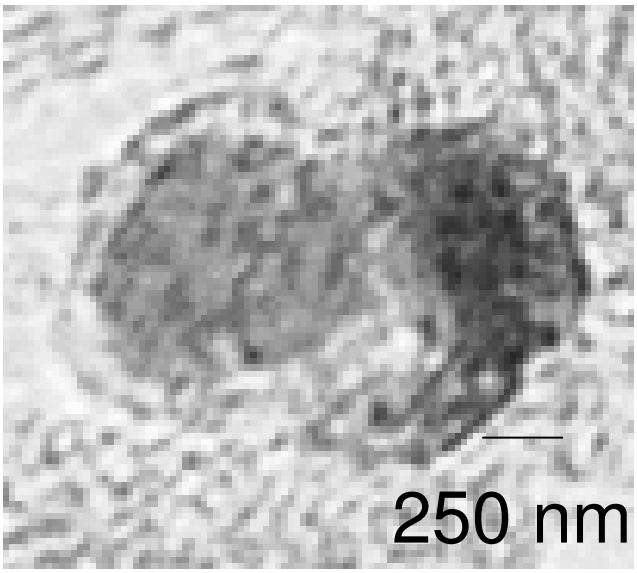

Figure 6.35 Formation of carbon cage around the metal particle

The second competing reaction that occurs is the nucleation of single-walled nanotubes as shown in Figure 6.34c. When the segregation velocity is high, the carbon flux is very high leading to the nucleation of tubes at the surface. Usually there are more than one nucleation site on a nanoparticle. The number of nucleation sites determine the number of tubes in the bundle. Figure 6.36 are TEM micrographs showing the formation of nanotube nucleation sites. Here, we observe that the outer carbon layer is not smooth but is made up of radial structures thus indicating that these are nucleation sites for the growth of tubes.

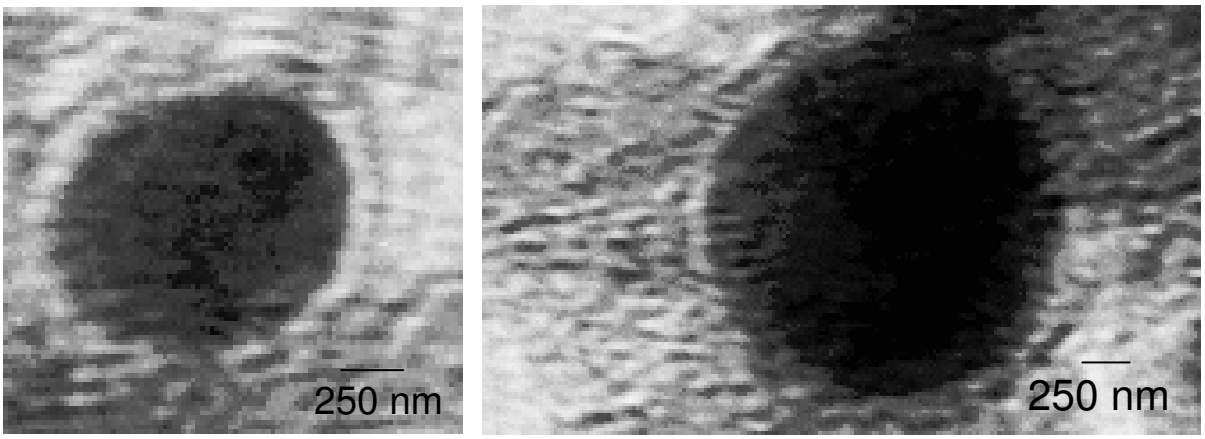

Figure 6.36 TEM micrographs showing nucleation of SWNTs

From the nanotube nucleus, the growth of the nanotube is continued by the incorporation of carbon atoms at the root by root growth mechanism [98]. During this stage, carbon atoms are continuously supplied from the vapor phase which diffuses into the particle. At this stage, the role of the metal catalyst is to provide a fluctuating M-C bonds during which new carbon atoms get incorporated in the tube. This leads to the formation of a tadpole-like structure where the metal particle is at the head of the SWNT bundle as shown schematically in Figure 6.34d and TEM image in Figure 6.37.

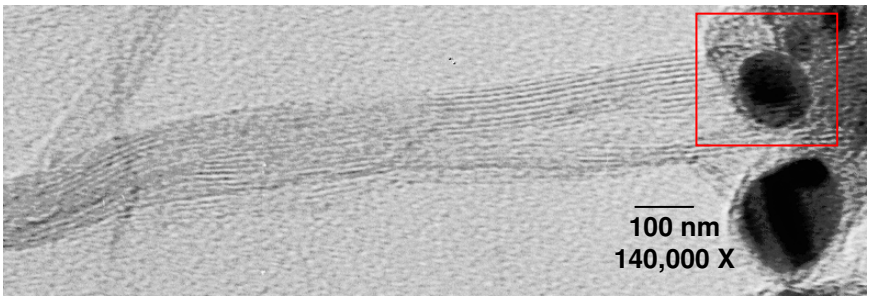

Figure 6.37 Formation of SWNT bundle.

Some times, the growth is halted just after nucleation of SWNTs leading to the sea-urchin-like structure [113] as shown schematically in Figure 6.34f and a TEM image in Figure 6.38. The SWNTs nucleate and grow from all directions but the growth did not continue to form a bundle. This may be due to rapid cooling or lack of carbon atoms towards root growth. Thus, the growth takes place only from the carbon atoms in the metal nanoparticle with no additional atoms added during growth.

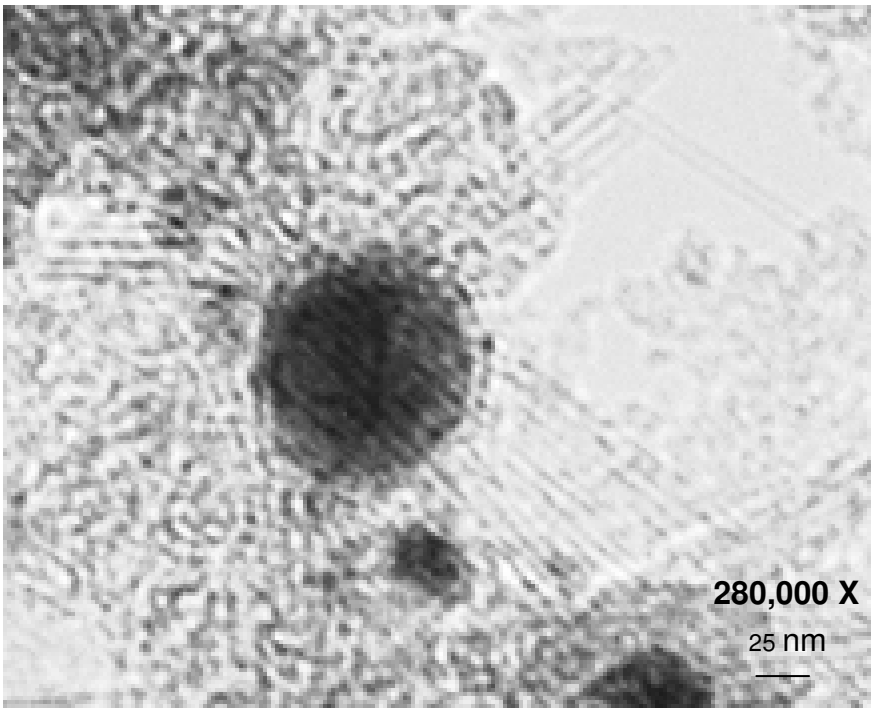

Figure 6.38 Sea urchins-like structure with closed ends

The other structure that was observed is the growth of SWNT in baby-rope from the metal particle. Here the metal particle has amorphous carbon condensed on the particle, schematically as shown in Figure 6.34(e) and a TEM micrograph in Figure 6.39. The central dark metal particle is covered with amorphous carbon layer with a bundle projecting from the particle. This is an intermediate situation between SWNT nuclei and bundle. The formation of different structures can be attributed to different composition of Ni-Y-C particle and quenching rates.

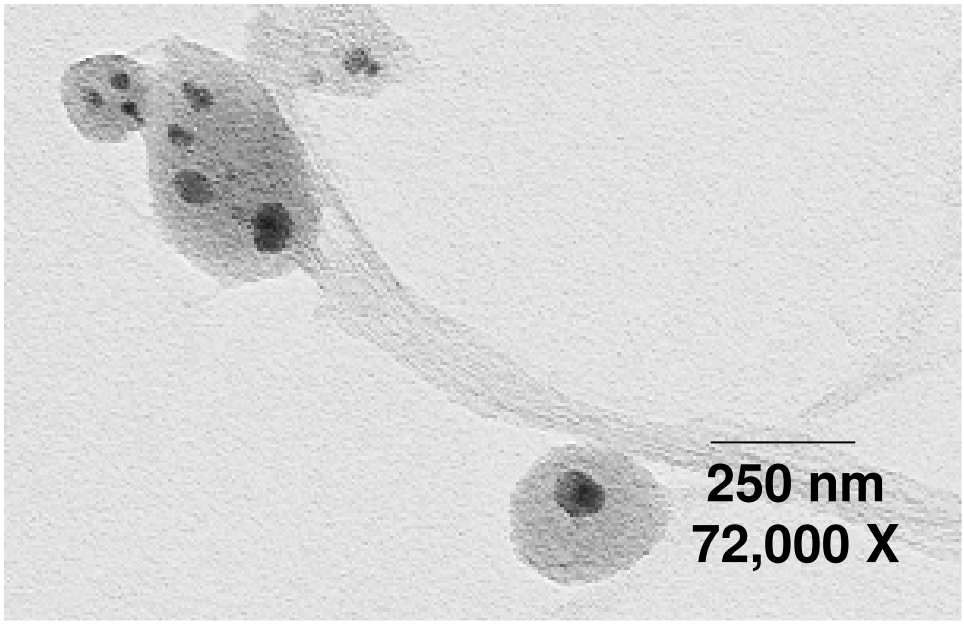

Figure 6.39 TEM micrograph of SWNT baby-rope

6.7.3 Effect of helium pressure

Carbon-metal vapor is formed due to vaporization of the graphite anode [112]. Cooling of this vapor leads to the formation of SWNT bundles [97]. At helium pressures above 630 torr, the metal-carbon vapor is cooled down very rapidly due to the presence of large number of helium atoms. This rapid cooling does not give enough time for the

segregation of carbon atoms from the nanoparticles. This leads to the formation of spherical particles as seen in Figure 6.19a. With decrease in helium pressure from 506 torr to 315 torr, the number of helium atoms that cool the metal-carbon-vapor also decreases leading to an increase in the thermal gradient on the cathode surface. The increase in thermal gradient increases the time of flight of the metal-carbon particle [48]. Thus the time spent by the particle in the supporting zone increases, giving time for the segregation and addition of carbon atoms at the root. So, maximum amount of SWNT bundles are formed in this pressure range. When the helium pressure is decreased to 250 torr, the thermal gradient becomes too high. This increases the time spent by the particle in the hot zone and prevents the growth of SWNT bundles.

As discussed earlier and observed in the SEM micrographs (Fig. 6.19) the helium pressure in the chamber plays a very important role in the formation of SWNT bundles on the cathode. The pressure determines the temperature gradient and the gradient determines the quenching rate and time of flight. The quenching rate determines the time for the segregation of carbon atoms. The segregation time determines the number of nucleation sites in a particle. High quenching rate leads to insufficient time for segregation and tube growth is not observed. Very low quenching rate also leads to lack of SWNT growth.

6.8 Other forms of carbon

During the course of the study some interesting carbon structures were observed in the TEM these are reported here and its structure is explained.

6.8.1 Graphite sheets

The use of iron nanoparticles in the form of magnetic fluid in the anode resulted in the formation of graphitic sheets shown in the TEM micrograph (Figure 6.40). Less than 1 ml of magnetic fluid was filled in a 0.125" diameter hole in the anode and the experiments were conducted at 760 torr helium atmosphere.

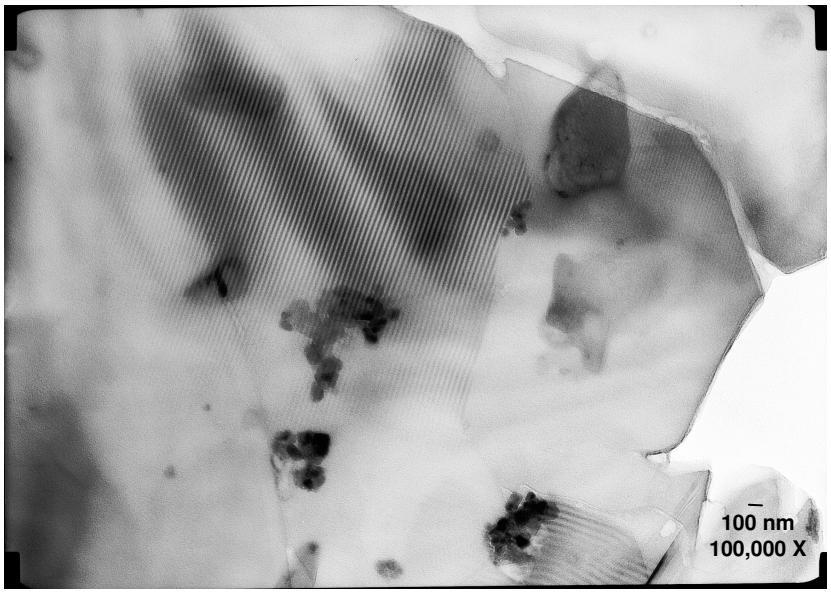

Figure 6.40 TEM micrograph of graphite sheets formed with the use of iron nanoparticles.

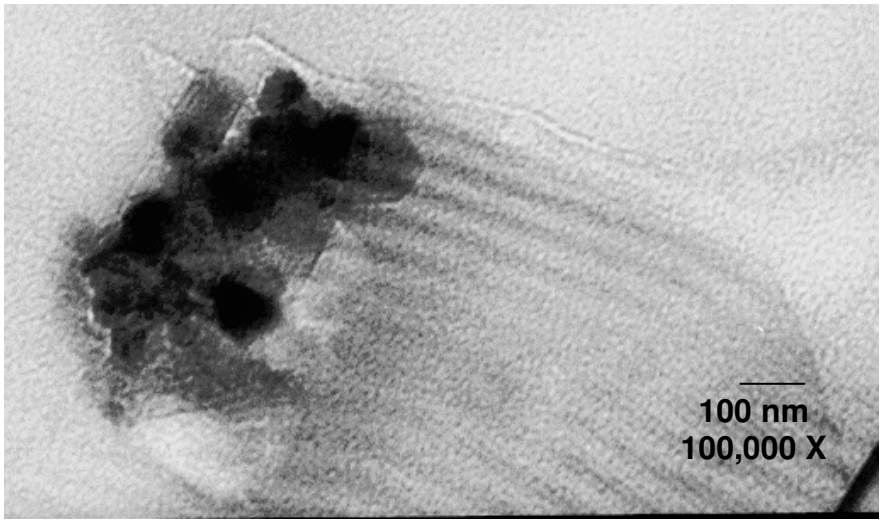

Figure 6.41 TEM micrograph of graphite sheets starting from the iron nanoparticles.

The graphite sheets are a few micrometers in length and width. It is observed that the distance between two graphite planes do not vary in a sheet. Figure 6.41 shows that these sheets appear to originate from the metal particles and grow in length. These sheets were not observed in the absence of metal catalyst.

6.8.2 Hexagonal graphite particles

The other interesting form of carbon observed during the study is hexagonal particles as shown in Figure 6.42. These particles were observed in Sample 2 (S2) prepared during the purification study. When the arc-produced MWNTs were heated to 700^0 C with air flow for 10 mins, these particles were observed along with MWNTs. From the TEM micrographs the edge of the plane is measured to be ~ 0.730 µm.

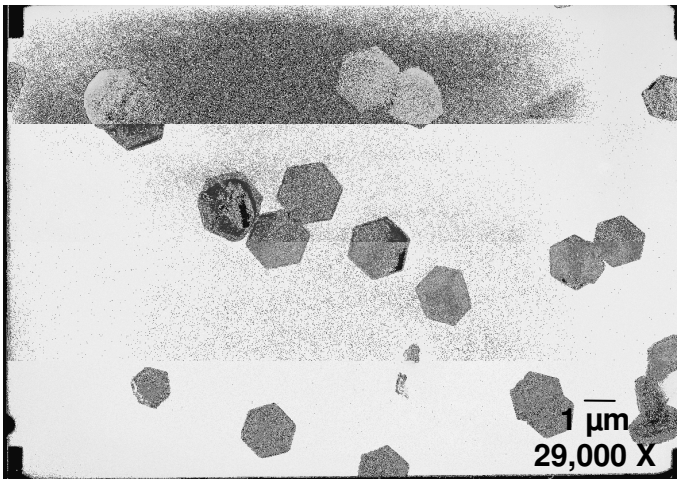

Figure 6.42 TEM micrograph of graphite basal planes.

CHAPTER 7

DISCUSSION

7.1 Arc Stability

A stable arc was found to be a necessary condition for the continuous synthesis of MWNTs containing black, core material. A stable arc can be sustained by maintaining constant anode-cathode distance, decreasing the anode-cathode distance, decreasing the current density, decreasing gas pressure, or decreasing gas flow rate. A stable arc produces a cathode deposit that is lustrous at the outer surface and is hollow in the inner region, as show in Figure 6.1. This could be explained by the fact that a stable arc favors more number of hexagonal structures than pentagon as explained by Maiti *et al*. [92]. Similar observations on arc stability were made by Ebbesen *et al*. [24].

7.2 Effect of buffer gas

The buffer gas is one of the important parameter that controls the yield of MWNTs. Argon is unfavorable due to the variation of chamber pressure and lack of arc stability. This could be attributed to the fact that the thermal conductivity of argon (162 W/m K) is very low compared helium (1415 W/m K).

7.3 Effect of helium pressure

Helium pressure determines the anode evaporation rate and cathode deposit as shown in Table 6.2 and Figures 6.3 to 6.5. Helium pressures above 650 torr are unfavorable due to formation of an unstable arc. Pressures below 100 torr are also unfavorable due to low

vaporization rates. The most favorable pressure range was found to be between 315 to 355 torr, where ~70% of the evaporated anode was converted into MWNTs containing cathode deposit. This is lower than 500 torr, the pressure reported by Seraphin *et al*. [50] and Zhangyz *et al.* [51] which could be due to differences in the chamber design and volume.

7.4 Purification of MWNTs

The effect of time, temperature, and air flow during purification was studied systematically. The purification time decreases with increase in temperature and vice versa. This can be explained on the basis that with increase in temperature the oxidation rate of amorphous carbon is increased thus reducing the time. The oxidation of nanotubes begins at the tips and proceeds along its length in the absence of air flow. This can be explained on the basis that the nanotube tips are made of pentagons which are easy to oxidize compared to hexagons at the tube surface [86]. When air is circulated the tube surfaces begin to oxidize even before the tips. This is attributed to the fact that when air circulation is maintained there is a continuous supply of fresh oxygen atoms that is directed on the tube surfaces. The most favorable conditions for purification are listed in Table 7.1.

Table 7.1 Purification conditions for MWNTs

Sample No.	Time (min)	Temperature (^{0} C)	Air flow
3	15	700	Yes
11	15	700	No
13	5	750	No

The purification time reported here is less than the time reported by Tsang *et al*. [64], Ajayan *et al*. [65] and Uchida *et al*. [67]. This can be due to smaller particle size of amorphous carbon, lower percentage of amorphous carbon or better dispersion of particles during sonication.

7.5 Single-walled carbon nanotubes

The effect of helium pressure showed that 506 torr is the desirable value of pressure for the formation of collar deposit, as shown in Table 6.7 and Figure 6.19. Similar observations have been made by Journet *et al*. [24], Shi *et al*. [95] and Ando *et al*. [48]. The collar deposit is maximum when the helium flow rate in the chamber is maintained at 2 l/min. At high flow rates, the yield is low due to very strong helium currents in the chamber which increase the quenching rates thus decreasing the time for SWNT growth [48]. When the helium flow rate is 2 l/min, the yield is highest at 250 mg. This can be attributed to gentle helium currents that are formed around the cathode. These currents help in depositing the metal-carbon vapor on the cathode surface in the form of collar deposit. This also provides the right thermal gradient and time of flight for the nanoparticles. The absence of helium flow decreases the collar deposit to 54 mg, which can be explained by the absence of helium currents.

7.6 Growth mechanism of SWNTs

The microscopic and macroscopic SWNT growth mechanism was identified based on the SEM and TEM analyses. The SEM images (Figures 6.30-6.32) show the various stages in the formation of collar deposit. The TEM images (Figures 6.34-6.39) show the intermediate

stages in the SWNT bundle formation. These images support the vapor-liquid-solid (V-L-S) model presented by Saito *et al.* [102, 112], Kanzow *et al.* [97] and Gavillet *et al*. [98].

To sum up the growth mechanism, it is established that graphite and metal vaporizes from the anode to forms metal-carbon nanoparticles. The cooling of the nanoparticles leads to the segregation of carbon atoms to the surface thus forming SWNT nucleation sites. The addition of carbon atoms to the root of the nucleation sites leads to the formation SWNT bundle. A large number of SWNT bundles grown for the same length leads to the formation of collar mat with metal at the top surface. The repeated formation of collar mats, one over the other, appears as the dark colored collar deposit on the cathode. The quenching rate determines the number of nucleation sites and the diameter of the nucleus. The number of nucleation sites determines the number of tubes in the bundle and the bundle diameter. The activity of catalyst determines the length of the bundle seen as mat thickness. The number of mats determines the thickness and amount of collar deposit.

CHAPTER 8

CONCLUSIONS AND FUTURE WORK

8.1 CONCLUSIONS

1. In this experimental study, carbon nanotubes (CNT) are obtained by vaporizing graphite in an inert atmosphere using arc-discharge method.
2. Stable arc is a necessary condition for the synthesis MWNTs. Helium is found to be favorable buffer gas for the synthesis of MWNTs compared to argon due to a stable chamber pressure and ease of control of the arc.
3. The helium pressure is found to have a significant effect on the yield of the MWNTs containing cathode deposit. Maximum yield of cathode deposit is obtained when the chamber pressure is maintained between 315 to 355 torr.
4. SEM analysis showed that MWNTs are found inside the cathode deposit in the form of bundles along with amorphous carbon.
5. Purification study of MWNTs showed that heating at 750^0 C for 5 mins or 700^0 C for 15 mins are desirable conditions for removing amorphous carbon.
6. Heating in the presence of air flow results in oxidation of tube surfaces leading to increase in number of open tips.
7. The vaporization of graphite anode with 4% Ni-1% Y in helium atmosphere leads to the formation of SWNTs.

8. The growth of SWNT bundles strongly depend on the chamber pressure. The bundles are formed in helium at a pressure in the range of 315 to 506 torr, with 506 torr being the most favorable.
9. The nucleation and growth of SWNT bundles can be explained using the V-L-S model [98].

8.2 Future work

Major efforts in this study have been towards building the apparatus and in identifying favorable conditions for the formation of carbon nanotubes. With this part done recommendations for future work include the following:

1. Yield of MWNTs containing cathode deposit can be studied by varying the diameter of the graphite anode.
2. The SWNT content in the samples can be analyzed using thermo gravimetric analysis (TGA).
3. Efforts towards purifying the SWNT raw material can be made to obtain pure SWNT samples which can be used for such applications as CNT-composites.
4. Variation of SWNT diameter with changes in argon-helium gas mixture ratio and pressure can be studied.
5. Effect of quench rate can be studied using water or liquid nitrogen cooled cathodes.
6. Effect of metal catalyst such as iron, cobalt or mixtures can be studied, to identify the optimal conditions and variation in tube diameter.

REFERENCES

1. Kroto, H. W., Heath, J. R., O'Brien, S. C., Curl, R. F. and R. E. Smalley, "C 60: Buckministerfullerene," Nature **318** (1985) 162-163.

2. Iijima, S., "Helical microtubules of graphitic carbon," Nature **354** (1991) 56-58.

3. Iijima, S., and T. Ichihashi, "Single-shell carbon nanotubes of 1-nm diameter," Nature **363** (1993) 603-605.

4. Bethune, D. S., Kiang, C. H., Vries de, M. S., Gorman, G., Savoy, R., Vazquez, J., and R. Beyers, "Cobalt-catalyzed growth of carbon nanotubes with single-atomic-layer walls," Nature **363** (1993) 605-607.

5. Graham, A. P., Duesberg, G. S., Hoenline, W., Kruepl, F., and M. I. Liebau, "How do carbon nanotubes fit into the semiconductor roadmap?," Applied Physics A **80** (2005) 1141 – 1151.

6. Dresselhaus, M. S., Dresselhaus, G., and R. Saito, "Physics of carbon nanotubes," Carbon **33** (1995) 883- 891.

7. Treacy, M. M., Ebbesen, T. W., and J. M. Gibson, "Exceptionally high young's modulus observed for individual carbon nanotubes," Nature **381** (1996) 678 – 680.

8. Wong, E. W., Sheehan, P. E., and C. M. Lieber, "Nanobeam mechanics: elasticity, strength, and toughness of nanorods and nanotubes," Science **277** (1997) 1971- 1975.

9. Meyyappan, M., Delzeit, L., Cassell, A., and D. Hash, "Carbon nanotube growth by PECVD: A review," Plasma Sources Sci. Technol. **12** (2003) 205-216.

10. Salvetat, J. P., Bonard, J. M., Thomson N. H., Kulik, A. J., Forr´o, L., Benoit, W., and L. Zuppiroli, "Mechanical properties of carbon nanotubes," Applied Physics. **A 69** (1999) 255-260.

11. Hone, J., Whitney, M., and A. Zetti, "Thermal conductivity of single walled carbon nanotubes," Synthetic Metals **103** (1999) 2498-2499.

12. Che, J., Cagin, T., and W. A. Goddard III, "Thermal conductivity of carbon nanotubes," Nanotechnology **11** (2000) 65–69.

13. Langer, L., Heremans J. P., Bayot V., Issi J. P., Stockman L., Haesendonck C. V., Y. Bruynseraede, Y., and C. H. Olk, "Electrical measurements on submicronic synthetic conductors : Carbon Nanotubes," Synthetic Metals, **70**, 1393-1396.

14. Ruoff, R.S., and D. C. Lorents, "Mechanical and thermal properties of carbon nanotubes," Carbon **33** (1995) 925-930.

15. Sinnott, S. B., Shenderova, O. A., White, C. T., and D. W. Brenner, "Mechanical properties of nanotubule fibers and composites determined from theoretical calculations and simulations," Carbon **36** (1998) 1-9.

16. Davey, A. P., Coleman, J., Dalton, A., Maier, S., Drury, A., Gray, D., Brennan, M., Ryder, K., Chapelle, M. L. D. L., Journet, C., Bernier,P., Carroll, D., Blau,

W., Byrne,H. J, Ajayan, P. M, and S. Lefrant, "Evolution and evaluation of the Polymer/Nanotube composite," Synthetic Metals, 103(1999) 2559-256.

17. Woolley, A. T., Cheung, C. L., Hafner, J. H. and C. M. Lieber, "Structural biology with carbon nanotube AFM probes," Chemistry & Biology **7** (2000) R193-R204.

18. Guo, L., Wang, R., Xu, H. and J. Liang, "Why can the carbon nanotube tips increase resolution and quality of image in biological systems?," Physica E: Low-dimensional Systems and Nanostructures **27** (2005) 240-244.

19. Hahn, J., Yoo, J.E., Han, J., Kwon, H.B., and J. S. Suh, "Field emission from the film of the finely dispersed arc-discharge black core material," Carbon **43** (2005) 937-943.

20. Jang, Y. T., Lee, Y. H., Ju, B. K., Ahn, J. H., Go, C. K., and G. S. Park, "Application of carbon nanotubes to the cathode ray tube-electron gun," Vacuum **68** (2002) 79-85.

21. Smalley, R.E., "From dopyballs to nanowires," Materials Science and Engineering B **19** (1993) 1-7.

22. Ströbel, R., Jörissen, L., Schliermann, T., Trapp, V., Schütz, W., Bohmhammel, K., Wolf, G., and J. Garche, "Hydrogen adsorption on carbon materials," Journal of Power Sources **84** (1999) 221-224.

23. Baughman, R. H., Cui, C., Zakhidov, A. A., Iqbal, Z., Barisci, J. N., Spinks, G. M., Wallace, G. G., Mazzoldi, A., De Rossi, D., Rinzler, G. A., Jaschinski, O, Roth, S., and M. Kertesz, Science **284** (1999) 1340.

24. Ebbesen, T. W. and P. M. Ajayan, “Large scale synthesis of carbon nanotubes,” Nature **358** (1992) 220-222

25. Ugarte, D., “Morphology and structure of graphitic soot particles generated in arc-discharge C_{60} production,” Chemical Physics Letters **198** (1992) 596-602.

26. Journet, C., Maser, W. K., Bernier, P., Loiseau, A., Chapelles, M., Lefrants., S, Deniards, P., Lee, R, and J. E. Fischer, “Large-scale production of single-walled carbon nanotubes by the electric-arc technique,” Nature **388** (1997) 756 – 758.

27. Guo, T., Nikolaev, P., Thess, A., Colbert, D. T., and R. E. Smalley, “Catalytic growth of single-walled manotubes by laser vaporization,” Chemical Physics Letters **243** (1995) 49-54.

28. Yakobson, B. I. and R. E. Smalley, "Fullerene Nanotubes: C1,000,000 and Beyond," American Scientist **85** 324 (1997).

29. Endo, M., Takeuchi, K., Igarashi, S., Kobori, K., Shiraishi, M., and H. W. Krotos, ”The production and structure of pyrolytic carbon nanotubes (PCNTs),” Journal of Physics and Chemistry of Solids **54** (1993) 1841-1848.

30. Ramakrishnan, M. P., “Experimental study on microwave assisted CVD growth of carbon nanotubes on silicon wafer using cobalt as a catalyst,” M.S., Thesis, Mechanical and Aerospace Engineering, Oklahoma State University, May 2005.

31. Hata, K., Futaba, D. N., Mizuno, K., Namai, T., Yumura, M., and S. Iijima, “Water-Assisted Highly Efficient Synthesis of Impurity-Free Single-Walled Carbon Nanotubes,” Science (2004), 1362-1364.

32. Huang, Z. P., Wang, D. Z., Wen, J. G., Sennett, M., Gibson, H., and Z. F. Ren, "Effect of nickel, iron and cobalt on growth of aligned carbon nanotubes," Applied Physics A, Materials Science & Processing **74** (2002) 387-391.

33. Nikolaev, P., Bronikowski, M.J., Bradley, R.K., Rohmund, F, Daniel, C. T., Smith, K. A., and R. E. Smalley, "Gas-phase catalytic growth of single-walled carbon nanotubes from carbon monoxide," Chemical Physics Letters **313** (1999) 91-97.

34. Resasco, D. E., Alwarez, W. E., Pompeo, F., Balzano, L., Herrera, J. E., Kitiyanan, B., and A. Borgna, "A scalable process for production of single-walled carbon nanotubes (SWNTs) by catalytic disproportionation of CO on a solid catalyst," Journal of Nanoparticle Research **4** (2002) 131-136.

35. Wal, V, Hall, R. L., Lee, J., and B. M. Gordon, "Optimization of Flame Synthesis for Carbon Nanotubes Using Supported Catalyst," Journal of Physical Chemistry B **106** (2002) 13122-13132.

36. Dresselhaus, M.S., Dresselhaus, G., Sugihara, K., Spain, I. L., and H. A. Goldberg, "Graphite Fibers and filaments", Springer Ser. Mater. Sci **5** (Springer, Berlin, Heidelberg 1988).

37. Tibbetts, G. G., Devour, M. G., and E. J. Rodda, "An adsorption-diffusion isotherm and its applications to the growth of carbon filaments on iron catalyst particles," Carbon **25** (1987) 367-375.

38. Hughes, T.V., and C. R. Chambers, "Manufacture of carbon filaments," U.S. Patent No. 405,480 dated June. 18, 1889.

39. Baker, R. T. K., and P. S. Harris, "Formation of filamentous carbon," In Chemistry and physics of carbon (edited by P.L. Walker, Jr. and P. A. Thrower) Dekker, New York Vol **14** (1978) 83.

40. Bacon, R., "Growth, Structure, and Properties of Graphite Whiskers," Journal of Applied Physics **31** (1960) 283–290.

41. Kratschmer, W., Lamb, L. D., Fostiropoulos, K. and D. R. Huffman, Nature **347** (1990) 354-358.

42. Mintmire, J. W., Dunlap, B. I., and C. T. White, "Are fullerene tubules metallic?," Phys. Rev. Lett. **68** (1992) 631–634.

43. Dresselhaus, M. S., Dresselhaus, G. and R. Saito, "Carbon fibers based on C_{60} and their symmetry," Phys. Rev. B **45** (1992) 6234–6242.

44. Saito, Y., Nishikubo, K., Kawabata, K. and T. Matsumoto, "Carbon nanocapsules and single-layered nanotubes produced with platinum-group metals (Ru, Rh, Pd, Os, Ir, Pt) by arc-discharge," Journal of Applied Physics **80** (1996) 3362-3367.

45. Bera, D., Brinley, E., Kuiry, S. C., McCutchen, M., Seal, S., Heinrich, H., and B. Kabes, "Optoelectronically automated system for carbon nanotubes synthesis via arc-discharge in solution," Review of Scientific Instruments **76** (2005) 033903.

46. Yumura, M., Ohshima, S., Uchida, K., Tasaka, Y., Kuriki, Y., Ikazaki, F., Saito, Y., and S. Uemura, "Synthesis and purification of multi-walled carbon nanotubes for field emitter applications," Diamond and Related Materials **8** (1999) 785–791.

47. Ishigami, M., Cumings, J., Zettl, A and S. Chen, "A simple method for the continuous production of carbon nanotubes," Chemical Physics Letters **319** (2000) 457–459.

48. Ando, Y., Zhaob, X., Hiraharab, K., Suenagab, K., Bandowb, and S., Iijima, “Arc plasma jet method producing single-wall carbon nanotubes,” Diamond and Related Materials **10** (2001) 1185-1189.

49. Haung, H., Kajiura, H., Tsutsui, S., Hirano, Y., Miyakoshi, M., Yamada, A., M. Ata, “Large scale rooted growth of aligned super bundles of single-walled carbon nanotubes by using directed arc plasma method,” Chemical Physics Letters **343** (2001) 7-14.

50. Seraphin, S., Zhou, D., Jiao, J., Withers, J.C., and R. Loutfy, “Effect of processing conditions on the morphology and yield of carbon nanotubes,” Carbon **31** (1993) 685-689.

51. Zhangyz, H., Wangz, D., Xuey, X., Chenz, B., and S. Peng, “The effect of helium gas pressure on the formation and yield of nanotubes in arc-discharge,” Journal of Applied Physics D **30** (1997) L1-L4.

52. Wang, X. K., Lin, X. W., Dravid, V. P., Ketterson, J. B., and R. P. H. Chang, "Carbon nanotubes synthesized in a hydrogen arc-discharge," Applied Physics Letters **66** (1995) 2430-2432.

53. Hahn, J., Yoo, J. E., ,Han, J., Kwon, H. B., and J. S. Suh, " Field emission from the film of the finely dispersed arc-discharge black core material," Carbon **43** (2005) 937–943.

54. Ando, Y., Zhao, X., Kataura, H., Achiba, Y., Kaneto, K., Tsuruta, M., Uemura, S., and S. Iijima, "Multiwalled carbon nanotubes prepared by hydrogen arc," Diamond and Related Materials **9** (2000) 847–851.

55. Jung, S. H., Kim, M. R., Jeong, S. H., Kim, S. U., Lee, O. J., Suh, J. H., and C. K. Park, "High yield synthesis of multi-walled carbon nanotubes by arc discharge in liquid nitrogen," Appl. Phys. A **76** (2003) 285-286.

56. Antisari, M. V., Marazzi, R., and R. Krsmanovic, "Synthesis of multiwall carbon nanotubes by electric arc discharge in liquid environments," Carbon **41** (2003) 2393-2401.

57. Sano, N., Wang, H., Alexandrou, I., Chhowalla, M., Teo, K. B. K., and G. A. J. Amaratunga, "Properties of carbon onions produced by an arc discharge in water," Journal of Applied Physics **92** (2002) 2783-2788.

58. Rosolen, J. M., Lofrano, R. C. Z., and L. A. Montoro, "Synthesis of single and multi-walled carbon nanotubes by arc water method," Carbon **43** (2005) 195-213.

59. Zhu, H. W., Li, X. S., Jiang, B., Xu, C. L., Zhu, Y. F., Wu, D. H., X. H. Chen, "Formation of carbon nanotubes in water by electric-arc technique," Chemical Physics Letters **366** (2002) 664-669.

60. Li, X., Zhu, H., Jiang, B., Ding, J., Xu, C., and D. Wu, "High yield synthesis of multi-walled carbon nanotubes by water protected arc discharge method," Carbon **411** (2002) 1645-1687.

61. Yokomichi, H., Sakima, H., Matoba, M., Ichihara, M., and F. Sakai, "Morphology and electronic properties of carbon nanotubes synthesized by arc discharge in CF_4 gas," Superlattices and Microstructures **25** (1999) 487-491.

62. Lai, H. J., Lin, M. C. C., Yang, M. H., and A. K. Li, "Synthesis of carbon nanotubes using polycyclic aromatic hydrocarbons as carbon sources in an arc discharge," Materials Science and Engineering C **16** (2001) 23-26.

63. Shimotani, K., Anazawa, K., Watanabe, H., and M. Shimizu, "New synthesis of multi-walled carbon nanotubes using an arc-discharge technique under organic molecular atmospheres," Applied Physics A **73** (2001) 451-454.

64. Tsang, S. C., Harris, P. F. J., and M. L. H. Green, "Purification of carbon nanotubes," Nature **362** (1993) 522-525.

65. Ajayan, P. M., Ebbesen, T. W., Hiura, H., Tanigaki, K., "Purification of nanotubes," Nature **367** (1994) 519.

66. Ebbesen, T., Ajayan, P.M., and H. Hiura, "Method of purifying carbon nanotubes," US Patent # 5641466, June 24, 1997.

67. Uchida, K., Yumura, M., Ohshima, S., Kuriki, Y., Yase, K., and F. Ikazaki, "Process for isolating carbon nanotubes from a mixture containing carbon nanotubes and graphite particles," US Patent # 5560898, October, 1, 1996.

68. Park, Y. S., Choi, C. Y., Kim, K. S., Chung, D. C., Bae, D. J., An, K. H., Lim, S. C., Zhu, X. Y., and Y. H. Lee, "High yield purification of multiwalled carbon nanotubes by selective oxidation during thermal annealing," Carbon **39** (2001) 655-661.

69. Seraphin, S., and D. Zhou, "Single-walled carbon nanotubes produced at high yield by mixed catalysts," Applied Physics Letter **64** (1994) 2087-2089.

70. Saito, Y., Koyama, T., and K. Kawabata, “Growth of single-layer carbon tubes assisted with iron-group metal catalysts in carbon arc,” Physics D **40** (1997) 421-424.

71. Saito, Y., Tani, Y., and A. Kasuya, “Diameter of single-wall carbon nanotubes depending helium gas pressure in an arc discharge,” Journal of Physical Chemistry B **104** (2000) 2495-2499.

72. Wang, Y., Zhang, Z., Liu, H., Xu, X., Pan, G., Guo, Z., Liu, Y., Han, X., and G. Lan, "The effect of catalyst concentration on the synthesis of single-wall carbon nanotubes," Spectrochimica Acta Part A **58** (2002) 2089–2095.

73. Takizawa, M.,Bandow, S., Yudasaka, M., Ando, Y., Shimoyama, H., and S. Iijima, “Change of tube diameter distribution of single-wall carbon nanotubes induced by changing the bimetallic ratio of Ni and Y catalysts," Chemical Physics Letters **326** (2000) 351–357.

74. Lv, X., Du, F., Ma, Y., Wu, Q., and Y. Chen, "Synthesis of high quality single-walled carbon nanotubes at large scale by electric arc using metal compounds," Carbon **43** (2005) 2013–2032.

75. Takizawa, M., Bandow, S., Torii, T., and S. Iijima, “Effect of environment temperature for synthesizing single-wall carbon nanotubes by arc vaporization method,” Chemical Physics Letters **302** (1999) 146-150.

76. Liu, Y., and T. Zhao, “Large scale and high purity synthesis of single-walled carbon nanotubes by arc discharge at controlled temperature,” Carbon **42** (2004) 2765-2768.

77. Farhat, S., Chapelle, M. L. L., Loiseau, A., Scott, C. D., Lefrant, S., Journet, C., and P. Bernier, "Diameter control of single-walled carbon nanotubes using argon-helium mixture gases," Journal of Chemical Physics **115** (2001) 6752-6759.

78. Zhao, X., Inoue, S., Jinno, M., Suzuki, T., and Y. Ando, "Macroscopic oriented web of single-wall carbon nanotubes," Chemical Physics Letters **373** (2003) 266-271.

79. Ando, Y., Zhao, X., Inoue, S., Suzuki, T., and T. Kadoya, "Mass production of high-quality single-wall carbon nanotubes by H_2-N_2 arc discharge," Diamond and Related Materials **14** (2005) 729-732.

80. Guo, Y., Okazaki, T., Kadoya, T., Suzuki, T., and Y. Ando, "Spectroscopic study during single-wall carbon nanotubes production by Ar, H_2, H_2-Ar D.C. arc discharge," Diamond and Related Materials **14** (2005) 887-890.

81. Waldroff, E.I., Wass, A.M., Friedmann, P.P., and M. Keidar, "Characterization of carbon nanotubes produced by arc discharge: Effect of background pressure," Journal of Applied Physics **95** (2004) 2749-2754.

82. Shi, Z., Lian, Y., Zhou, X., Gu, Z., Zhang, Y., Iijima, S., Li, H., Yue, K.T., and S. L. Zhang, "Production of single-wall carbon nanotubes at high pressure," Journal of Physical Chemistry B **103** (1999) 8698-8701.

83. Park, Y.S., Kim, K.S., Jeong, H.J., Kim, W.S., Moon, J.M., An, K.H., Bae, D.J., Lee, Y.S., Park, G.S., and Y. H. Lee, "Low pressure synthesis of single-waled carbon nanotubes by arc discharge," Synthetic Metals **126** (2002) 245-251.

84. Hinkov, I., Farhat, S., and C. D. Scott, “Influence of gas pressure on single wall carbon nanotube formation,” Carbon **43** (2005) 2453–2462.

85. Iijima, S., Ajayan, P. M., and T. Ichihashi, “Growth model for carbon nanotubes,” Physical Review Letters **69** (1992) 3100-3106.

86. Crespi, V. H., "Local tempearture during the growth of multiwalled carbon nanotubes," Physical Review Letters **82** (1999) 2908-2901.

87. Colbery, D.T., and R. E. Smalley, “Electric effects in nanotube growth,” Carbon **33** (1995) 921-924.

88. Gamaly, E.G., and T. W. Ebbesen, “Mechanism of carbon nanotube formation in the arc discharge,” Physical Review B 52 (1995) 2083-2089.

89. Guo, T., Nikolaev, P., Rinzler, A. G., Tomanek, D., Colbert, D. T., and R. E. Smalley, “Self assembly of tubular fullerenes,” Journal of Physical Chemistry **99** (1995) 10694-10697.

90. Charlier, J. C., Vita, A. D., Blasé, X., and R. Car, “Microscopic growth mechanisms for carbon nanotubes,” Science **275** (1997) 647-649.

91. Robertson, D. H., Brenner, D. W., and C. T. White, “On the way to fullerenes: Molecular dynamics study of the curling and closure of graphitic ribbons,” Journal of Physical Chemistry **96** (1992) 6133-6135.

92. Maiti, A., Brabec, C.J., Roland, C.M., and J. Bernholc, “Growth energitics of carbon nanotubes,” Physical Review Letters **73** (1994) 2468-2472.

93. Kwon, Y.K., Lee, Y.H., Kim, S.G., Jund, P., Tomanek, D., and R. E. Smalley, "Morphology and stability of growing multiwall carbon nanotubes," Physical Review Letters **79** (1997) 2065-2068.

94. Shi, Z., Zhou, X., Jin, Z., Gu, Z., Wang, J., Feng, S., Xu, X., Liu, and Zhenquan, "High yield synthesis and growth mechanism of carbon nanotubes," Solid State Communications **97** (1996) 371-375.

95. Shi, Z., Lian, Y., Zhou, X., Gu, Z., Zhang, Y., Iijima, S., Zhou, L., Yue, K.T., and S. Zhang, "Mass-production of single-wall carbon nanotubes by arc discharge method," Carbon **37** (1999) 1449-1453.

96. Shi, Z., Lian, Y., Liao, F.H., Zhou, X., Gu, Z., Zhang, Y., Iijima, S., Li, H., Yue, K.T., and S. L. Zhang, "Large scale synthesis of single-wall carbon nanotubes by arc discharge method," Journal of Physics and Chemistry of Solids **61** (2000) 1031-1036.

97. Kanzow, H., Lenski, C., and A. Ding, "Single-wall carbon nanotube diameter distributions calculated from experimental parameters," Physical Review B **63** 1254021-12540215.

98. Gavillet, J., Loiseau, A., Ducastelle, F., Thair, S., Bernier, P., Stephan, O., Thibault, J., and J. C. Charlier, "Microscopic mechanism for the catalyst assisted growth of single-wall carbon nanotubes," Carbon **40** (2002) 1649-1663.

99. Zhou, D., Seraphin, S., and S. Wang, "Single-walled carbon nanotubes growing radially from YC_2 particles," Applied Physics Letters **65** (1994) 1593-1595.

100. Itkis, M. E., Perea, D. E., Niyogi, S., Love, J., Tang, J., Yu, A., Kang, C., Jung, R., and R. C. Haddon, "Optimization of the Ni-Y catalyst composition in bulk electric arc synthesis of Single-walled carbon nanotubes by use of Near-Infrared spectroscopy," Journal of Physical Chemistry B **108** (2004) 12770-12775.

101. Saito, Y., Yoshikawa, T., Okuda, M., Ohkohchi, M., Ando, Y., Kasuya, A., and Y. Nishina, "Synthesis and electron-beam incision of carbon nanocapsules encaging YC_2," Chemical Physics Letters **209** (1993) 72-76.

102. Saito, Y., Kawabata, K., and M. Okuda, "Single-layered carbon nanotubes synthesized by catalytic assistance of rare-earths in a carbon arc," Journal of Physical Chemistry **99** (1995) 16076-16079.

103. Ugarte, D., "Morphology and structure of graphitic soot particles generated in arc-discharge C_{60} production," Chemical Physics Letters **198** (1992) 596-602.

104. Rodriguez, N. M., Kim, M. S., Fortin, F., Mochida, I., and R. T. K. Baker, "Carbon deposition on iron-nickel alloy particles," Applied Catalysis A General **148** (1997) 265-282.

105. Ugarte, D., "Formation mechanism of quasi-spherical carbon particles induced by electron bombardment," Chemical Physics Letters **207** (1993) 473-476.

106. Ugarte, D., "Onion-like graphite particles," Carbon **33** (1995) 989-993.

107. Graham, D., and W. S. Kay, "Morphology of thermally graphitized P-33 carbon black in relation to absorbent uniformity," Journal of Colloid Science **16** (1961) 182-186.

108. Marsh, P. A., Voet, A., Mullins, T. J., and L. D. Price, "Quantitative micrography of carbon black microstructure," Carbon **9** (1971) 797-799.

109. Ando, Y., Zhao, X., and H. Shimoyama, "Carbonaceous products in hydrogen arc discharge," Crystal Research Technology **34** (1999) 597-603.

110. Stone, A. J. and D. J. Wales, "Theoretical studies of icosahedral C_{60} and some related species," Chemical Physics Letters **128** (1986) 501-503.

111. Cadek, M., Murphy, R., McCarthy, B., Drury, A., Lahr, B., Barklie, R.C., Panhuis, M., Coleman, J. N., and W. J. Blau, "Optimization of arc-discharge production of multi-walled carbon nanotubes," Carbon **40** (2002) 923-928.

112. Saito, Y., Okuda, M., Tomita, M., and T. Hayashi, "Extrusion of single-wall carbon nanotubes via formation of small particles of condensed near an arc evaporation source," Chemical Physics Letters **236** (1995) 419-426.

113. Subramoney, S., Ruoff, R. S., Lorents, D. C., and R. Malhotra, "Radial single-layer nanotubes," Nature **366** (1993) 637.

114. Saito, Y., "Nanoparticles and filled nanoparticles," Carbon **33** (1995) 979-988.

VITA

HARIPRASAD RAMAKRISHNAN VENKATANATH

Candidate for the Degree of

Master of Science

Thesis: EXPERIMENTAL INVESTIGATION ON THE SYNTHESIS OF CARBON NANOTUBES (CNTs) BY ARC-DISCHARGE METHOD USING A MIG WELDER

Major Field: Mechanical Engineering

Biographical:

Personal Data: Born in Bangalore, Karnataka, India, on November 18. 1979, the son of Ramakrishnan and Santha

Education: Received Bachelor of Engineering degree in Mechanical Engineering from University of Madras, Chennai, India, in August 2002.

Completed the requirements for the Master of Science degree with a major in Mechanical and Aerospace Engineering at Oklahoma State University in December 2005.

Experience:

Graduate Teaching Assistant in the School of Mechanical and Aerospace Engineering, Oklahoma State University, Stillwater, Oklahoma, Jan 2003- May 2004.

Graduate Research Assistant in the School of Mechanical and Aerospace Engineering, Oklahoma State University, Stillwater, Oklahoma, Aug 2004 – present.

Name: Ramakrishnan Venkatanath Hariprasad Date of Degree: December, 2005

Institution: Oklahoma State University Location: Stillwater, Oklahoma

Title of Study: EXPERIMENTAL INVESTIGATION ON THE SYNTHESIS OF CARBON NANOTUBES (CNTs) BY ARC-DISCHARGE METHOD USING A MIG WELDER

Pages in Study: 154 Candidate for the Degree of Master of Science

Major Field: Mechanical Engineering

Scope and Method of study:

Nanotubes are considered the most useful molecules in nanotechnology due to their unique mechanical, electronic, and physical properties. The arc-discharge is a simple and inexpensive method for producing carbon nanotubes (CNTs) on a large scale. The arc-discharge apparatus in the vertical configuration in conjunction with a MIG welder was built for conducting this study. To synthesize multi-walled carbon nanotubes (MWNTs) a 0.25" diameter graphite anode was used. For the synthesis of single-walled carbon nanotubes (SWNTs), 4 at% nickel, 1 at% yttrium, 95 at% carbon anode was used. Critical process parameters, such as process gas, gas flow rate, and gas pressure have been varied to study its effect on MWNT yield.

Findings and conclusion:

In this experimental study, carbon nanotubes (CNT) are obtained by vaporizing graphite in an inert atmosphere using the arc-discharge method. Helium is found to be a favorable buffer gas for the synthesis of MWNTs compared to argon. Maximum yield of cathode deposit is obtained when the chamber pressure is maintained between 315 to 355 torr. Purification study of MWNTs showed that heating at 750^{o} C for 5 mins or 700^{o} C for 15 mins are desirable conditions for removing amorphous carbon. The vaporization of graphite anode containing 4% Ni-1% Y in a helium atmosphere leads to the formation of SWNTs. The growth of SWNT bundles strongly depends on the chamber pressure. CNT bundles are formed in helium at a pressure in the range of 315 to 506 torr. Maximum yield was obtained when the helium pressure was 506 torr, at a flow rate of 2 l/min. The nucleation and growth of SWNT bundles are explained according the vapor-liquid-solid (V-L-S) model.

ADVISER'S APPROVAL: Dr. Ranga Komanduri